Lagrangian transport

WAVACS 2009
B. Legras, legras@lmd.ens.fr, http://www.lmd.ens.fr/legras

The Lagragian point of view

position $\vec{x}(\vec{a},t)$
velocity $\vec{u}(\vec{x}(\vec{a},t),t)$
tracer concentration $c(\vec{x}(\vec{a},t),t)$
where $\vec{a}=\vec{x}(\vec{a},0)$
is the initial position
of the parcel

Eulerian point of view

Lagrangian point of view

velocity $\vec{u}(\vec{x},t)$
tracer concentration $c(\vec{x},t)$

Lagrangian versus Eulerian point of view

Lagrangian dispersion (Taylor)

We neglect here molecular diffusion and show that at large scales where dispersion exceeds the size of most energetic eddies, transport is again diffusive.

In Lagragian coordinates, motion of a parcel is

$$\boldsymbol{x}(\boldsymbol{a},t)=\boldsymbol{x}(\boldsymbol{a},0)+\int_0^t \boldsymbol{u}(\boldsymbol{x}(\boldsymbol{a},s),s)\,ds$$

where $x(\boldsymbol{a},t)$ is position at time t of parcel which was in $\boldsymbol{a}$ at time 0 (hence $\boldsymbol{x}(\boldsymbol{a},0)=\boldsymbol{a}$)

For each parcel with initial position $\boldsymbol{a}_i$, define

$$\boldsymbol{x}_i(t)=\boldsymbol{x}(a_i,t) \text{ and } \boldsymbol{v}_i(t)=\boldsymbol{u}(\boldsymbol{x}(\boldsymbol{a}_i,t),t)$$

Hence, $\frac{d}{dt}(\boldsymbol{x}_i-\boldsymbol{a}_i)^2=2(\boldsymbol{x}_i-\boldsymbol{a}_i)\boldsymbol{v}_i=2\int_0^t \boldsymbol{v}_i(t)\boldsymbol{v}_i(s)\,ds$,

and after averaging over ensemble

$$\frac{d}{dt}\langle(\boldsymbol{x}_i-\boldsymbol{a}_i)^2\rangle=2\int_0^t S(t-s)\,ds=2\int_0^t S(s)\,ds$$

where $S(t-s)=\langle \boldsymbol{v}_i(t)v_i(s)\rangle$ is the Lagrangian velocity correlation, assuming homogeneity and stationnarity.

This can be solved as

$$\boxed{\langle(\boldsymbol{x}_i-\boldsymbol{a}_i)^2\rangle=2\int_0^t (t-s)\,S(s)\,ds}$$

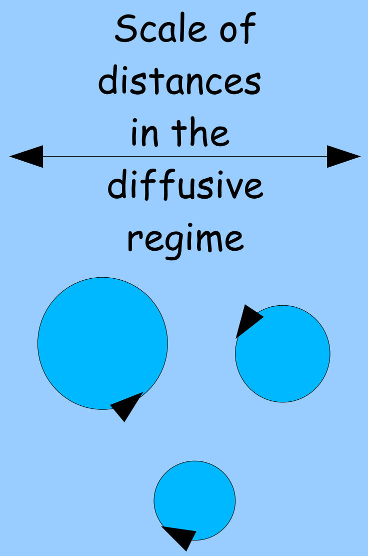

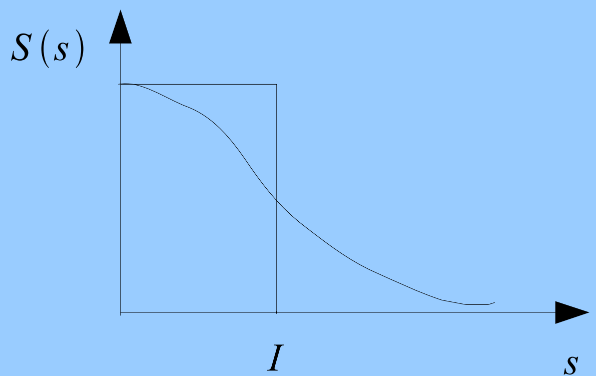

Integral scale I

$$\int_0^\infty S(s)\,ds=\langle v^2\rangle I$$

Diffusive regime: If $S(s)$ decays fast enough, and for $t \gg I$

$$\langle (\boldsymbol{x}_i - \boldsymbol{a}_i)^2 \rangle \sim 2Dt \text{ with } D = \int_0^\infty S(s)\,ds$$

If the integral $\int_0^\infty S(s)\,ds$ diverges, the diffusive regime does not exis

For instance if $S(s) \sim s^{-\eta}$ with $0 < \eta < 1$, the regime is super-diffusive

$$\langle \boldsymbol{x}^2 \rangle \sim t^{2-\eta}$$

If now $\int_0^\infty S(s)\,ds = 0$, but if $\int_0^t (t-s) S(s)\,ds$ diverges with t, we have a sub-diffusive regime. For instance if $S(s) \sim s^{-\eta}$ with $1 < \eta < 2$ for large enough times, we have again $\langle \boldsymbol{x}^2 \rangle \sim t^{2-\eta}$ but with an exponent less than 1

Reconstruction of tracer fields

Reconstruction of a tracer field is obtained by reverse time integration of particle trajectories initialised from their final position from t_0 to $t_0 - \tau$, using analysed winds (e.g. ECMWF winds).

- assignment of the chemical tracer value or PV at $t_0 - \tau$ location from low resolution CTM (chemical transport model) or analysed fields

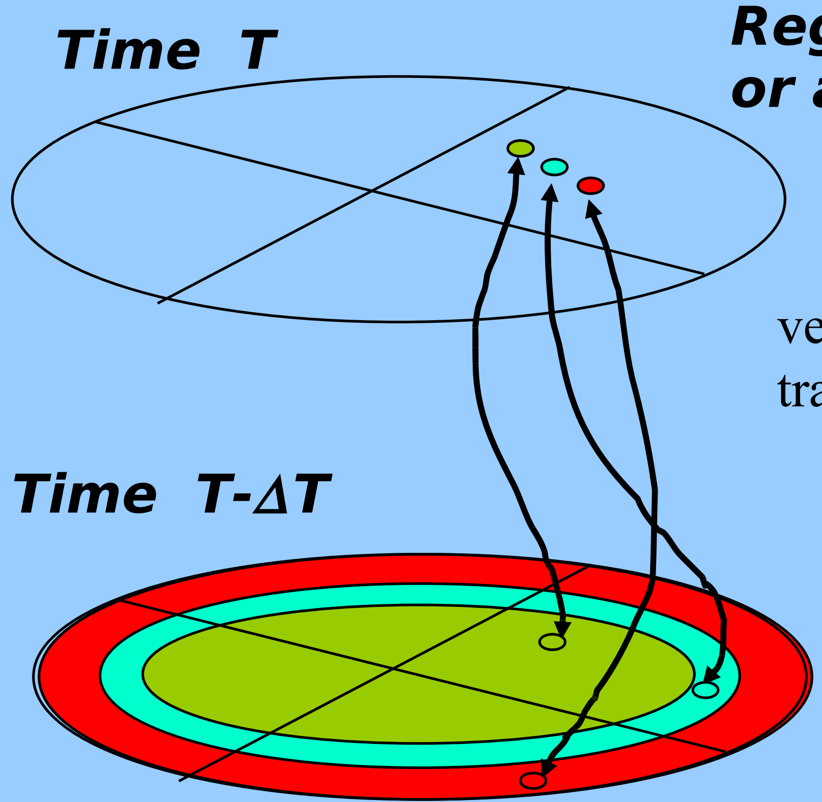

velocity $\vec{u}(\vec{x}(\vec{a},t),t)$
tracer concentration $c(\vec{x}(\vec{a},t),t)$

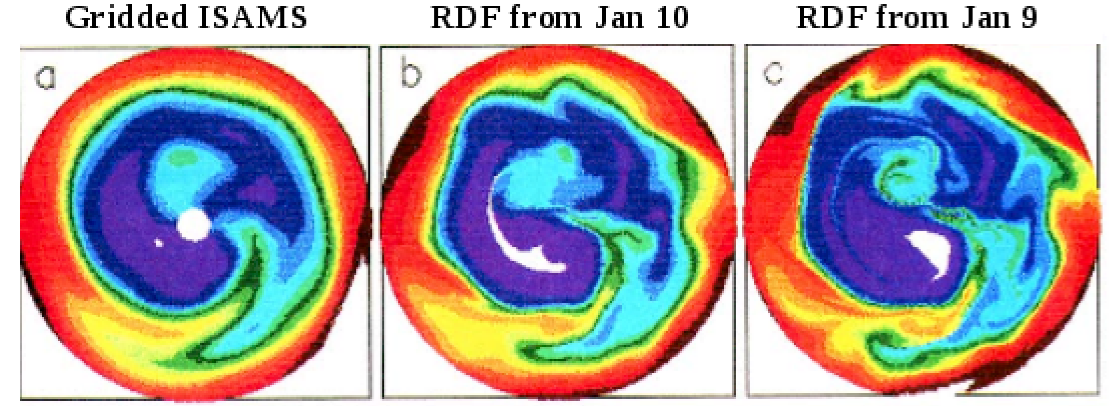

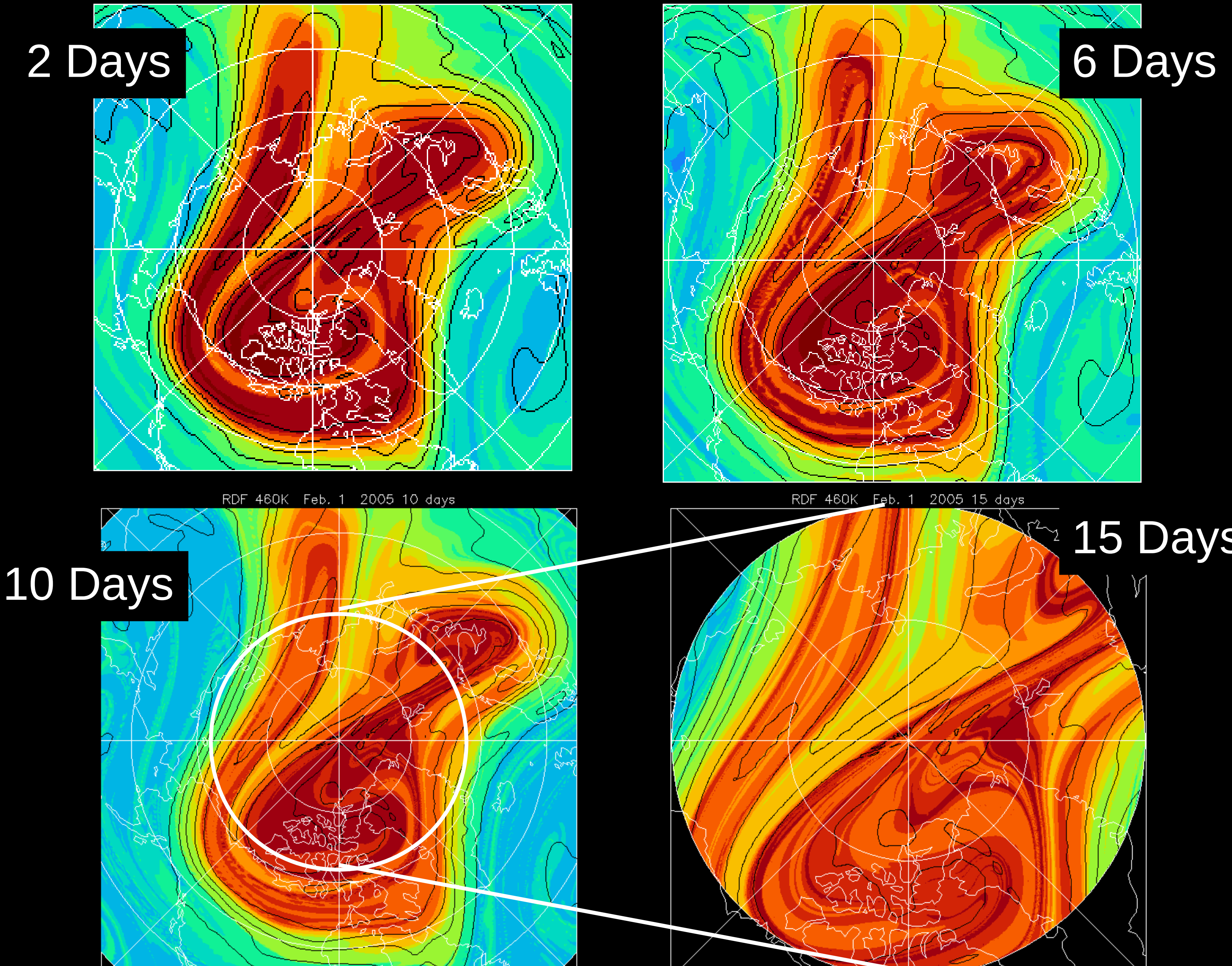
2 Days
6 Days
RDF 460K Feb. 1 2005 10 days
10 Days
RDF 460K Feb. 1 2005 15 days
15 Days

Mariotti et al., 1997, JGR D102, 6131-6142

Layerwise motion and the generation of filaments in the lower stratosphere -> laminae in the ozone vertical profile

ozone profile from Lerwick

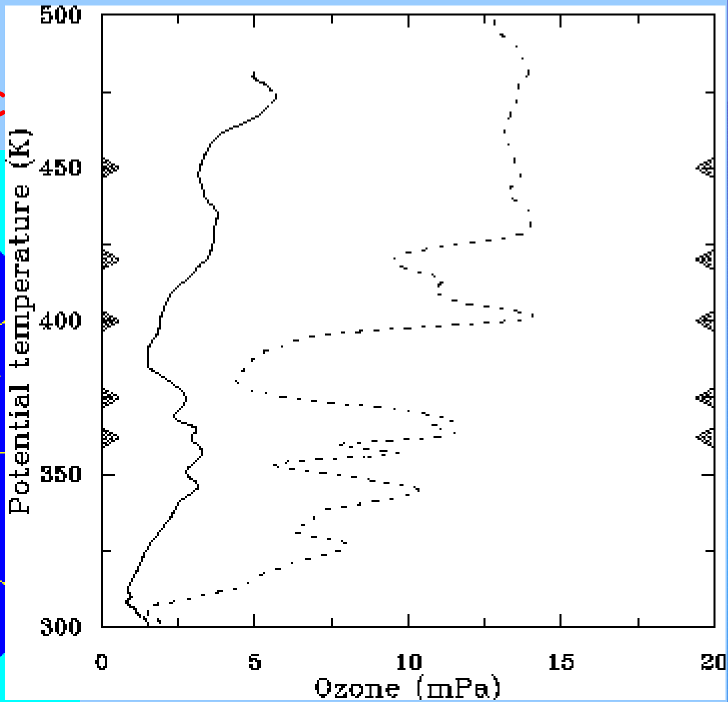

PV reconstruction by isentropic advec

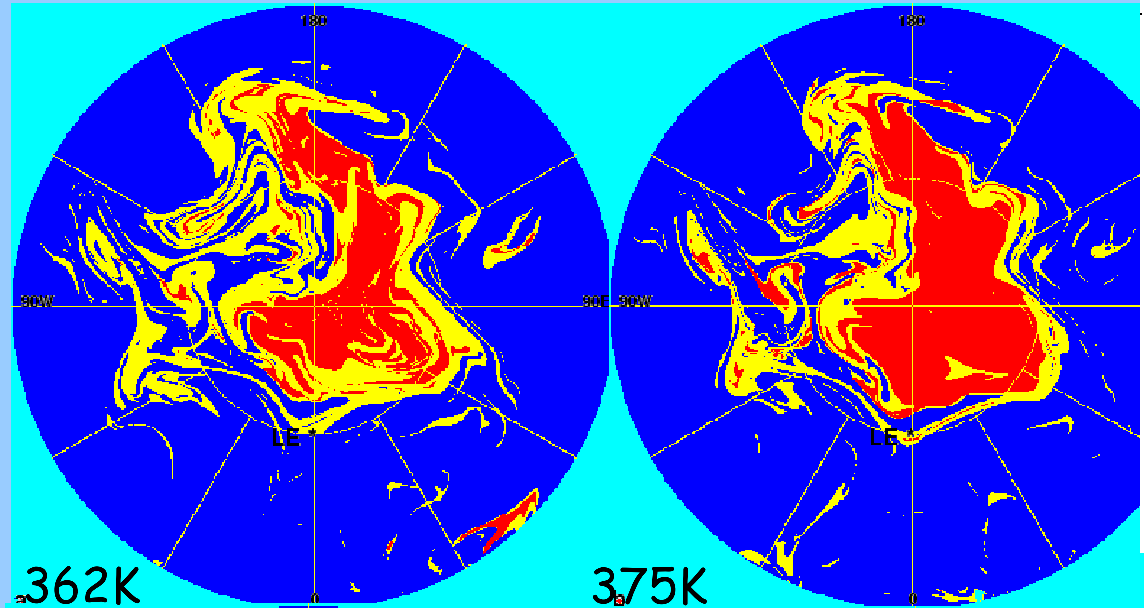

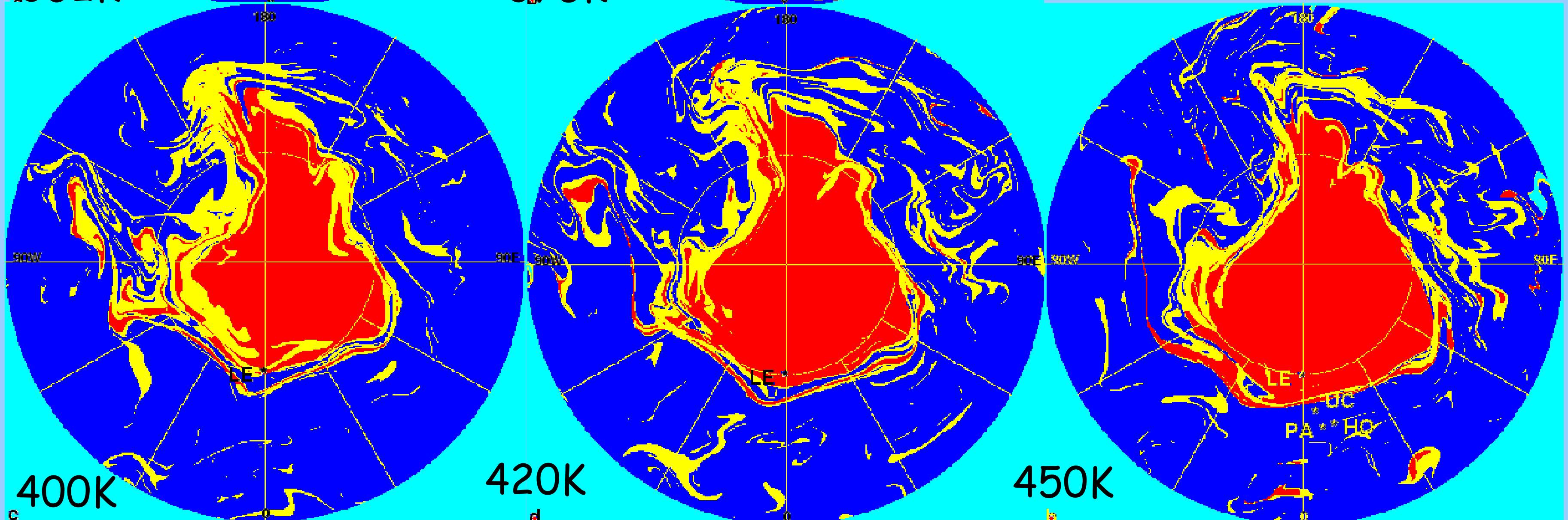

The ERTEL potential vorticity

$$P = \frac{(\overrightarrow{rot}\,\vec{v} + 2\vec{\Omega}) \cdot \vec{\nabla}\theta}{\rho} \approx \frac{(f + \zeta_\theta)}{\rho_\theta}$$

with the isentropic density $\rho_\theta = -g\,\partial p / \partial \theta$,
measuring static stability

The potential vorticity P (PV) is a material invariant under inviscid and adiabatic approximation

A discontinuity in static stability must show up equally well in PV

Unit: 1PVU = 10^{-6} m^2 s K kg^{-1}

Appenzeller, Davies & Norton, 1996, JGR, D101(1), 1435-1456

PV reconstruction by isentropic contour advection at 320 K

Meteosat water-vapour

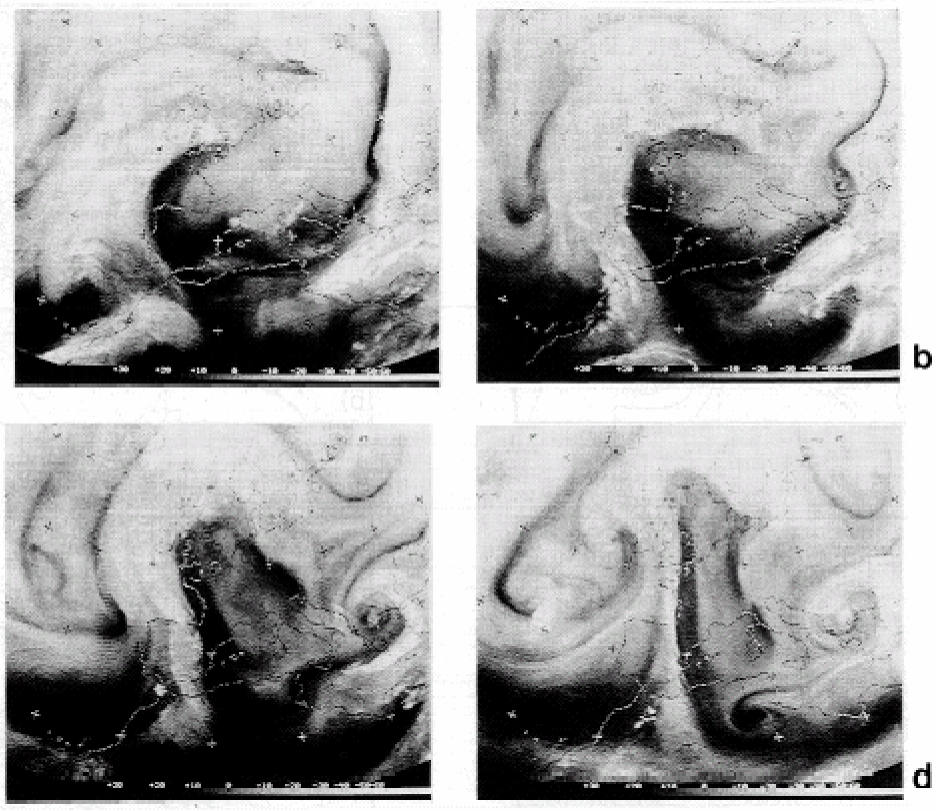

Figure 8. Satellite radiance images (compare Figure 3) at 12-hour intervals from 0000 UT, May 13, 1992 (compare panels for the same time periods as in Figure 7 and Plate 2).

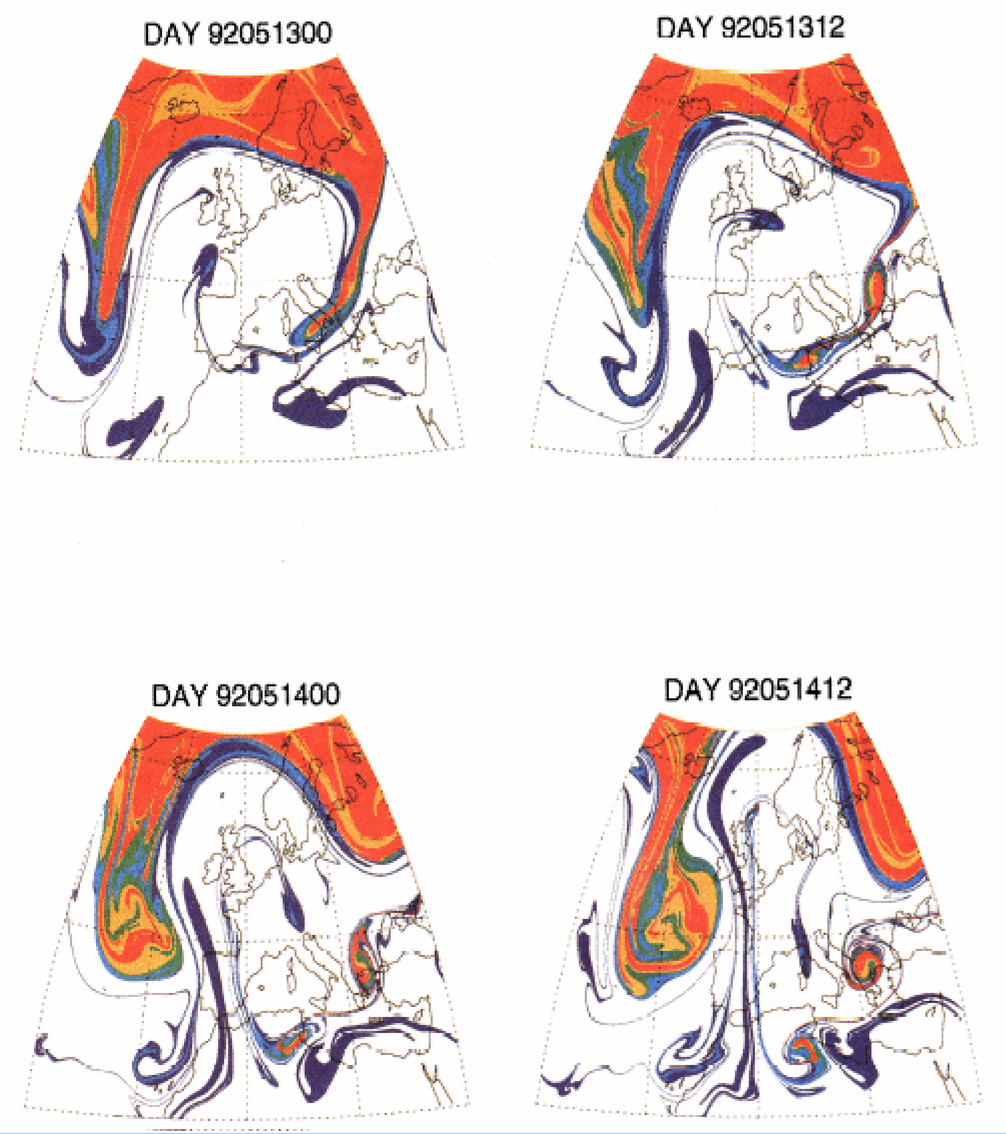

Lagrangian trajectories are able to reconstruct small-scale structures well beyond the resolution of the observed/analysed winds.

Why does this work?
What are the limitations?

Large-scale motion (L>100 km in the atmosphere, L>10 km in the ocean) is dominated by layerwise quasi two-dimensional motion as a result of aspect-ratio, rotation and stratification

Numerically simulated two-dimensional turbulence

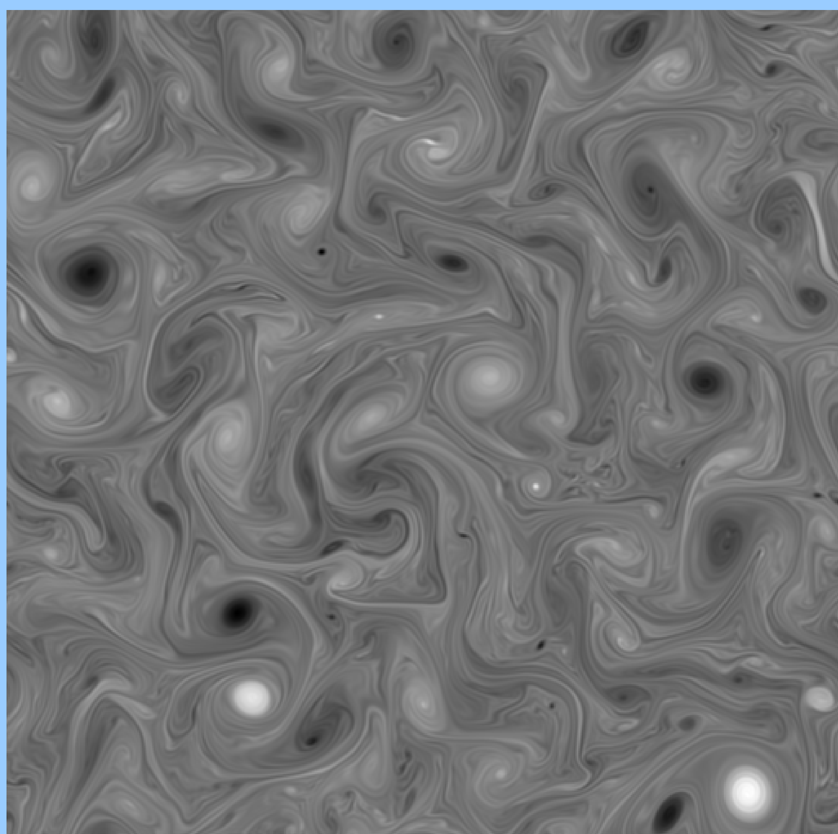

Chlorophyll in the ocean

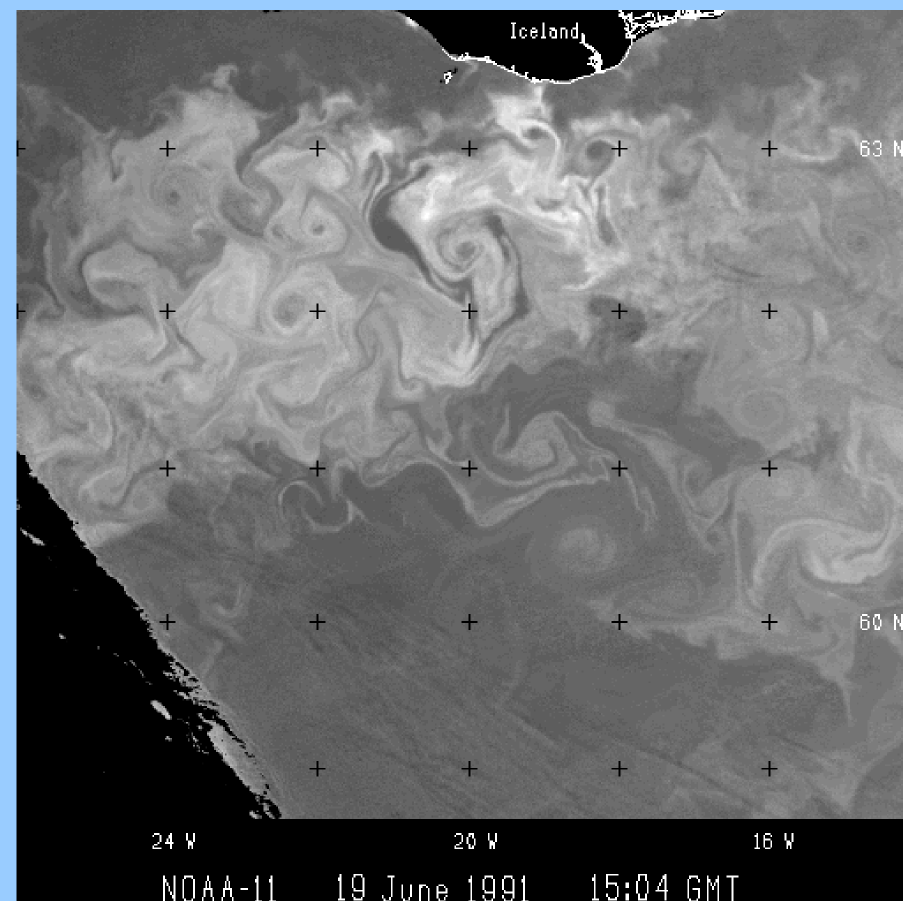

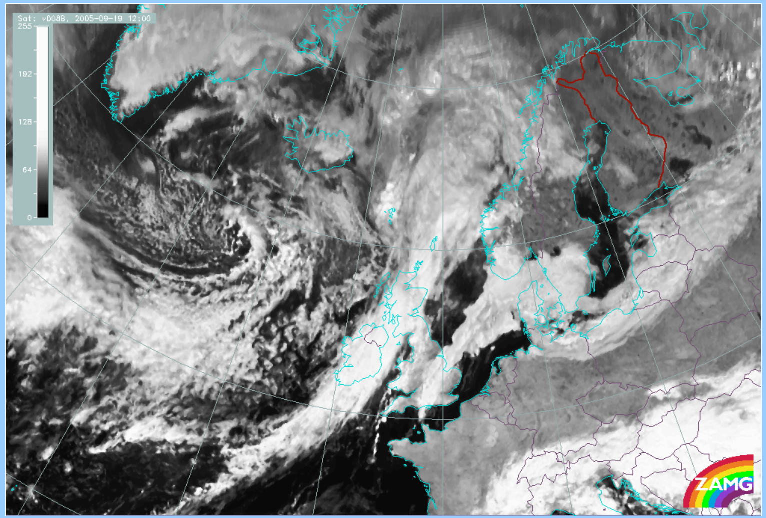

Visible channel
Meteosat

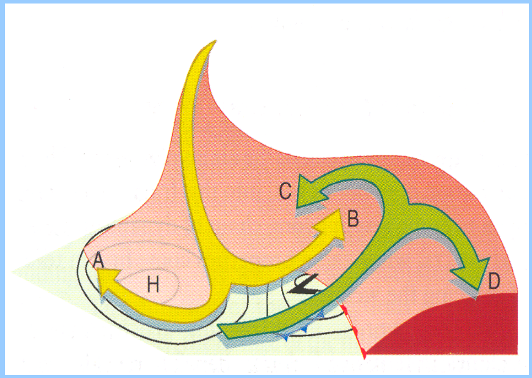

Water vapour channel Meteosat

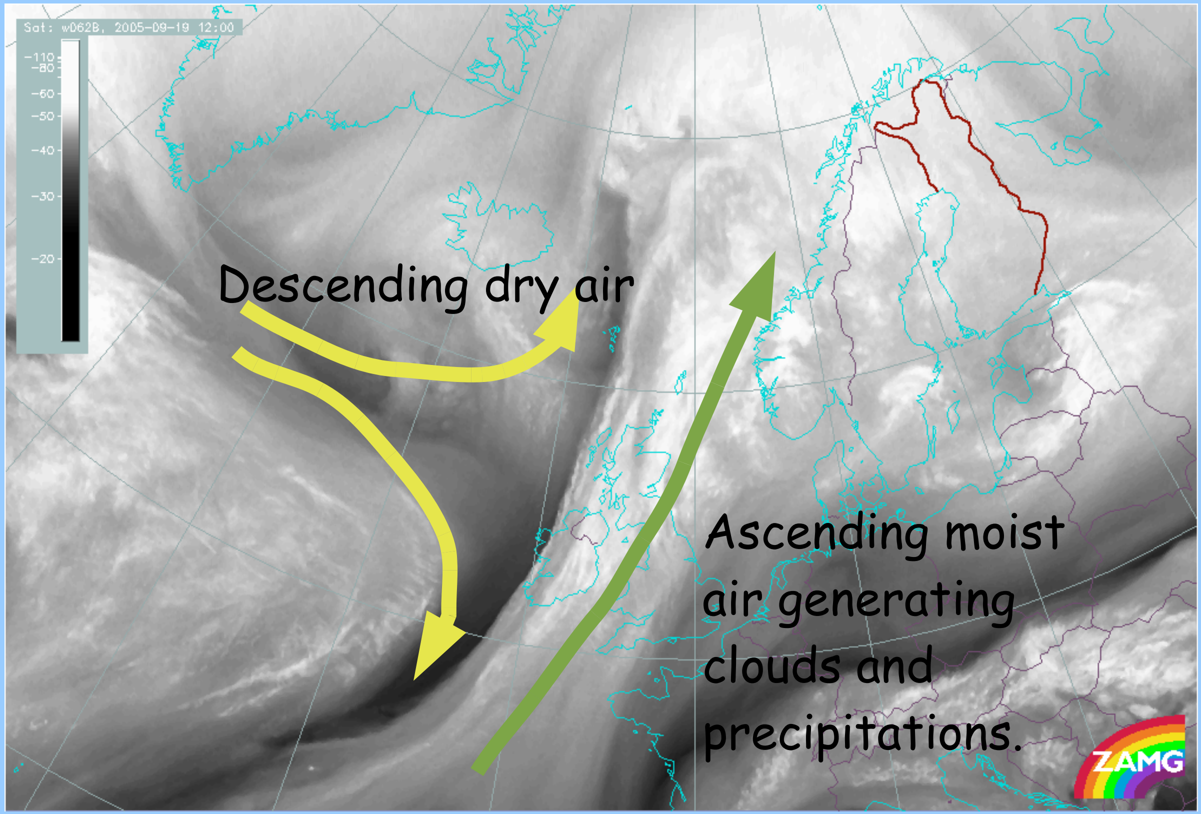

Although mixing and convective instability do occur during the development, the main ingredient is adiabatic baroclinic instability, that is isentropic motion.

II.4

Ubiquity of quasi-horizontal layers in the troposphere

Reginald E. Newell*, Valerie Thouret*†, John Y. N. Cho*, Patrick Stoller*‡, Alain Marenco† & Herman G. Smit§

Nature, 25 March 1999

About 15% of the atmosphere is occupied by layers.

Mainly due to stratospheric intrusions

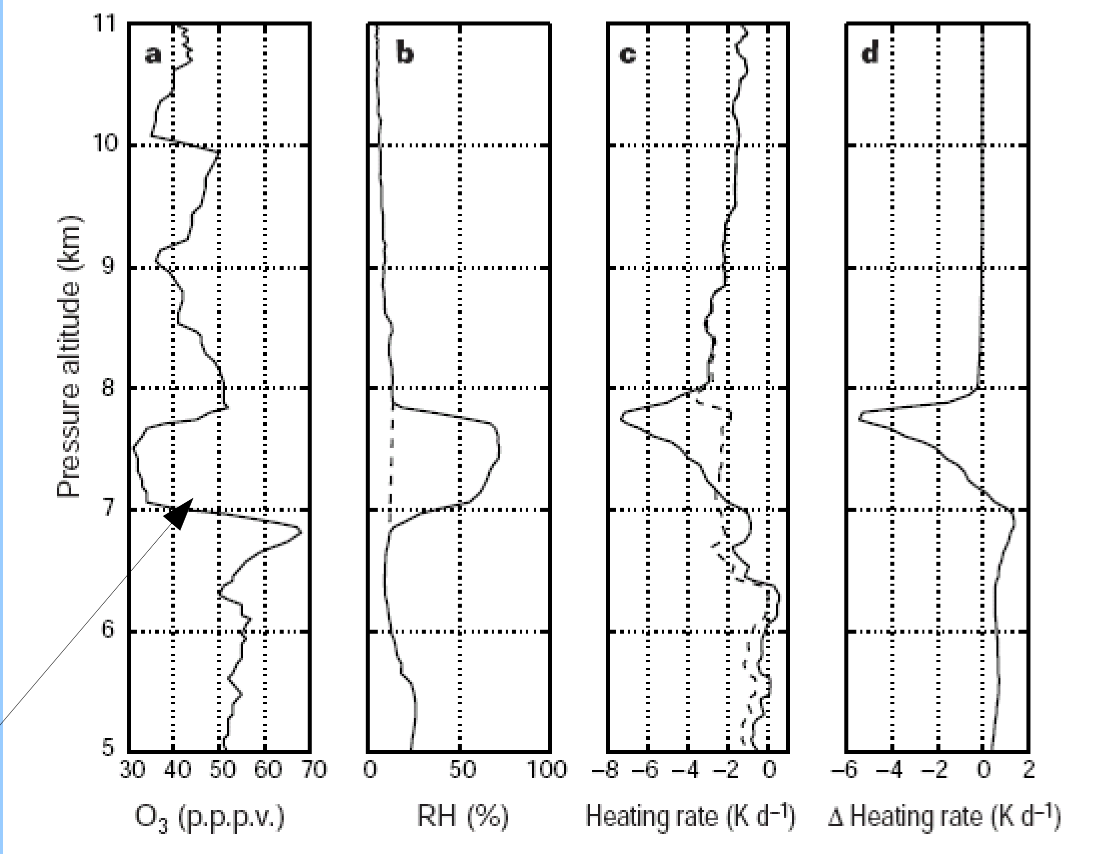

Ozone layer in the troposphere a few km under the tropopause

Example of layering in the free troposphere

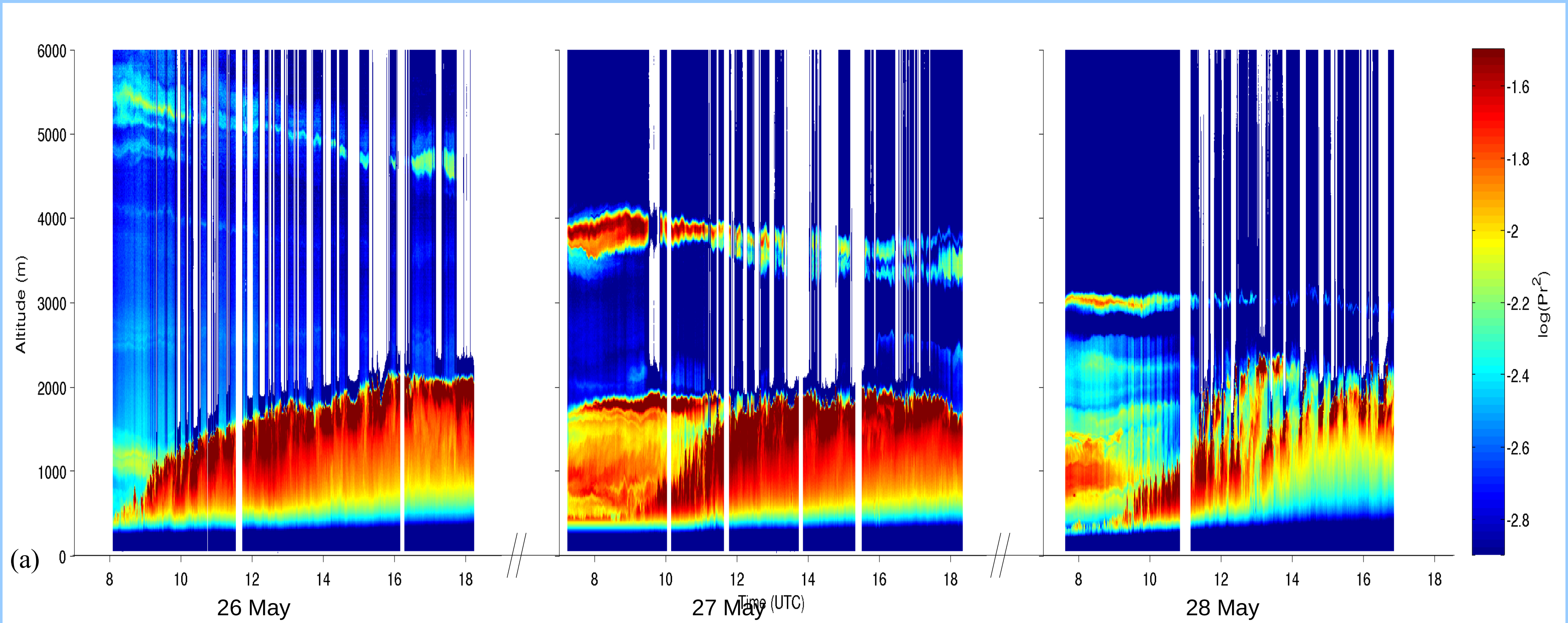

SIRTA aerosol lidar on 26-28 May 2003
Ecole Polytechnique / LMD

Turbulent versus chaotic mixing

- Turbulent mixing in 3D flows with a large number of degrees of freedom
- Kolmogorov scale law
  - ivelocity increment $\delta\ U(r) \sim r^{1/3}$
  - The velocity gradient is singular in the inviscid limit

- Chaotic *stirring* in layerwise (quasi-2D) flows is dominated by the advection of the large-scale energetic eddies
- Batchelor flow
  - Velocity increment

    $\delta\ U(r) \sim r$
  - Velocity gradient is everywhere bounded

Atmospheric spectra from commercial aircraft data

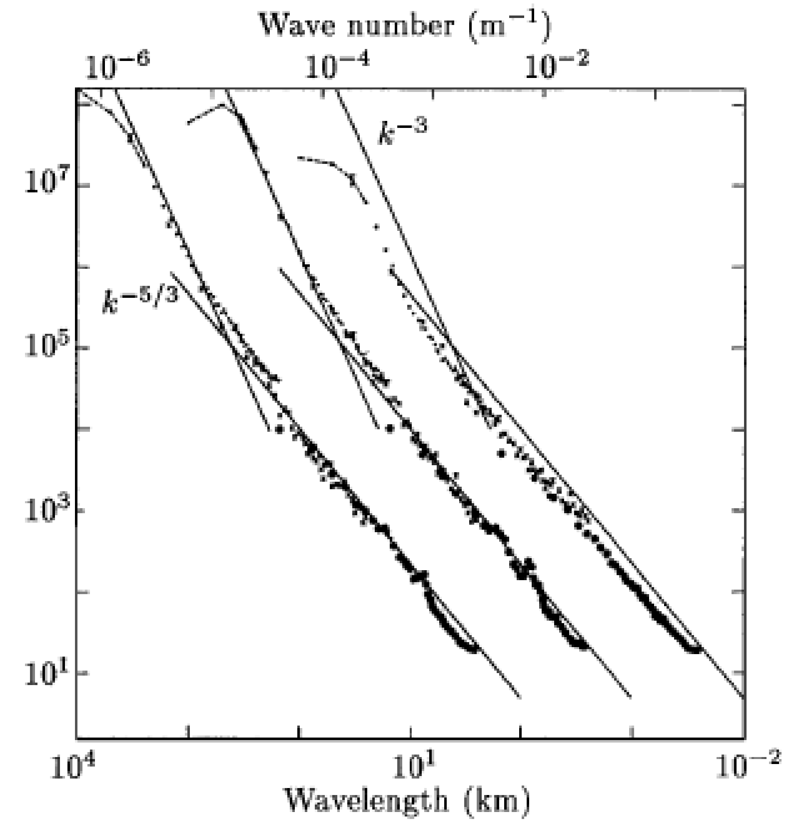

FIG. 1. From left to right: variance power spectra of zonal wind, meridional wind ($m^3 s^{-2}$), and potential temperature (K^2 m) near the tropopause from Global Atmospheric Sampling Program aircraft data. The spectra for meridional wind and temperature are shifted one and two decades to the right, respectively. Reproduced from [7].

Nastrom & Gage, J. Atmos. Sci., 1985

Dispersion of atmospheric tracers.
EOLE balloon experiment.

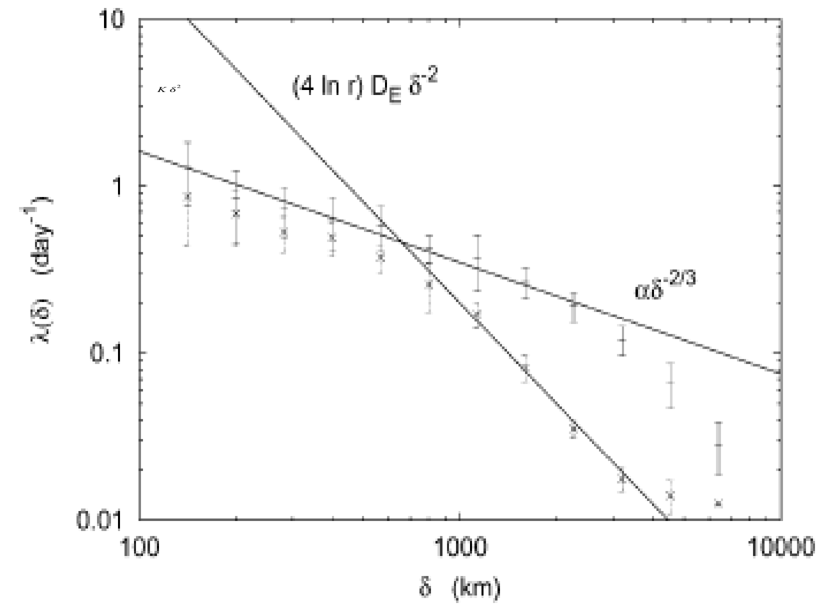

FIG. 5. FSLE of the balloon pairs, (–) describing total and (×) meridional dispersion, with initial 100-km threshold. The meridional FSLE is λ_{mer} defined in Eq. (2.7). The meridional eddy diffusion coefficient is $D_E \simeq 1.5 \times 10^6$ m^2 s^{-1}.

Lacorata et al., J. Atmos. Sci., 1984

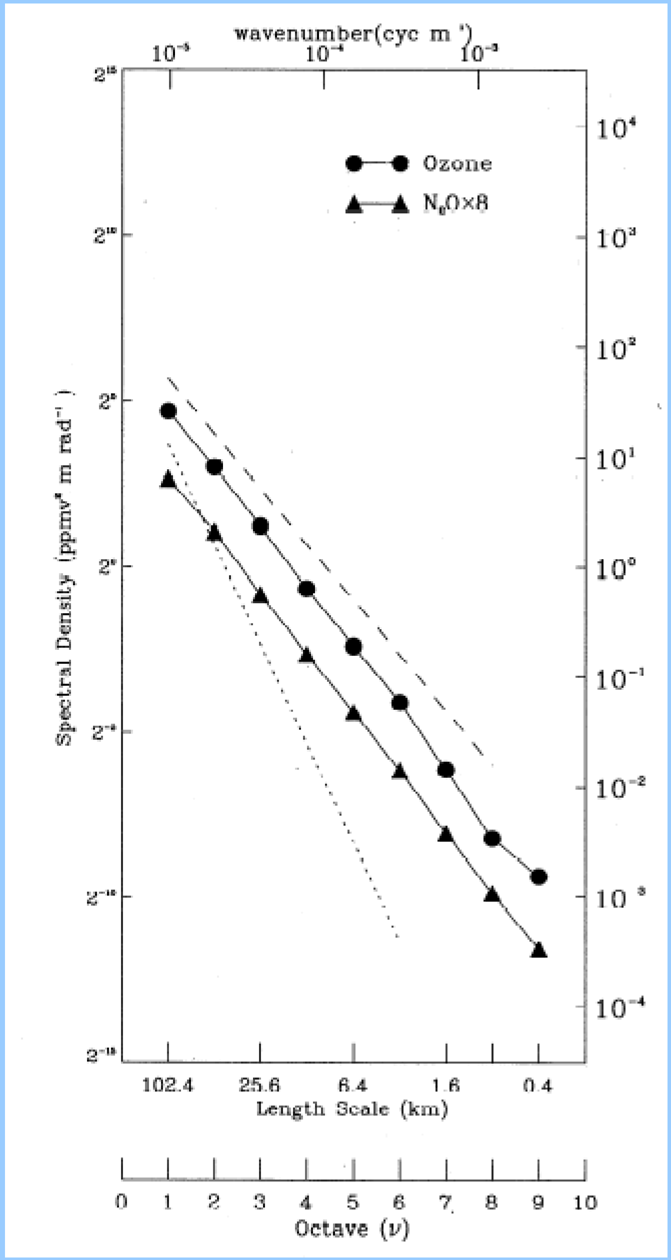

Figure 7. Log-averaged DWT power spectra of ozone and N_2O mixing ratio variance. Log averages are taken over the entire set of available 1024 s spectra of each quantity. Solid circles show log-averaged spectrum of ozone mixing ratio variance. Solid triangles show N_2O variance. Mixing ratios N_2O were arbitrarily multiplied by 8 to make them comparable to ozone mixing ratios. Short dashed line shows −3 slope. Long dashed line shows −5/3 slope.

Tracer spectra in the lower stratosphere display slope of about -1.7 that can be explained by a combination of isentropic advection and diffusion.

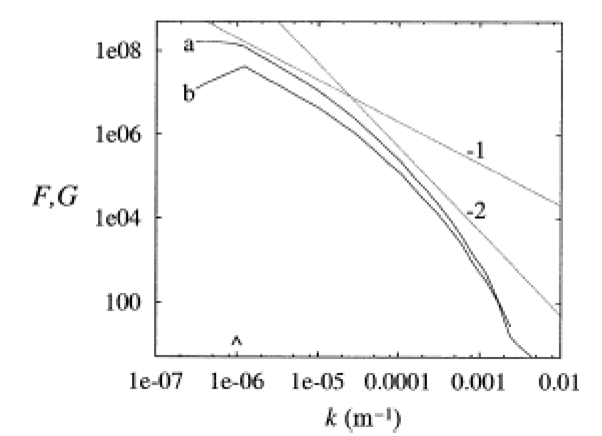

FIG. 8. Comparison between (a) 1D spectrum $G(k)$ and (b) 2D isotropic spectrum $F(k)$ obtained after 30 days with $\kappa = 10^{-2}$ m² s⁻¹.

Bacmeister et al., JGR, 1996

ER2 data

Haynes & Vanneste, JAS, 2004

theory

Deformation of a tracer blob by 2D turbulent flow

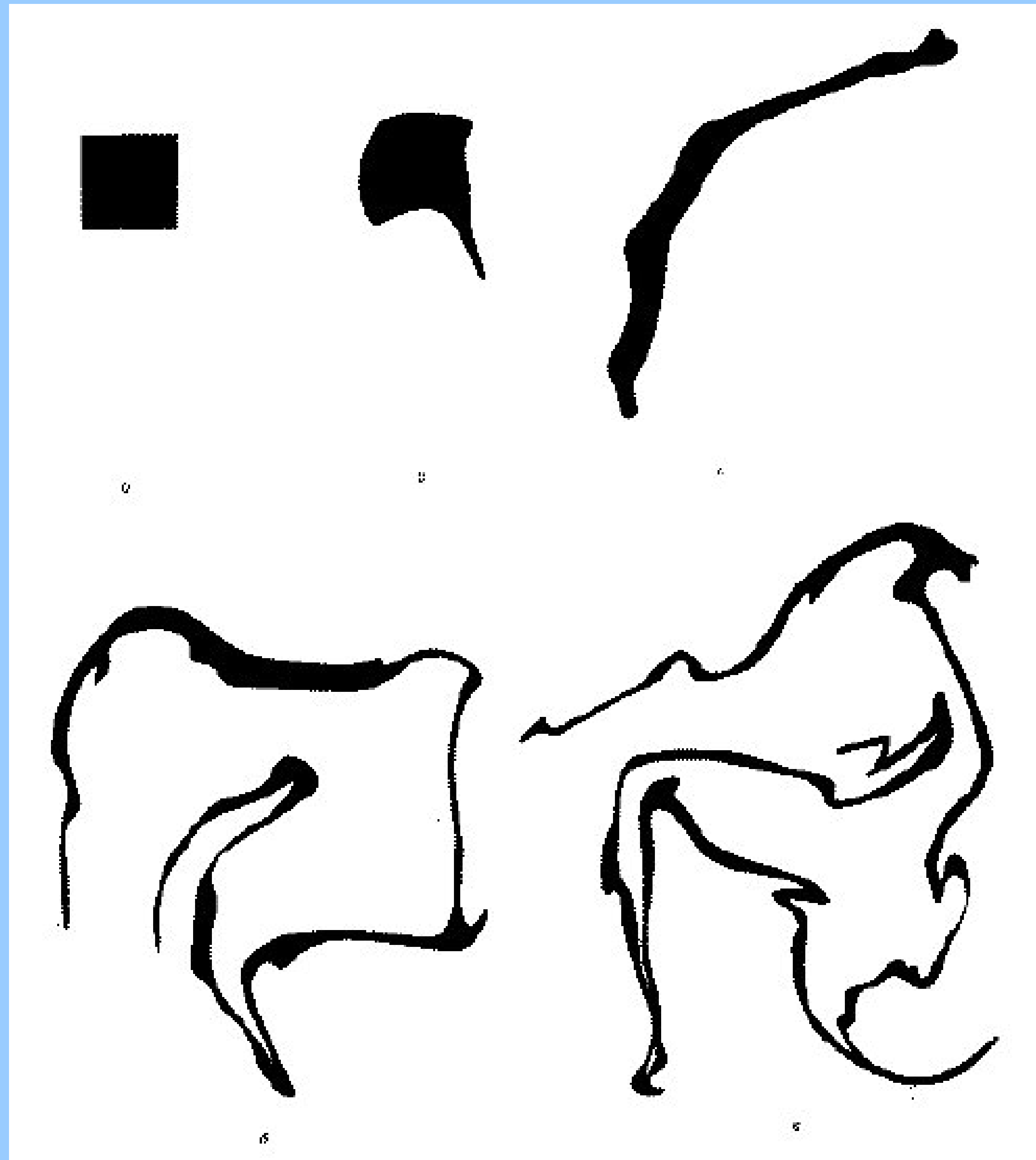

Efficient stirring is performed by a periodic flow

Trajectories may be chaotic in 2D for a periodic flow, in 3D for a stationary flow.

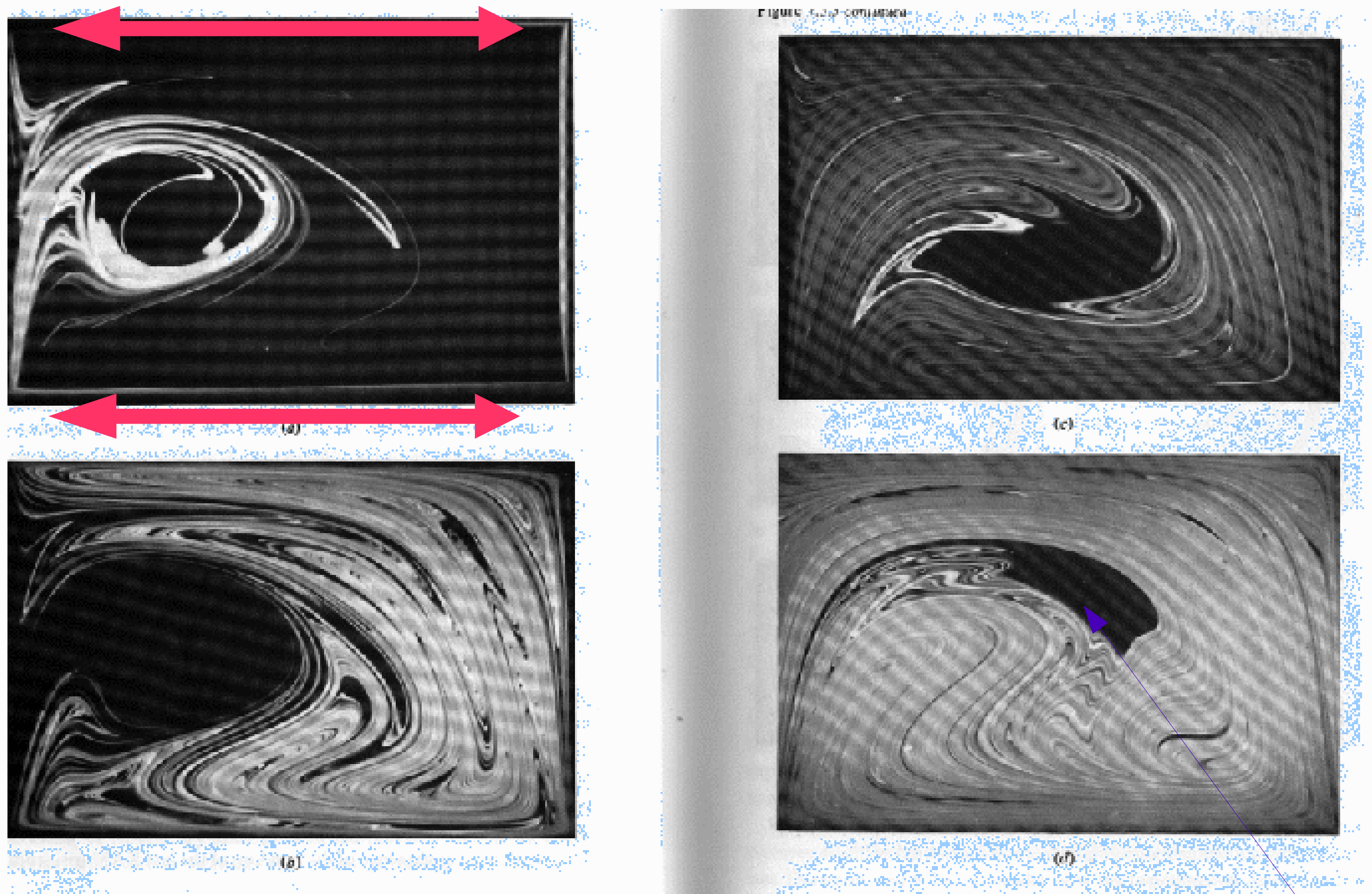

J.M. Ottino, The kinematics of mixing: stretching, chaos, and transport (Cambridge, 1989)

Lyapunov exponent

Evolution equations for a line element and the passive scalar gradient in the absence of diffusion and source are very similar since $\nabla\theta\cdot\mathbf{x}=\delta\theta$ is preserved

$$\frac{D}{Dt}\delta x_i=\frac{\partial u_i}{\partial x_j}\delta x_j \qquad\qquad \frac{D}{Dt}\frac{\partial\theta}{\partial x_i}=\frac{-\partial u_j}{\partial x_i}\frac{\partial\theta}{\partial x_j}$$

$$\left(\frac{D}{Dt}\text{ time derivation along a given trajectory }\mathbf{x}(t)\right)$$

Over a time interval $[t_{0,}t_0+\tau]$:

$$\delta\mathbf{x}(t_0+\tau)=\mathbf{M}(t_{0,}t_0+\tau)\,\delta\mathbf{x}(t_0) \qquad \nabla\theta(t_0+\tau)=-\mathbf{M}^T(t_{0,}t_0+\tau)\,\nabla\theta(t_0)$$

Finite-time Lyapunov exponent

$$\lambda(\tau,\mathbf{x}(t_0))=\frac{1}{\tau}\ln\frac{|\mathbf{M}\,\delta\mathbf{x}|}{|\delta\mathbf{x}|}=\frac{1}{\tau}\ln\frac{|\mathbf{M}^T\nabla\theta|}{|\nabla\theta|}$$

At large τ, if the flow is ergodic, $\lambda(\tau,\mathbf{x}(t_0))$ tends to a unique $\bar{\lambda}$.
At intermediate τ, λ exhibits large spatial and temporal variations.

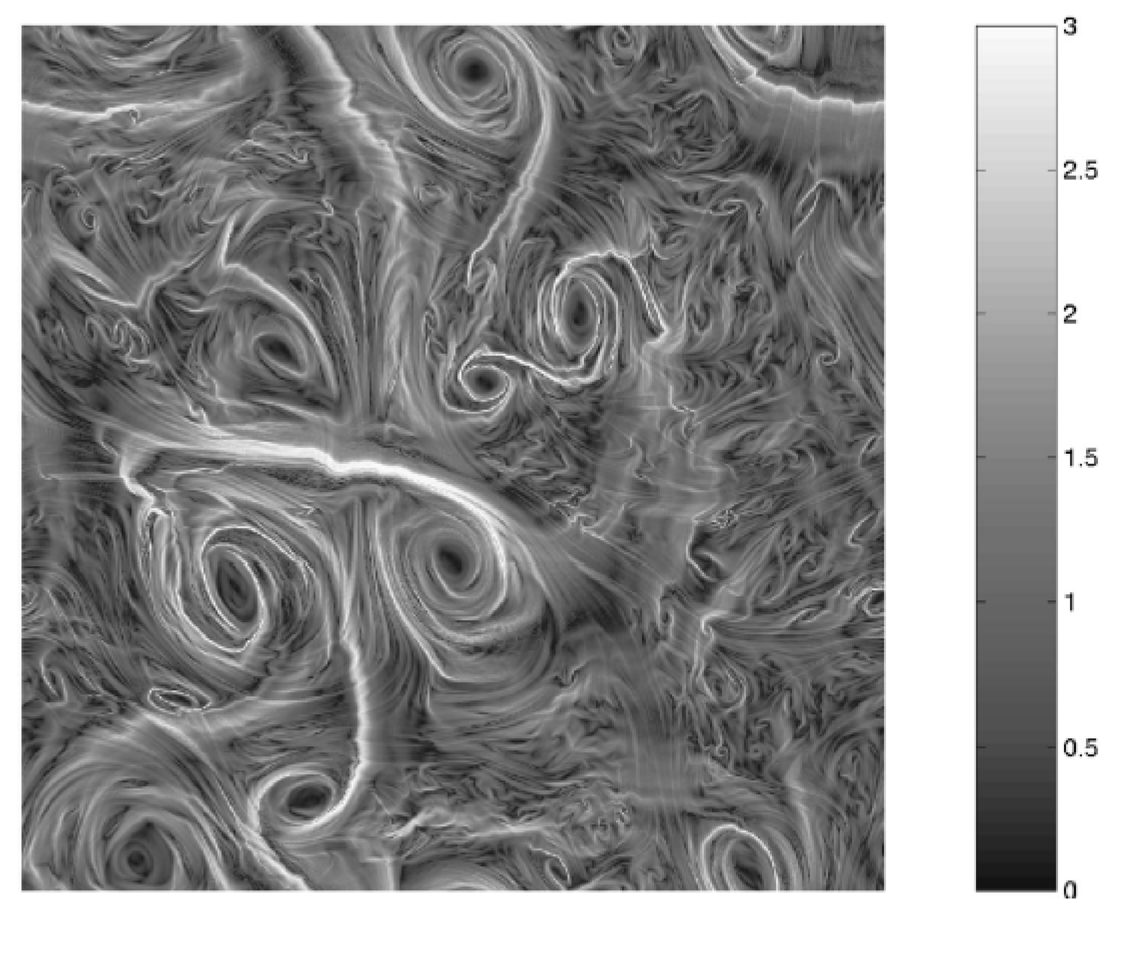

Local Lyapunov exponent in a two dimensional flow

Evolution of a tracer blob under the combined action of stretching and diffusion

l_0

Advection
diffusion

over duration τ

$l_d \approx \sqrt{\frac{\kappa}{\lambda}}$

Length $L \sim l_0 \, Exp(\lambda\tau)$

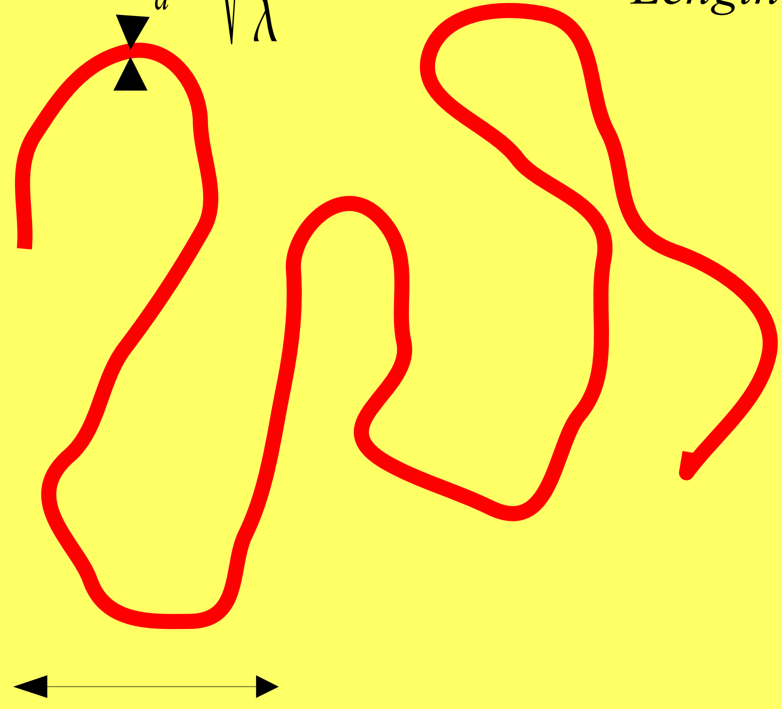

L_s *Characteristic size of sync*
(energetic) advecting structu

Size of the dispersed blob

$R \sim \sqrt{\tau} \; for \; \tau \gg \tau_0 = \bar{\lambda}^{-1} \ln(L_s / l_0)$

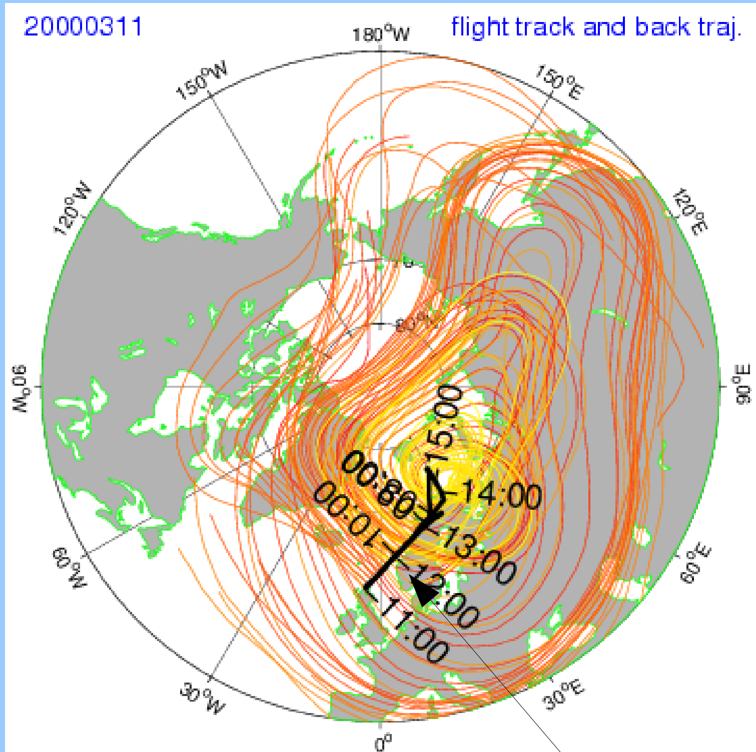

Potential temperature

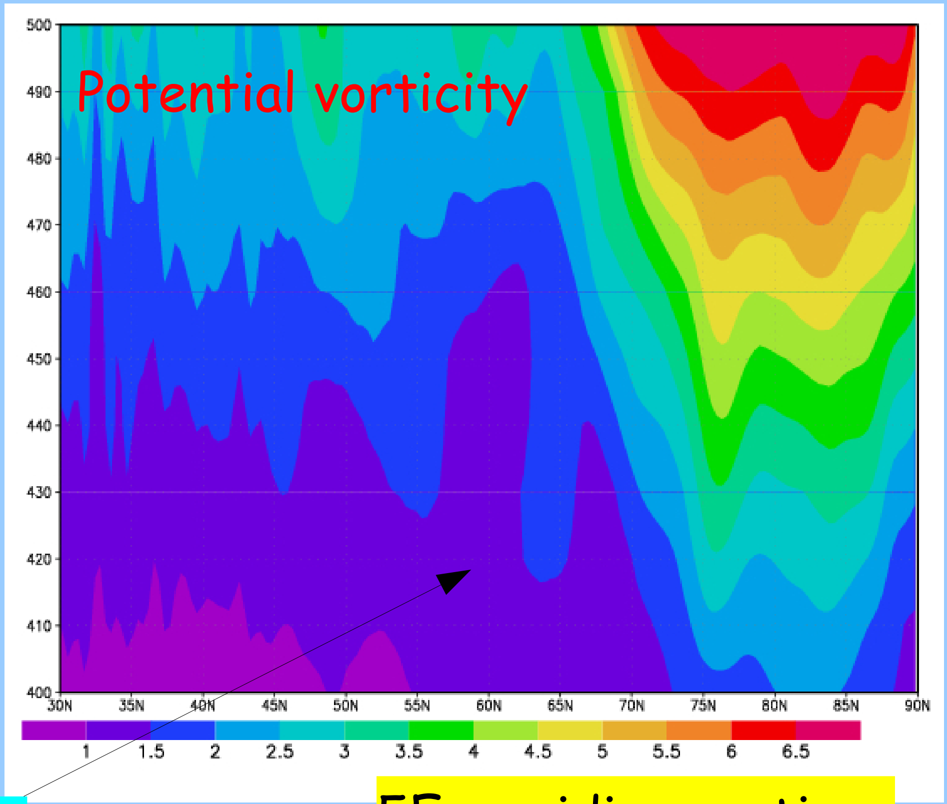

5E meridian section

filament

Filament encounter on 3 March 2000 SOLVE campaign

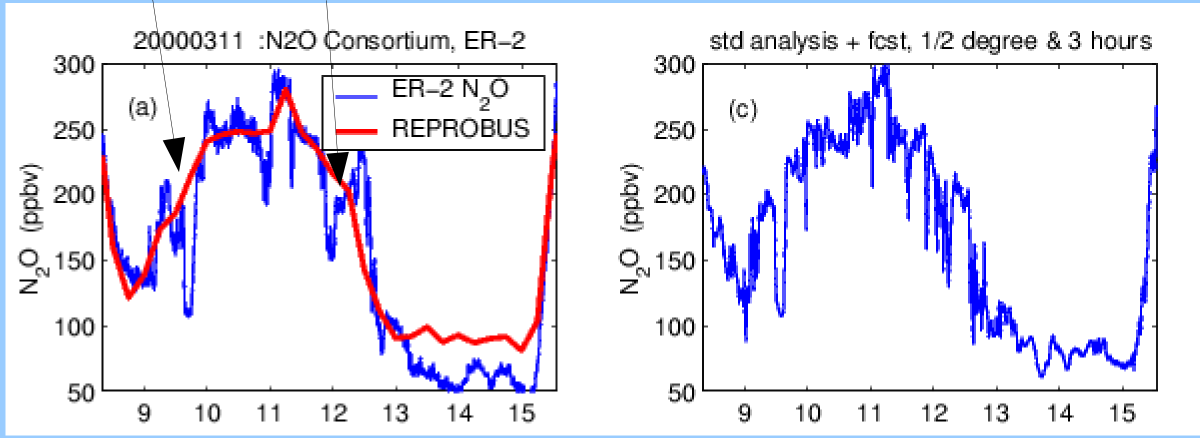

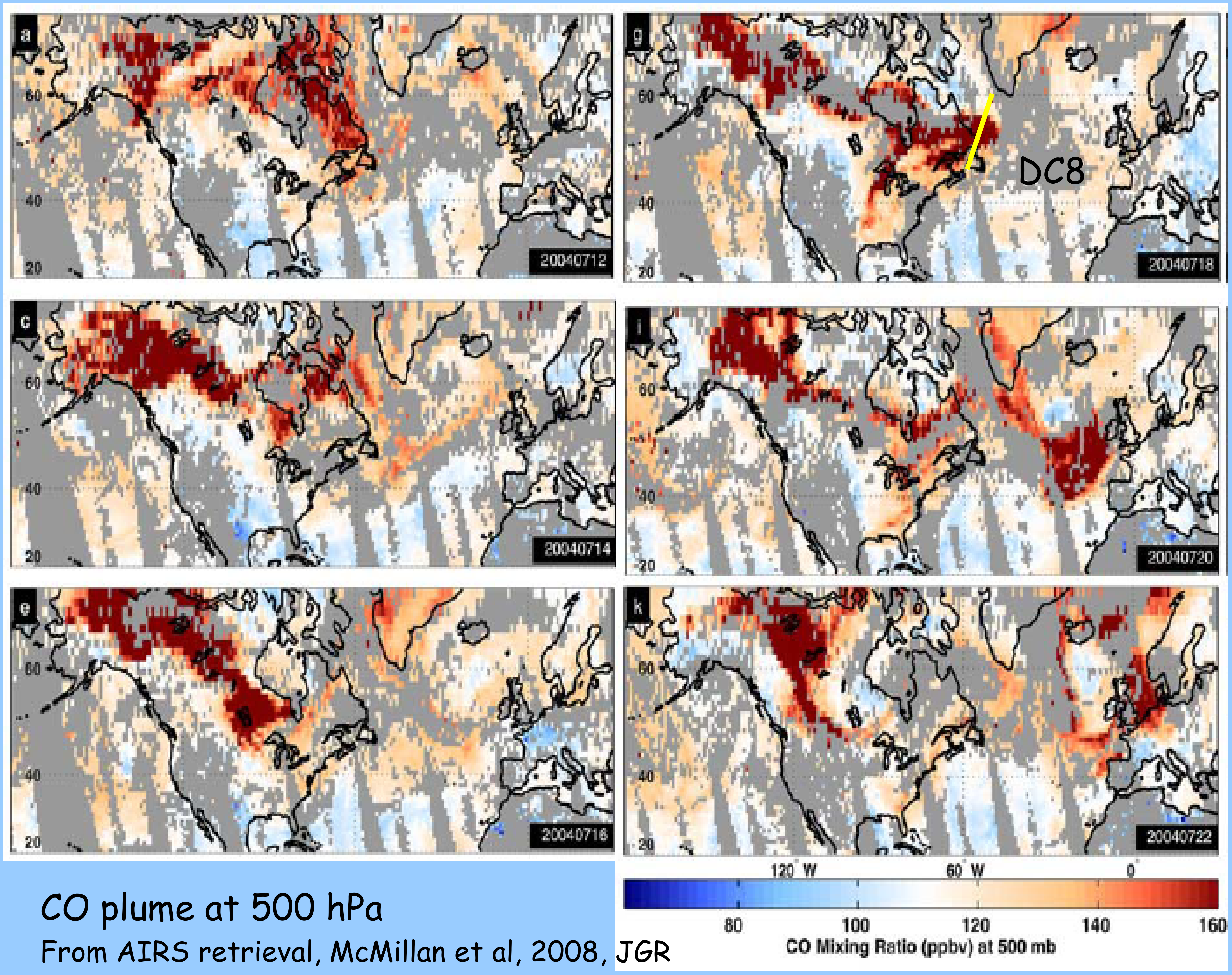

CO plume at 500 hPa

From AIRS retrieval, McMillan et al, 2008, JGR

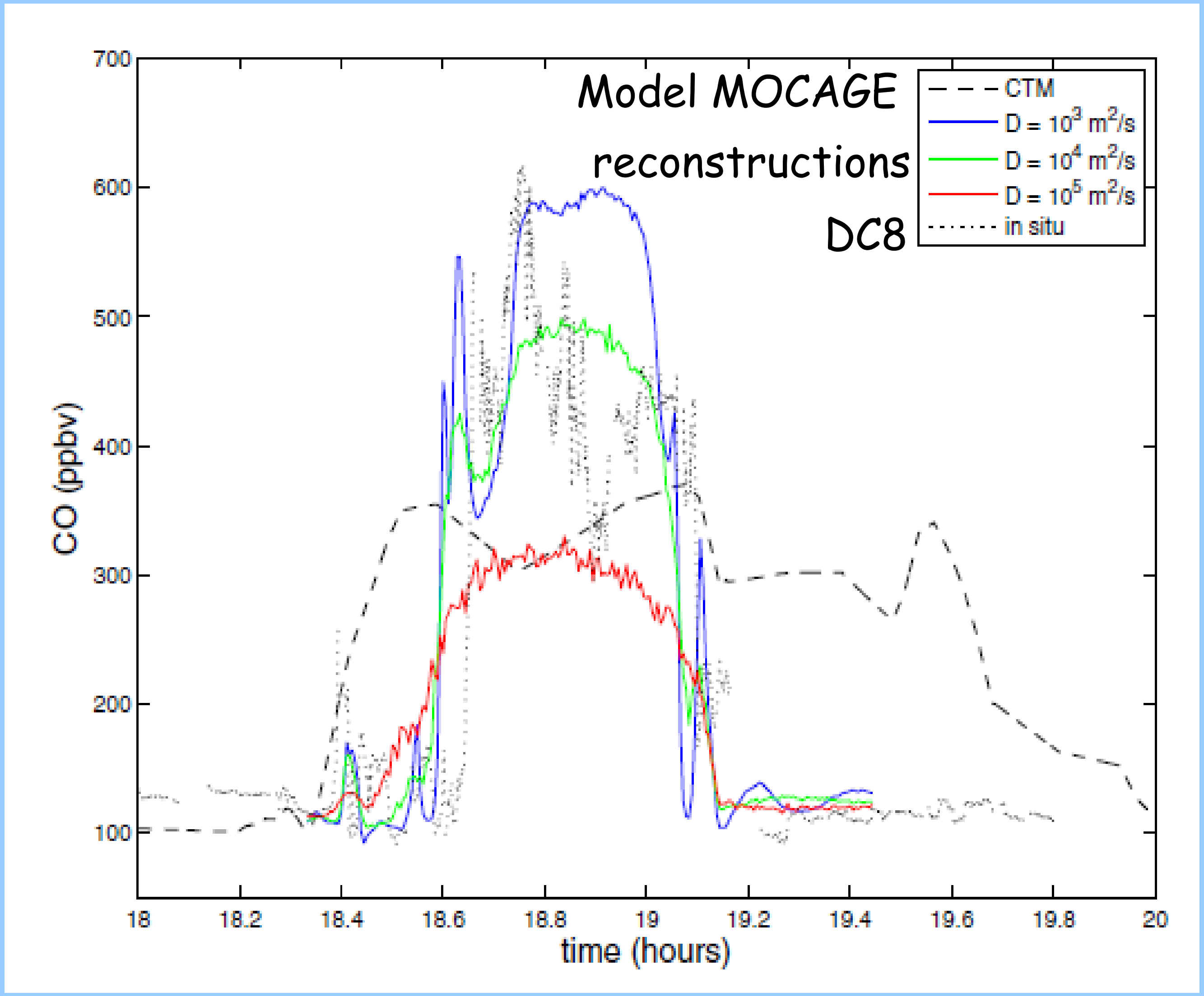

Improvement of CTM MOCAGE by Lagrangian reconstructions

Pisso et al., 2009, JGR

Lagrangian reconstructions
and diffusion

Observations

Reconstructions

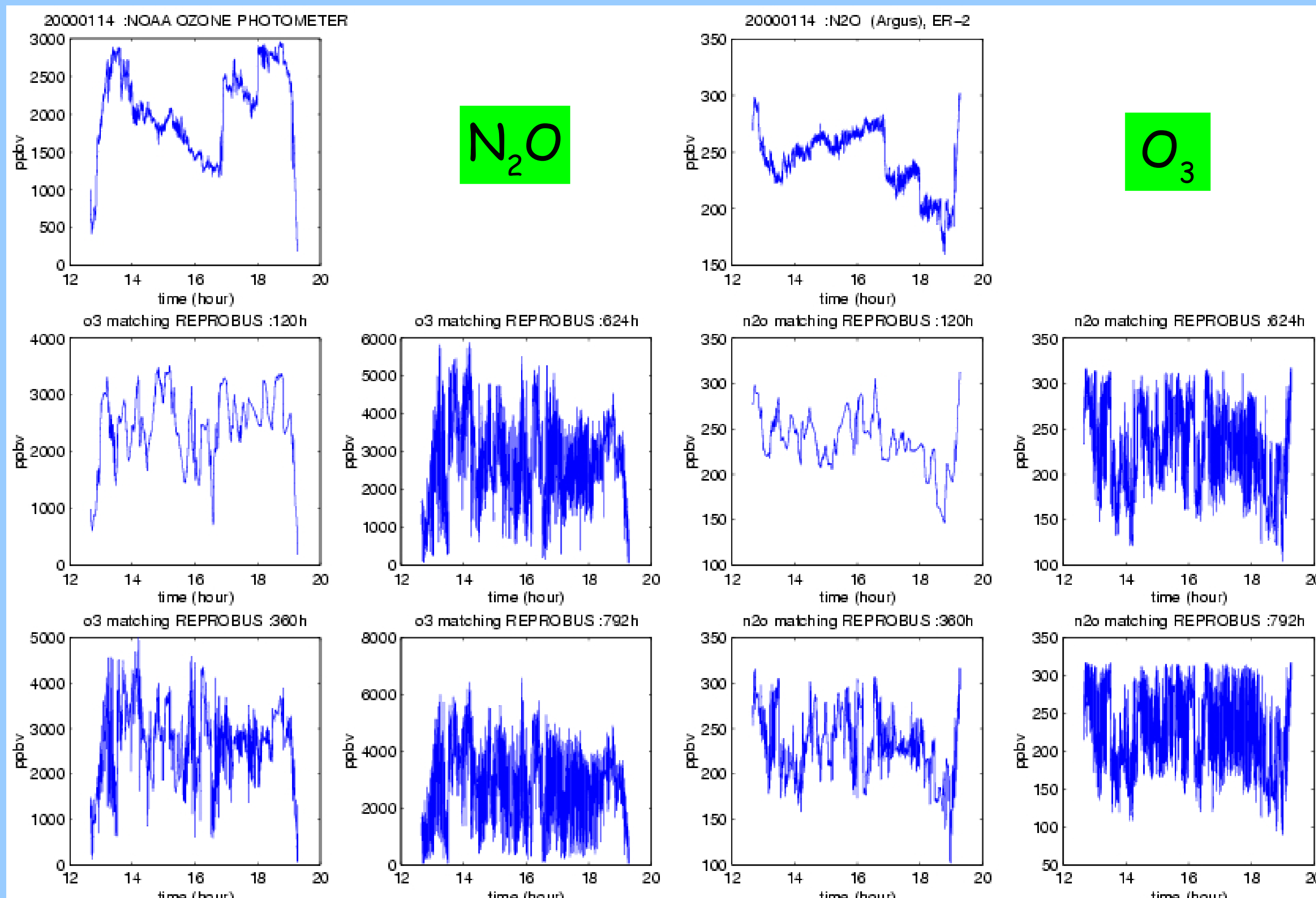

For comparison: deterministic reconstructions for τ = 5, 15, 26 and 33 days

Diffusion and random vertical motion

Let vertical motion be $\delta z = w\,\delta t + \eta\,\delta t$
where η *is a white noise and* δt
is the time step.
Over a large number of time steps,
this is equivalent to a diffusive
process with $D = \frac{1}{2} < \eta^2 > \delta t$.

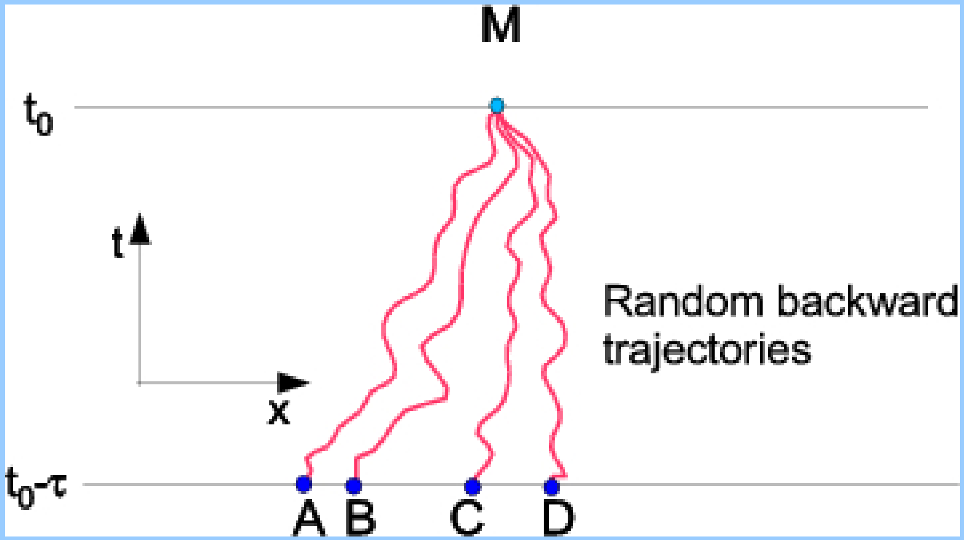

How to estimate Lagrangian diffusivity?

Pure advection (no diffusion) generates a number of spurious laminae which are not observed in the tracer profiles.

D can be estimated by adjusting diffusion until the reconstructed transect exhibits the same *roughness* as the observed transect r when well identified structures are similar.

The advection -diffusion equation

$$\frac{\partial \theta}{\partial t} + u \nabla \theta = \kappa \Delta \theta$$

can be solved as

$$\theta(x,t) = \int \rho(y,s) G(x,t;y,s) \theta(y,s) d^{3y}$$

where G is a Green function solution of

$$\frac{\partial G}{\partial t} + u(x,t) \nabla_x G - \frac{\kappa}{\rho(x,t)} \nabla_x \rho(x,t) \nabla_x G = \frac{1}{\rho(y,s)} \delta(t-s) \delta(y-s) \quad (1)$$

or

$$\frac{\partial G}{\partial s} + u(y,s) \nabla_y G + \frac{\kappa}{\rho(y,s)} \nabla_y \rho(y,s) \nabla_y G = \frac{1}{\rho(x,t)} \delta(t-s) \delta(y-s) \quad (2)$$

The Green function of the advection-diffusion equation describes the probability of transit of a particle from (y,s) to (x,t).
The statistical average of mixing ration over random backward trajectories is equivalent to solving (2).

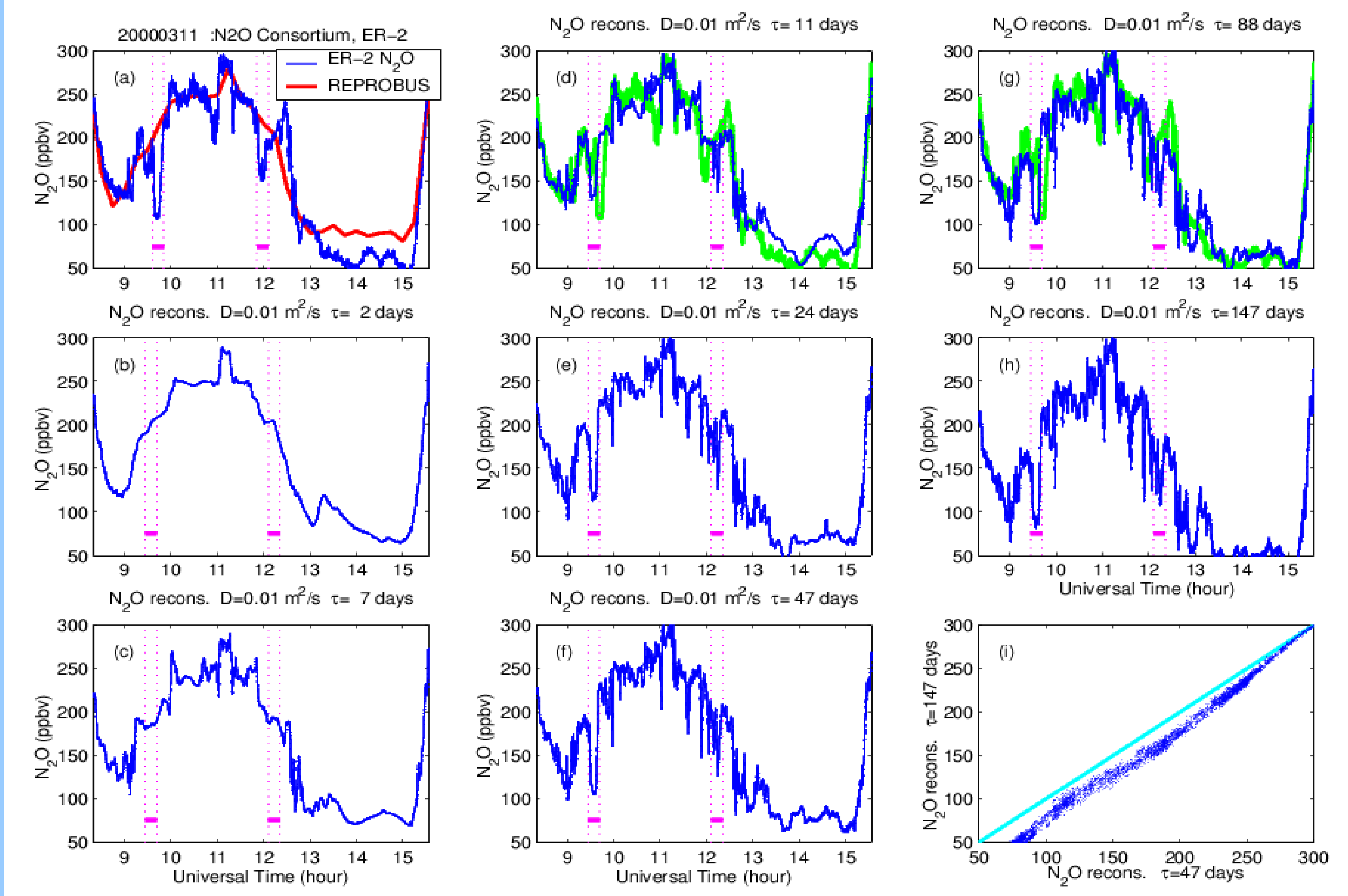

Tracer N_2O

Convergence of diffusive reconstructions

Reactive O_3

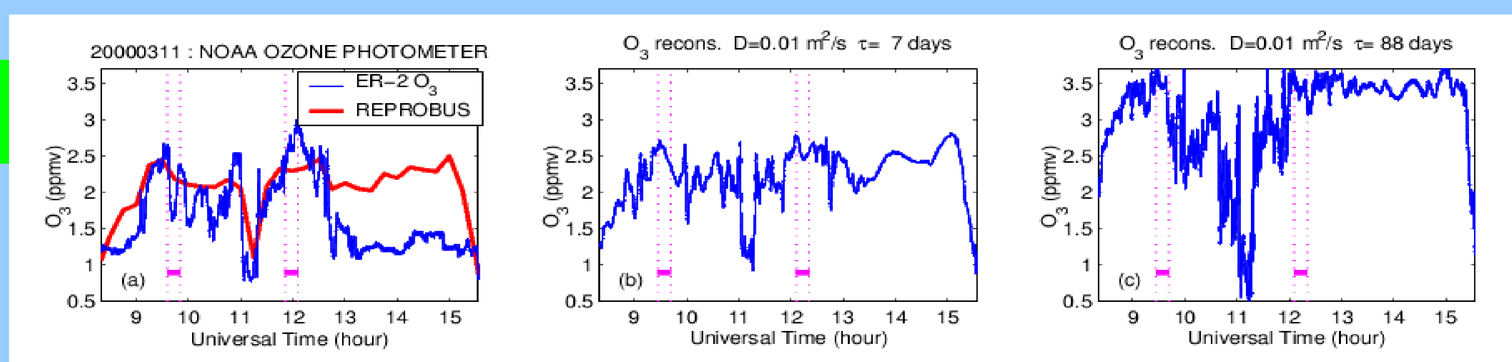

Local variations of Lagrangian turbulent diffusion

Filament width 100km
right edge 36 km
left edge 2.5 km

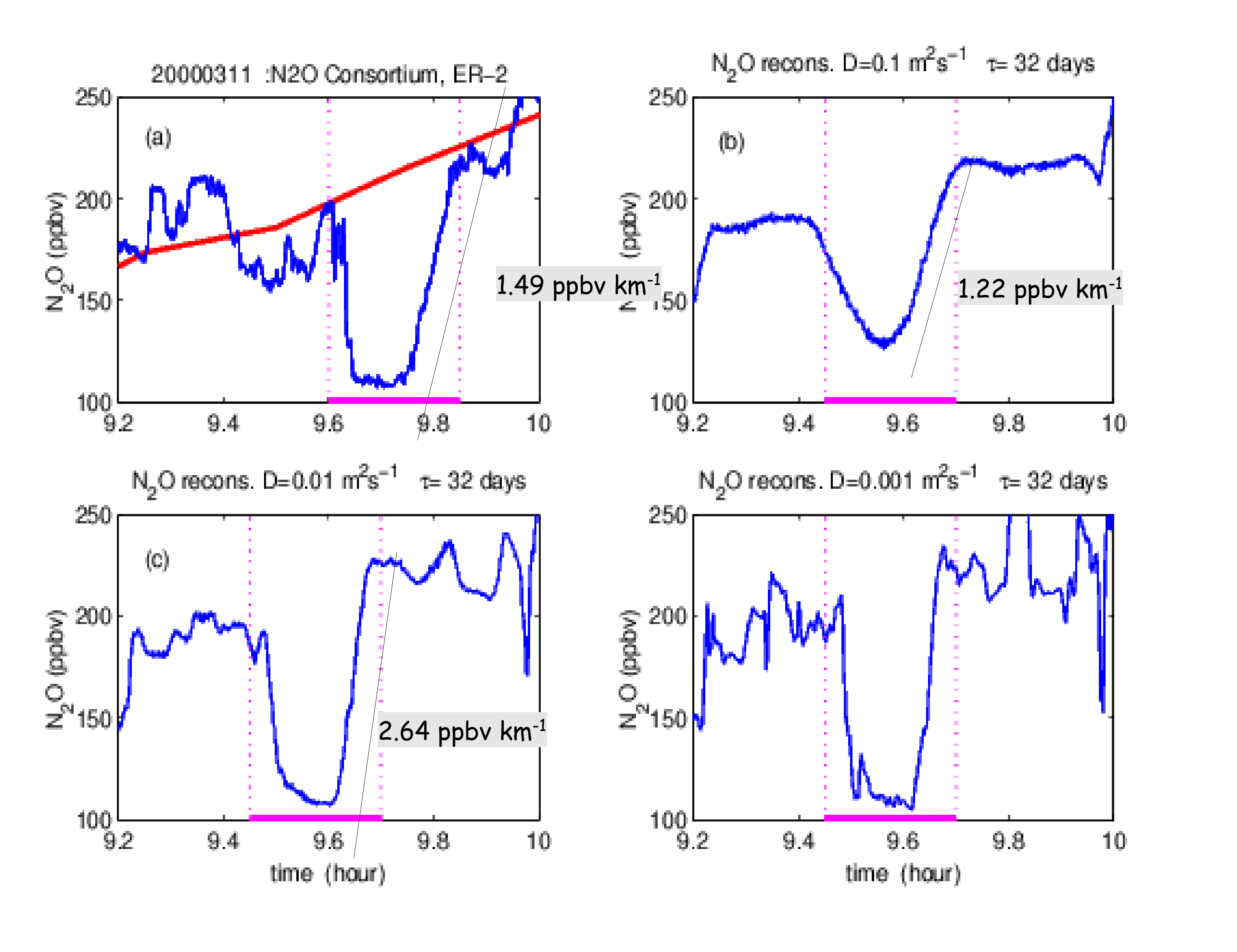

Legras et al., ACP, 2005

Vertical mixing versus horizontal stirring

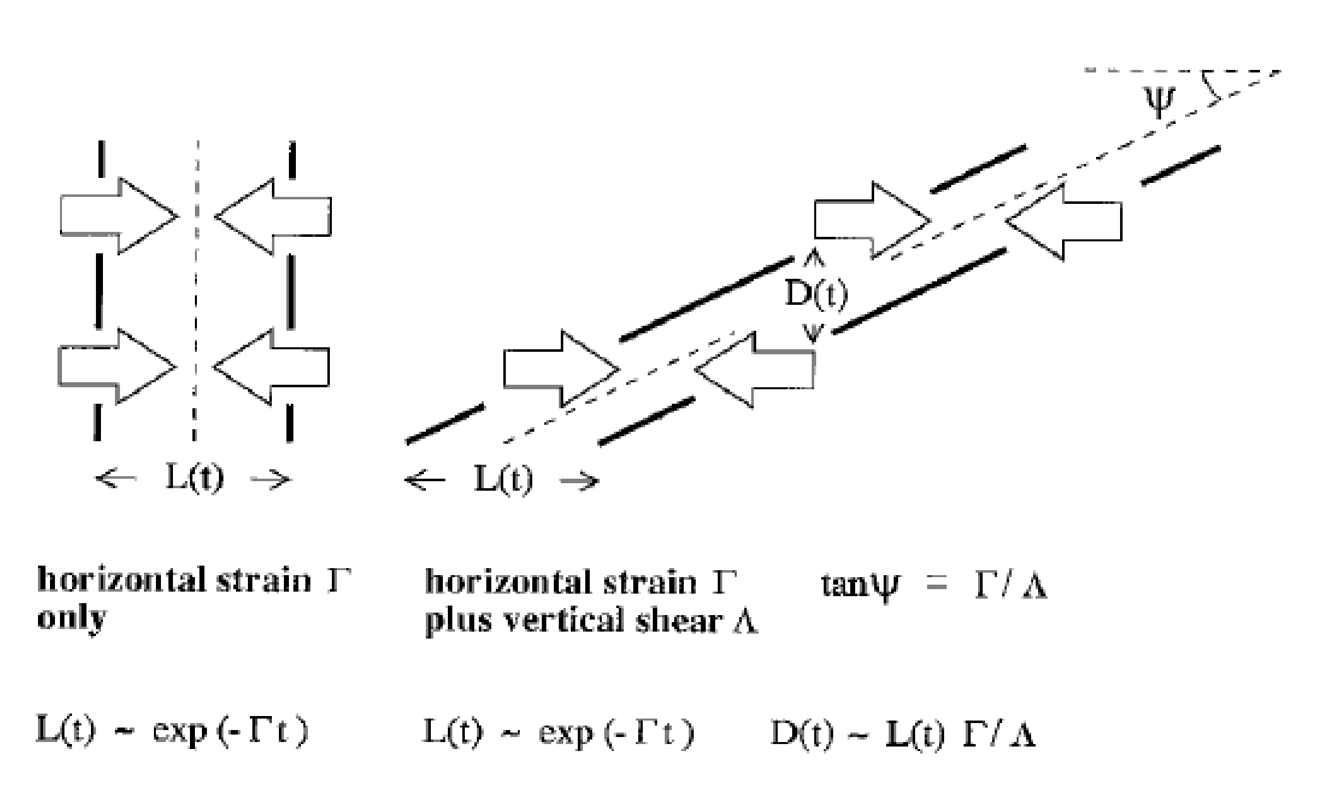

Haynes & Anglade, JAS, 1997

Building sloping sheets by combining vertical shear Λ and horizontal strain Γ. In the lower stratosphere: Λ / Γ≈ 250. This is in good agreement with observations of tracer sheet aspect ratios.
Lower aspect ratios (O(50)) are observed for tropopause folds near jet streams but still the aspect ratio is large.

Due to the high aspect artio (1 km in the horizontal ⇔ 4 m in the verical) aircraft measurements have generally much higher equivalent resolution than balloon soundings.

Intermediate Summary

Basic facts about transport and mixing in the non convective atmosphere

- Quasi-layerwise motion generates a large amount of small-scale sheets by advection seen as filaments in 2D maps and laminae in profiles or transects.
- Advection is dominated by structures in the wind field that are of sufficiently large scale to be resolved by operational analysis $\Rightarrow$ chaotic folding and stretching.
- Slow vertical motion.
- Laminae in the tracers are observed by in situ instruments at scales unresolved by NWP models.
- Sheets are sloping with an aspect ratio determined by the ratio between vertical shear and horizontal strain, $\approx$ 250 (Haynes & Anglade, 1997) in the lower stratosphere (1 km in the horizontal $\Leftrightarrow$ 4 m in the vertical). *As a result aircraft measurements have generally much higher equivalent resolution than standard balloon soundings.*
- Sheet thickness is bounded by 3D unresolved turbulence that is primarily acting as vertical mixing.

Quasi-Lagrangian numerical methods

A number of numerical methods have been introduced to preserve flow invariants better than finite-difference or spectral methods. Most of them are in the family of finite-volume or ENO (essentially non oscillating) methods.

CLAMS numerical advection scheme

Regridding is applied locally where the Lyapunov exponent exceeds some threshold

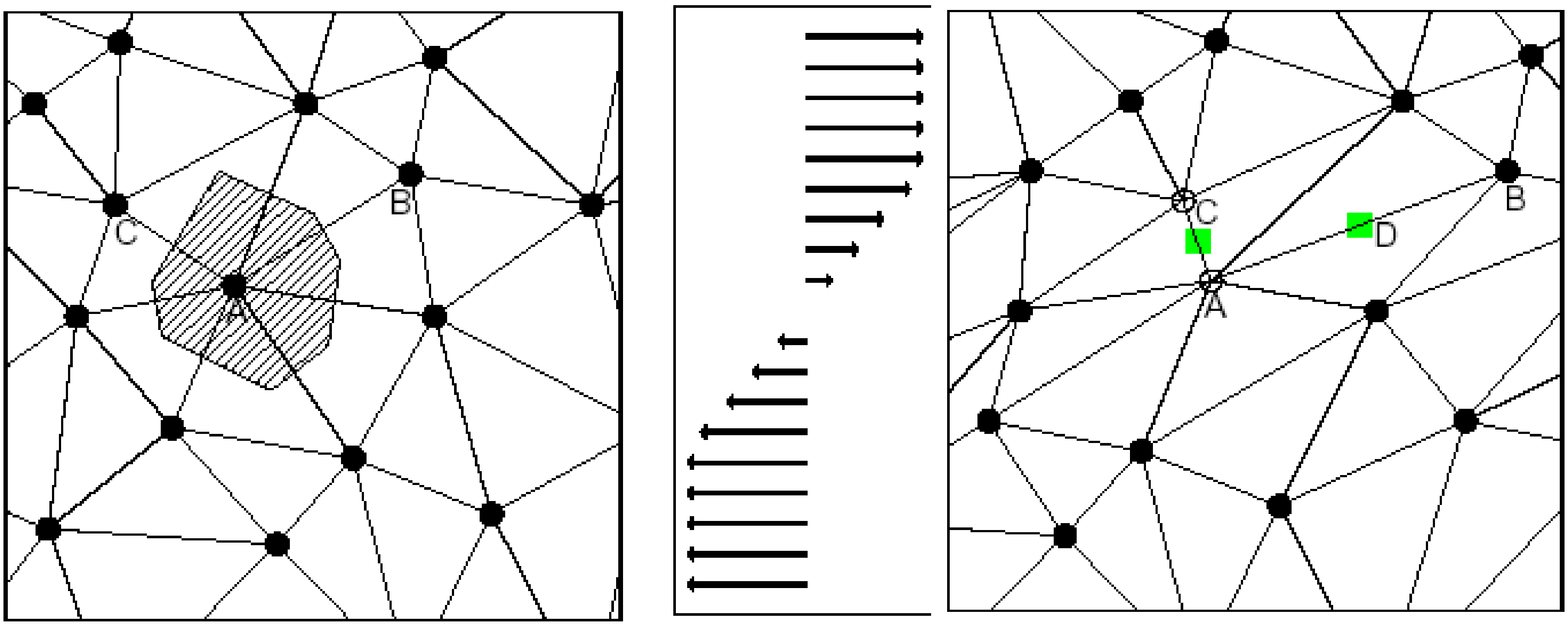

quasiuniform distribution of air parcels
Delaunay triangulation $\Rightarrow$
next neighbors

sheared flow
$\Delta t = 6 - 24$
hours

grid adaptation =
regridding of the deformed grid
$\Rightarrow$ new air parcels
$\Rightarrow$ interpolations (num. diffusion)
$\Rightarrow$ mixing

Mc Kenna et al., 2002, JGR, 107, 2000JD000114;
Konopka et al., 2004, JGR, 109, 2003JD003792

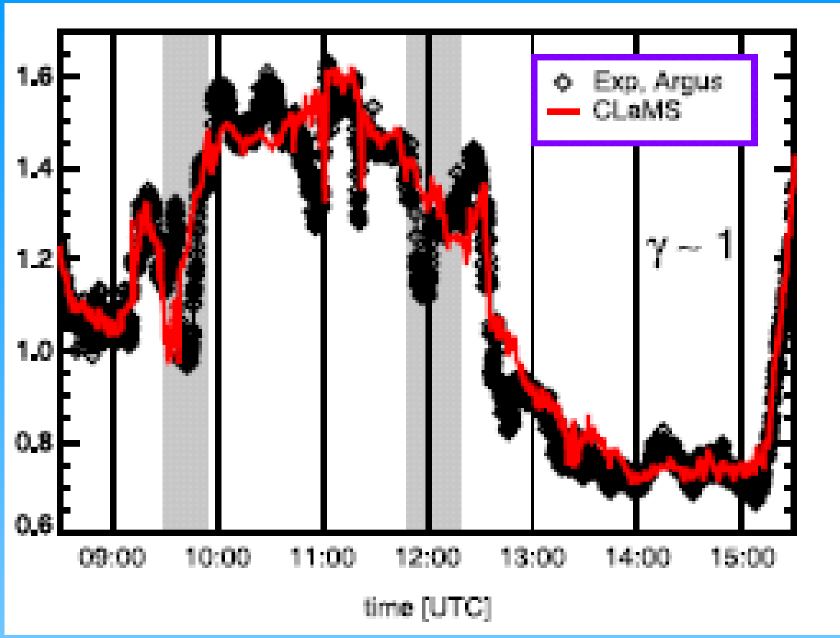

CLAMS results
for SOLVE campaign

Argus CH4 versus
CLAMS

Konopka et al.,
2004, JGR, 109,
2003JD003792

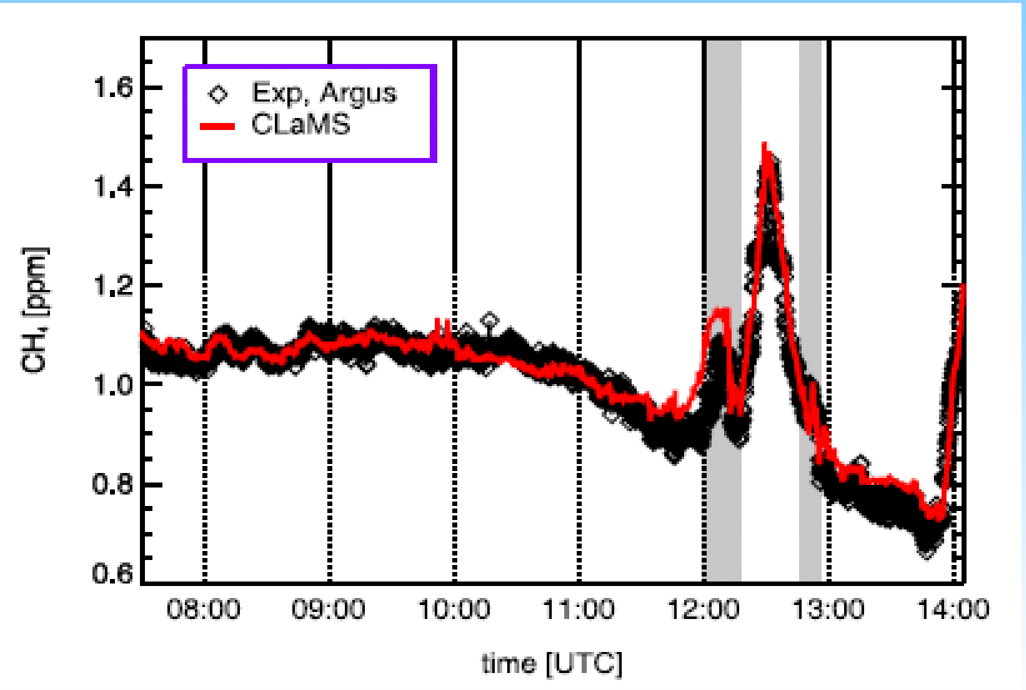

Transport barriers

I isentropic transport barriers

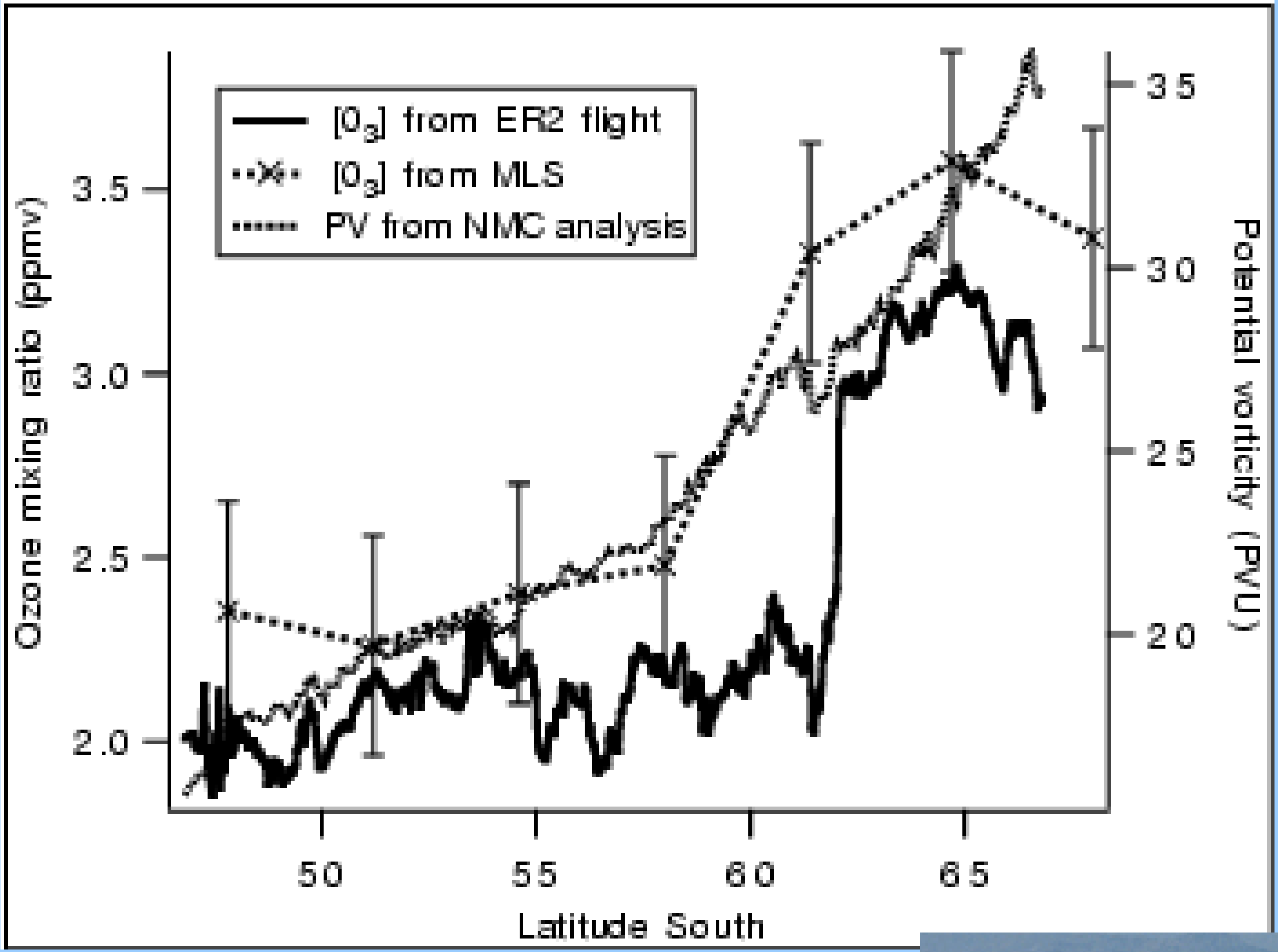

NASA ER-2 transect
across the edge of the
Antarctic polar vortex

sharp transition over a few km

Vortex erosion submitted to an external shear
Generation of filamenst and gradients on its periphery

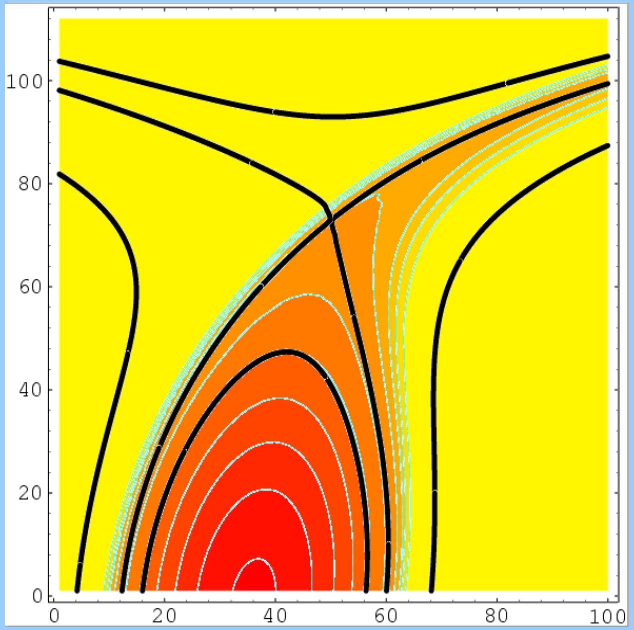

Streamfunction and vorticity chart (vorticity can ne replaced by a passive tracer)
Case of slow erosion

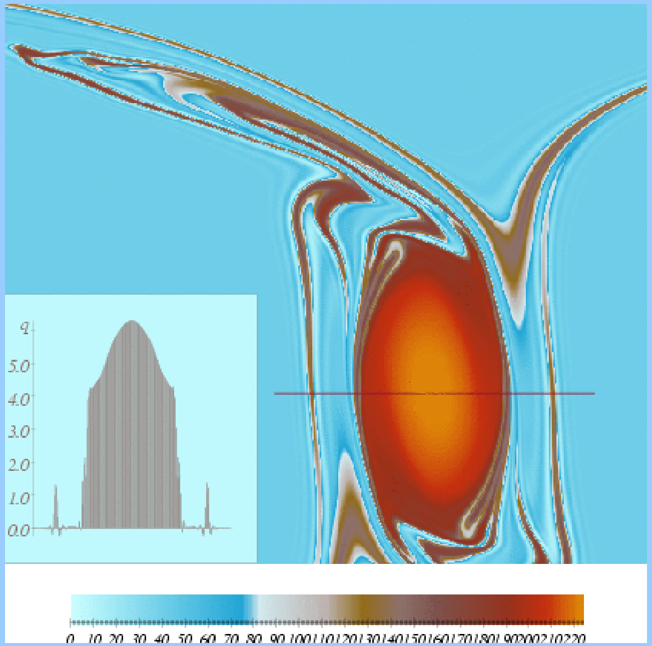

Vorticity chart and transverse section.
Case of fast erosion.

Chart of the polar Antarctic vortex. PV and stretching line maxima (Lyapunov) (backward and forward).

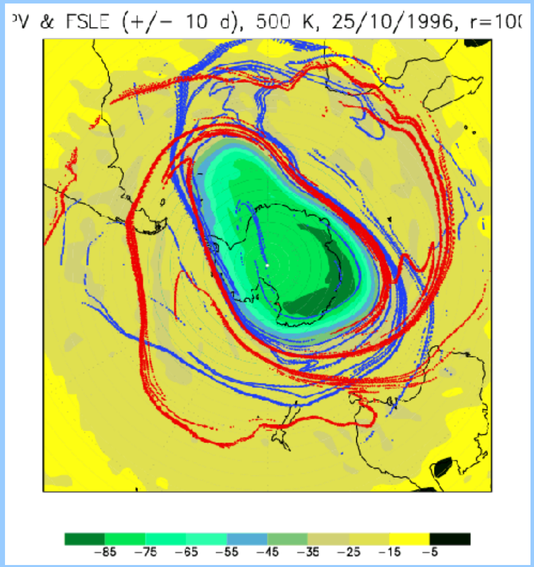

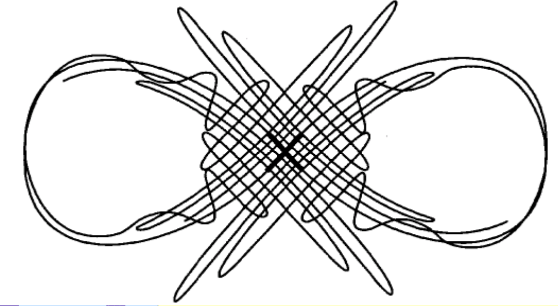

Stretching rate - Lyapunov exponent

Over a time interval $[t_{0}, t_0+\tau]$: $\delta\mathbf{x}(t_0+\tau)=\mathbf{M}(t_{0},t_0+\tau)\,\delta\mathbf{x}(t_0)$ $\nabla\theta(t_0+\tau)=-\mathbf{M}^T(t_{0},t_0+\tau)\,\nabla\theta(t_0)$

Finite-time Lyapunov exponent $\lambda(\tau,\mathbf{x}(t_0))=\frac{1}{\tau}\ln\frac{|\mathbf{M}\,\delta\mathbf{x}|}{|\delta\mathbf{x}|}=\frac{1}{\tau}\ln\frac{|\mathbf{M}^T\nabla\theta|}{|\nabla\theta|}$

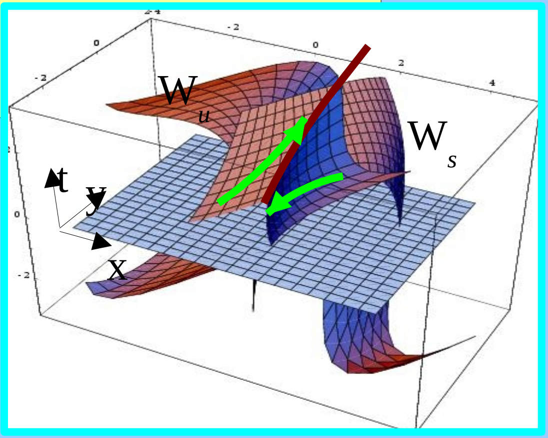

- Finite-time (FTLE) or finite-size (FSLE) Lyapunov exponent measures stretching experienced by a parcel during a time interval.
- Pro: Easily calculated and physically sound. Standard tool in the theory of dynamical systems. Not limited to 2D. Provides maps of dynamical barriers.
- Con: Complicated patterns when short lived structures. Is usually dominated by shear and hence is not a measure of mixing for distributed tracer. Does not correlate with effective diffusivity

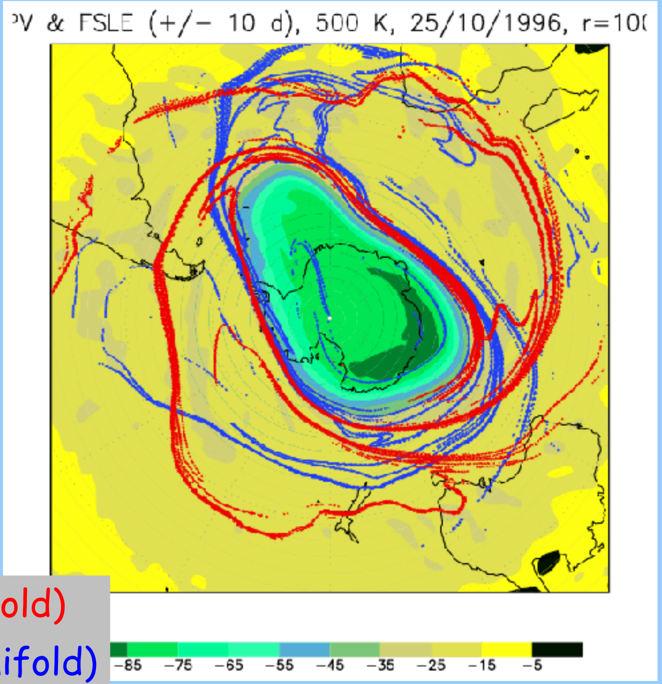

Red: large forward Lyapunov <=> unstable (past) material line (manifold)

Blue: large backward Lyapunov <=> stable (future) material line (manifold)

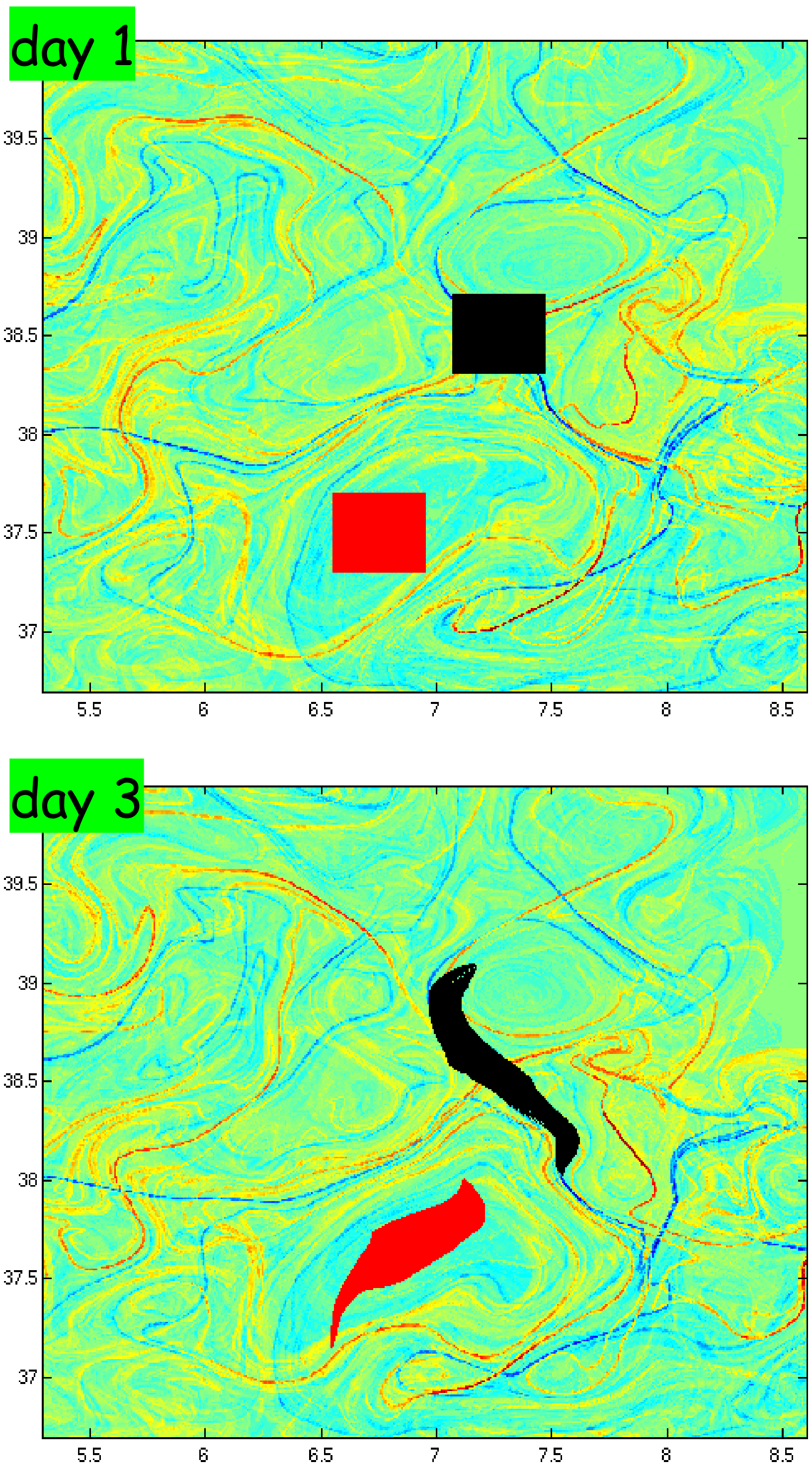

Courtesy of F. d'Ovidio

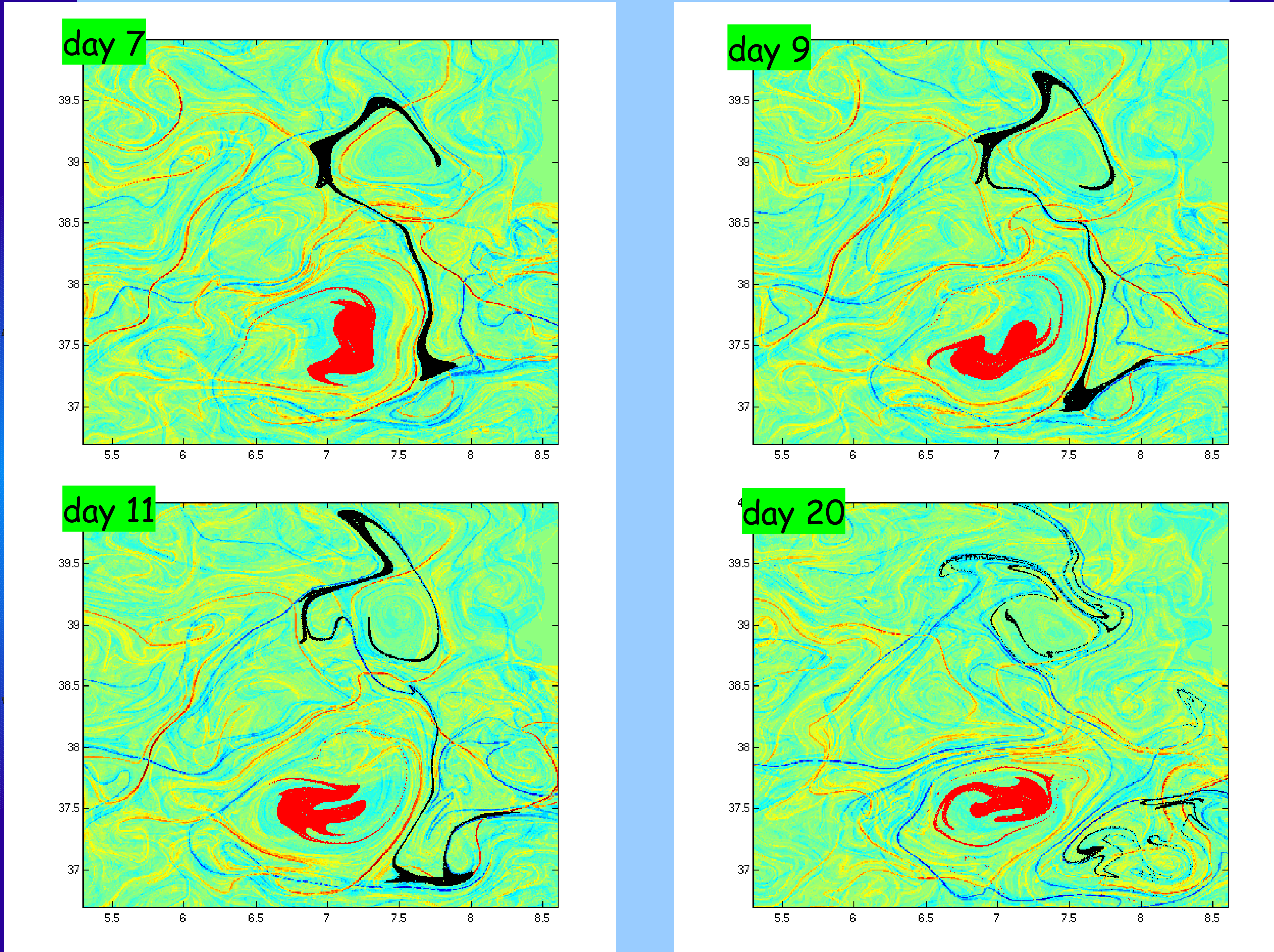
day 7
day 9
day 11
day 20
39.5
39
38.5
38
37.5
37
5.5
6
6.5
7
7.5
8
8.5

Intersection of stable and unstable material lines: hyperbolic trajectories

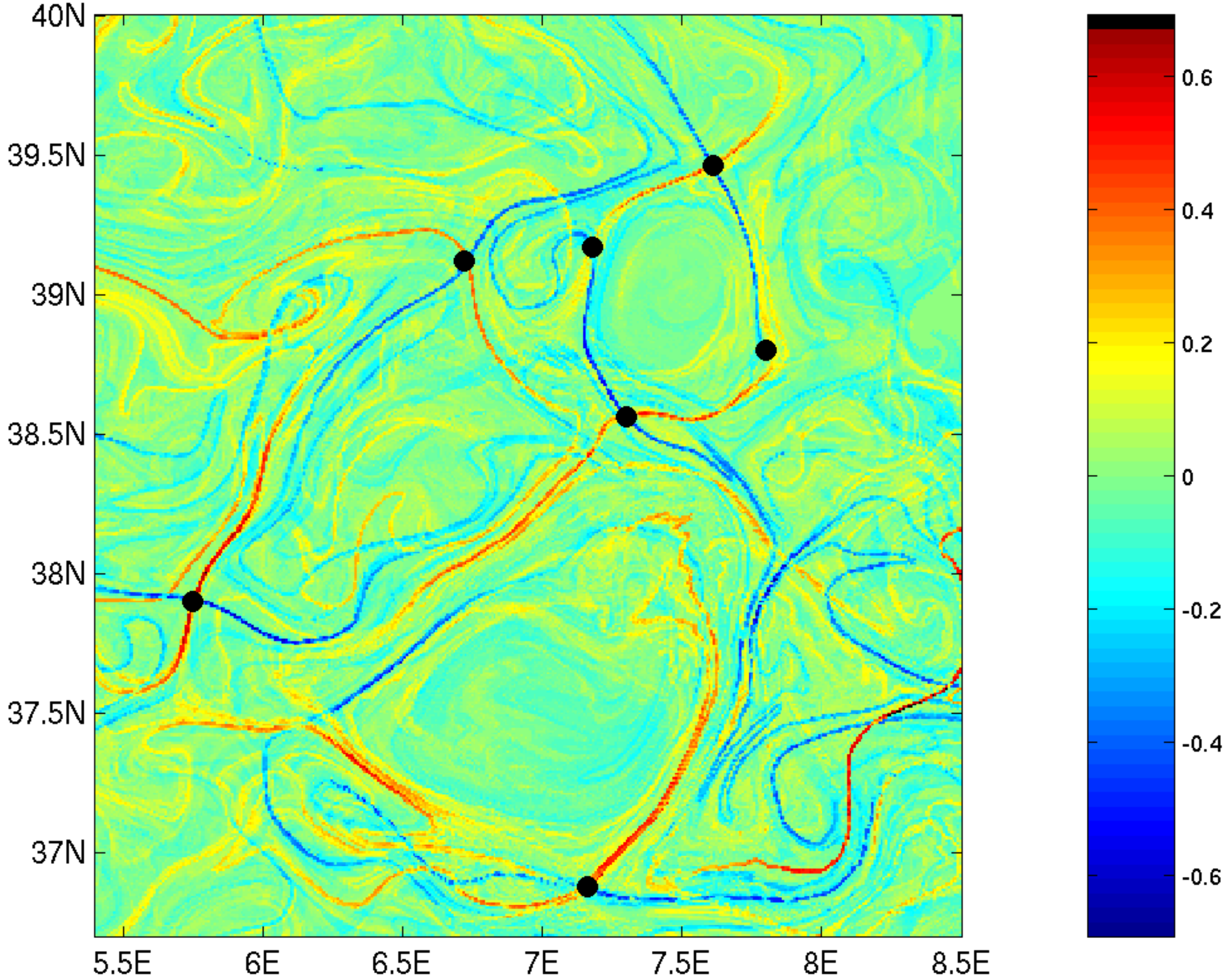

Effective diffusivity in practice

$$K_{\text{eff}}(A,t) = \frac{\partial A}{\partial C} \oint_{\gamma(C,t)} \kappa |\nabla c| \, dl = \frac{\langle \kappa |\nabla c|^2 \rangle}{(\partial C / \partial A)^2}$$

- Keff (Leq) is well defined from contour averaging on isentropic surfaces
- Measures mixing as the amount of foldings beared by a given contour.
- Pro: Is a diffusivity. Easily calculated. Depends weakly on the quantity being contoured. Usable as a turbulent parameterization in 2D vert-lat models.
- Con: Limited to isentropic motion. Does not diagnose variation of diffusion along contours.

L_{eq} as a function of log-pressure height and ϕ_e.

Increased mixing in the summer lower stratosphere

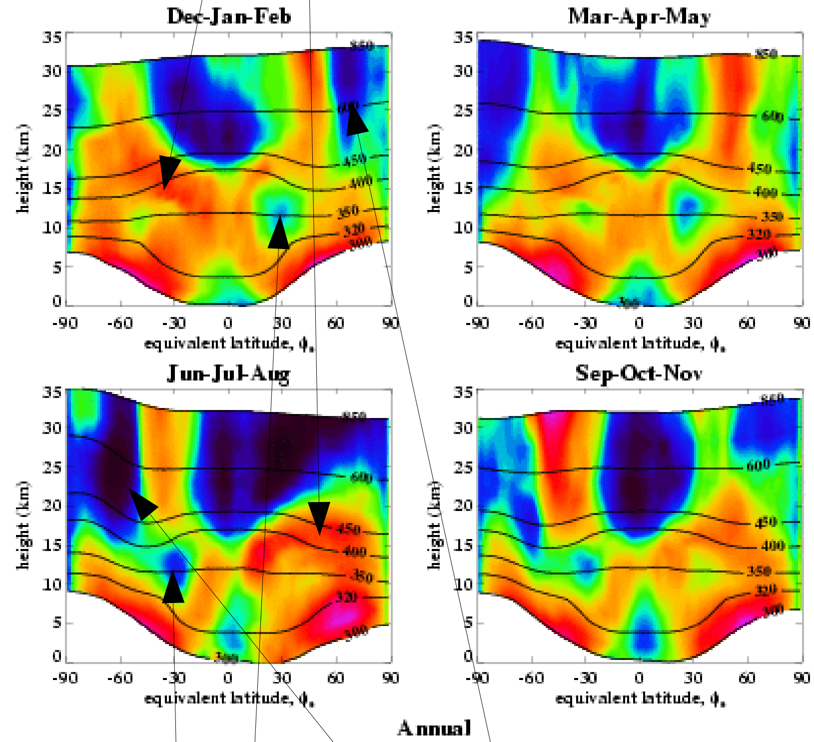

see Haynes and Shuckburgh, 2000, JGR, 105, 22777-22810.

Subtropical jets and polar vortex jets as minima (barriers) in effective diffusivity

Filament stretched until it reaches a width $l_d = \sqrt{\kappa / \lambda}$
where λ is the average Lyapunov exponent

Effective diffusivity $\kappa_{eff} = \kappa \frac{L^2}{l_O^2}$ where L
is the length of the contour.

Wide packing hypothesis $L \, l_d \approx l_0^2$
implies $\kappa_{eff} \approx \lambda l_0^2$

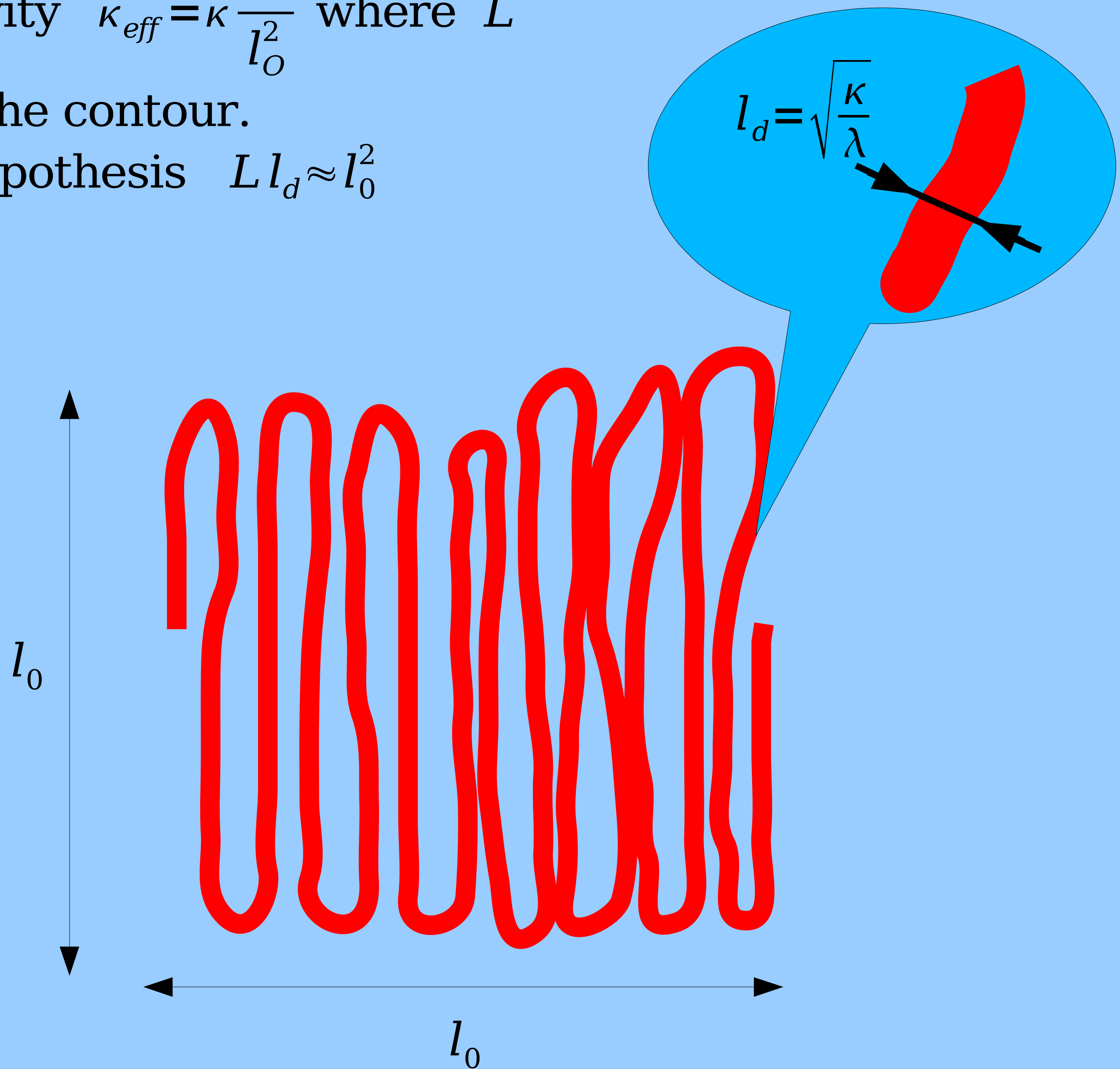

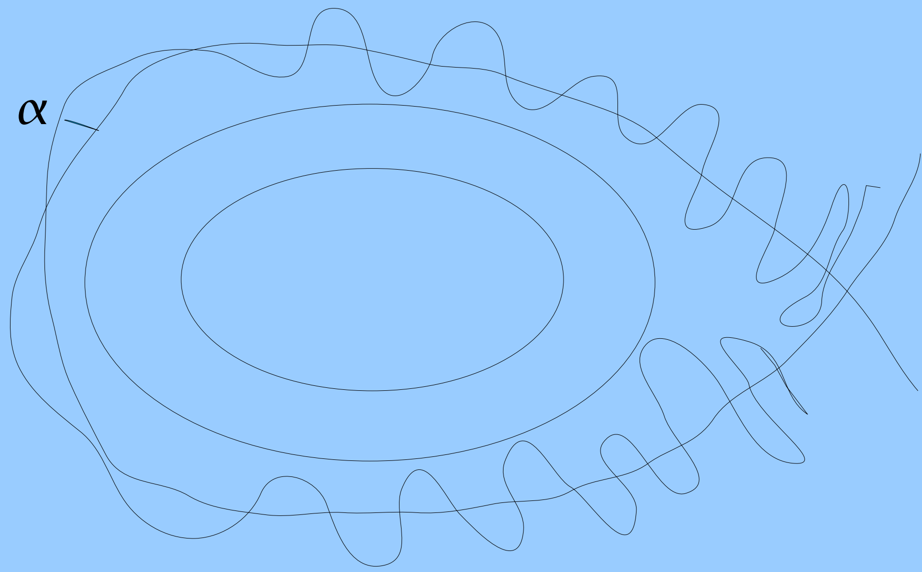

Within a shear zone, the width of the region invaded by filaments is bounded by barrier effects.

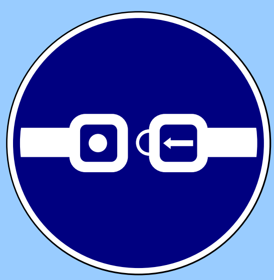

Under narrow packing hypothesis

$$L\, l_d \approx l_0^2 \sin\alpha$$

and hence $\kappa_{eff} \approx l_0^2 \lambda \sin^2\alpha$

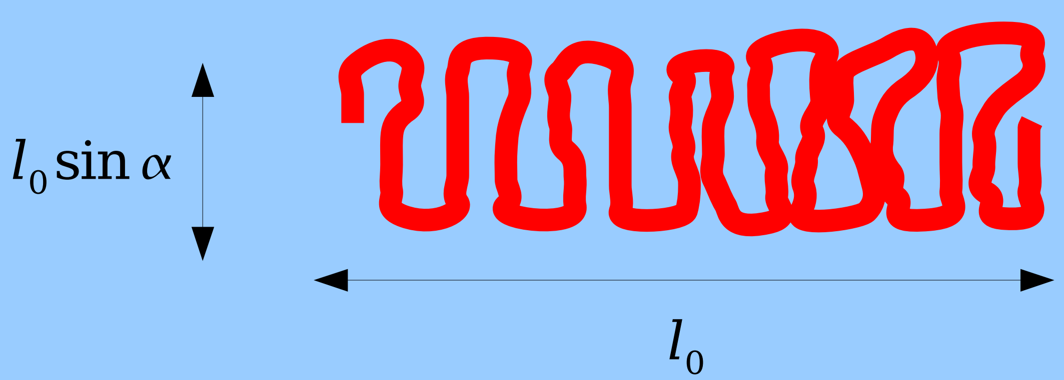

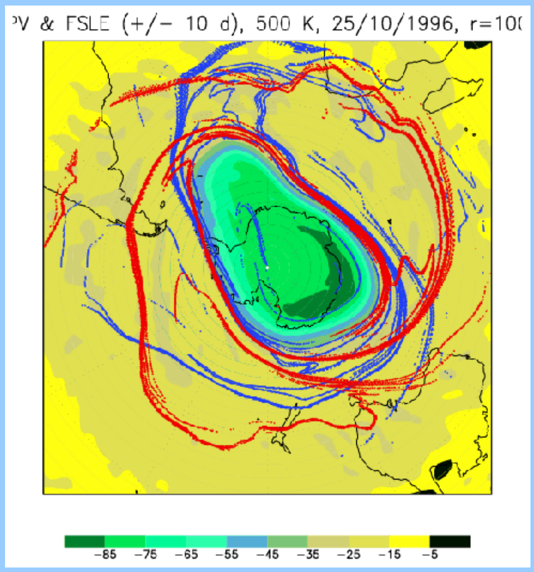

D'Ovidio etal., JAS, 2009

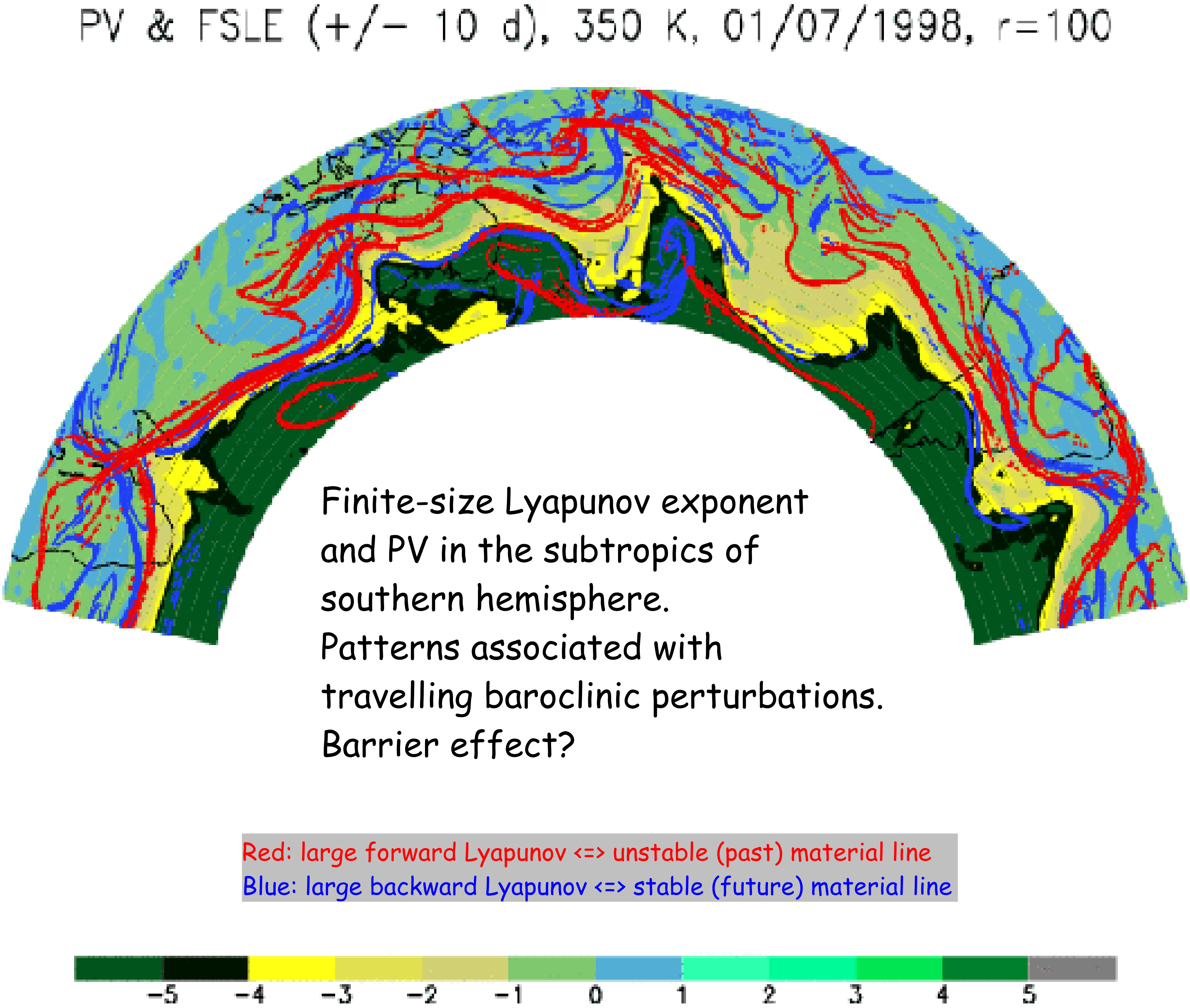

Finite-size Lyapunov exponent and PV in the subtropics of southern hemisphere.
Patterns associated with travelling baroclinic perturbations.
Barrier effect?

Red: large forward Lyapunov <=> unstable (past) material line
Blue: large backward Lyapunov <=> stable (future) material line

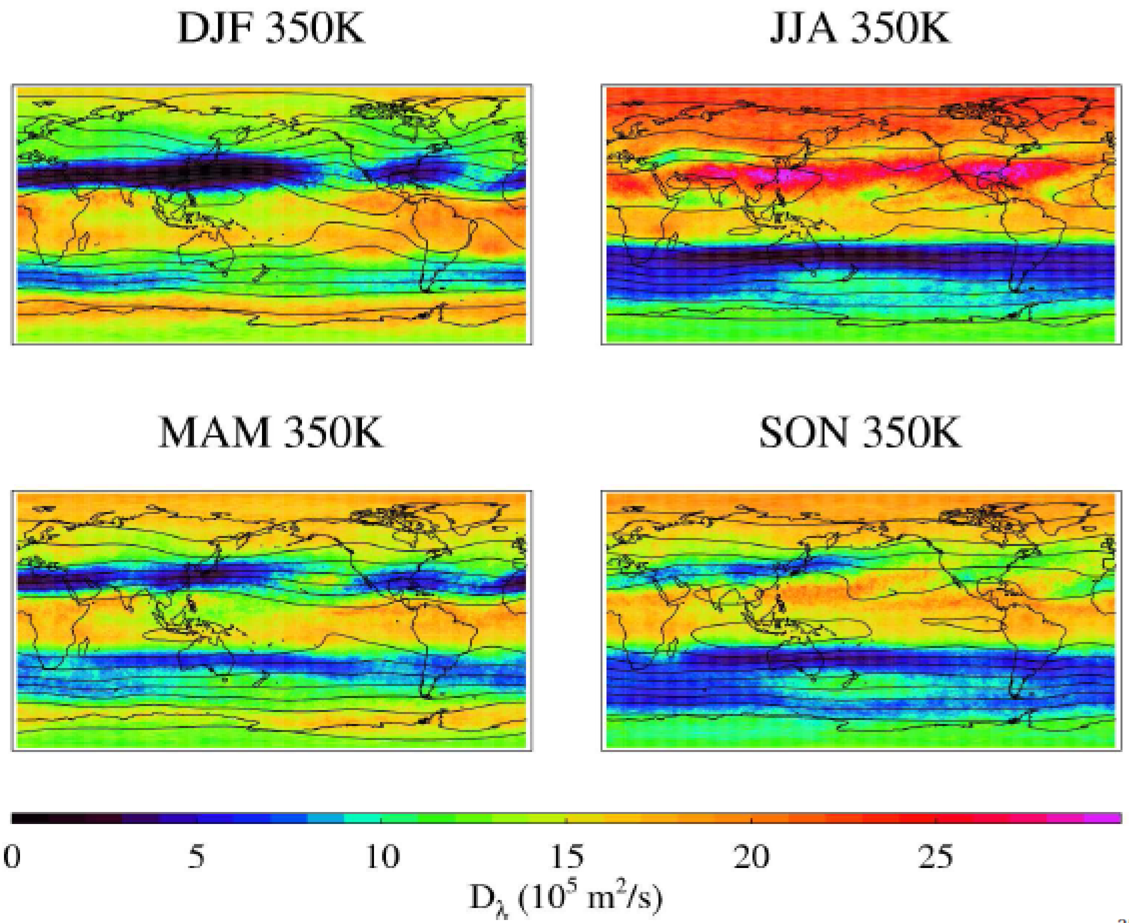

Lyapunov diffusivity

Lyapunov exponent x $\sin^2$ (angle between stable & unstable direction) x coefficient(latitude)

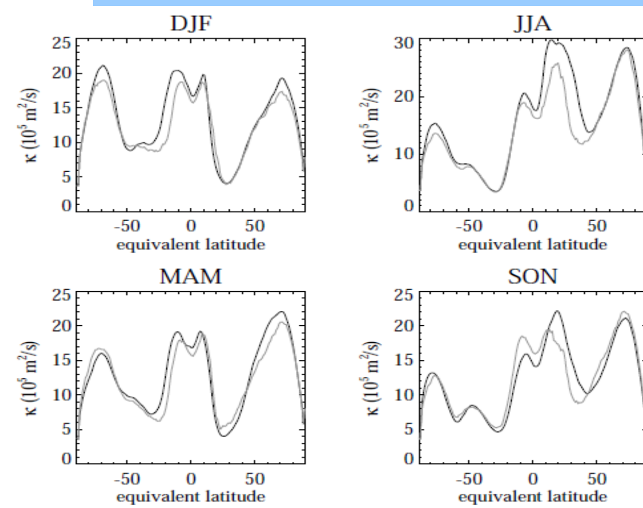

FIG. 8. The effective diffusivity $\kappa_{\rm eff}$ as a function of equivalent latitude (black) and the Lyapunov diffusivity D_λ averaged around contours of equivalent latitude (gray), for each season averaged over the period 1980-2001.

D'Ovidio et al., JAS, 2009

Schuckburgh et al., JAS, 2009

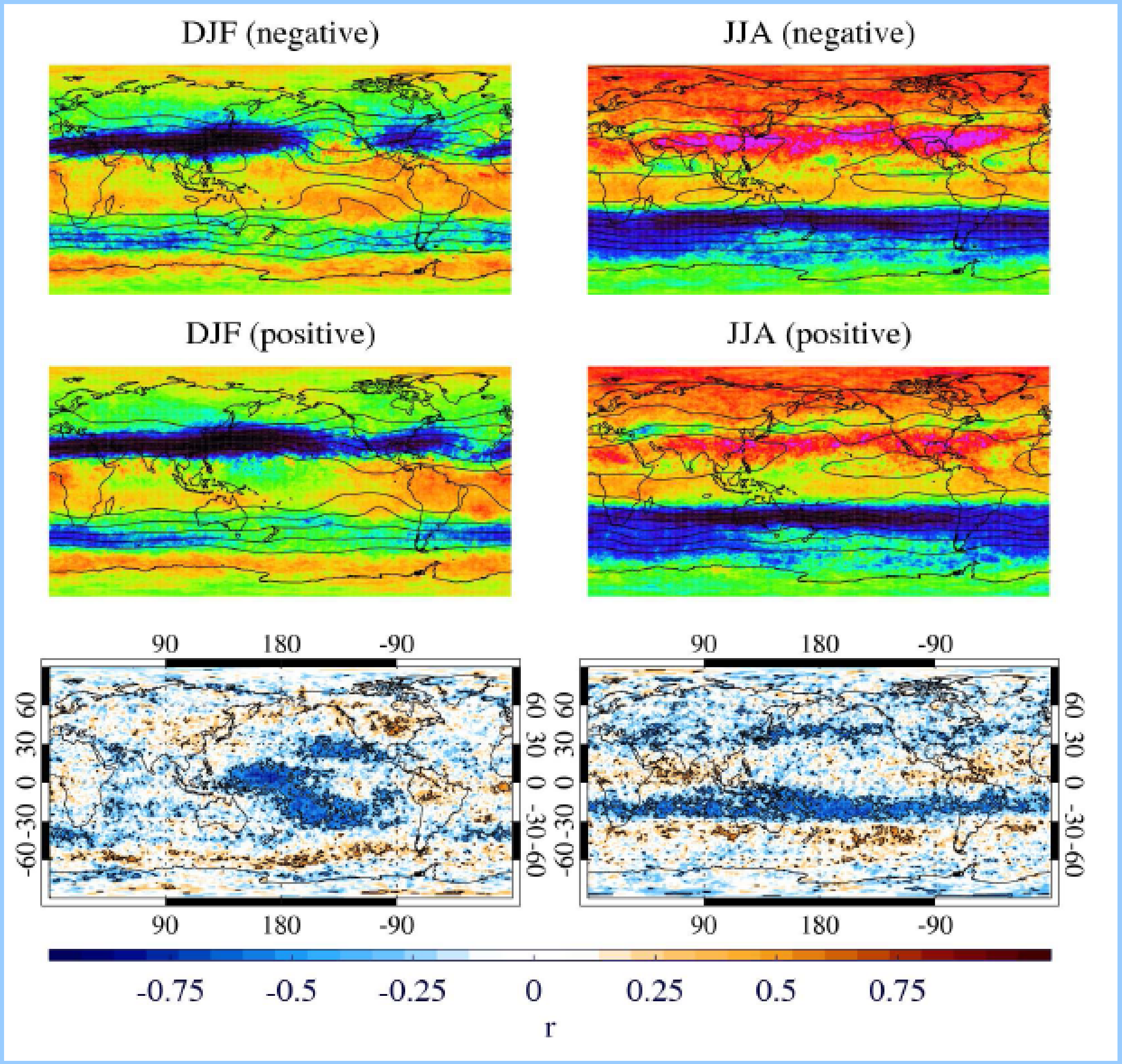

Schuckburgh et al., JAS, 2009

Upper-level frontogenesis and tropopause fold (II)

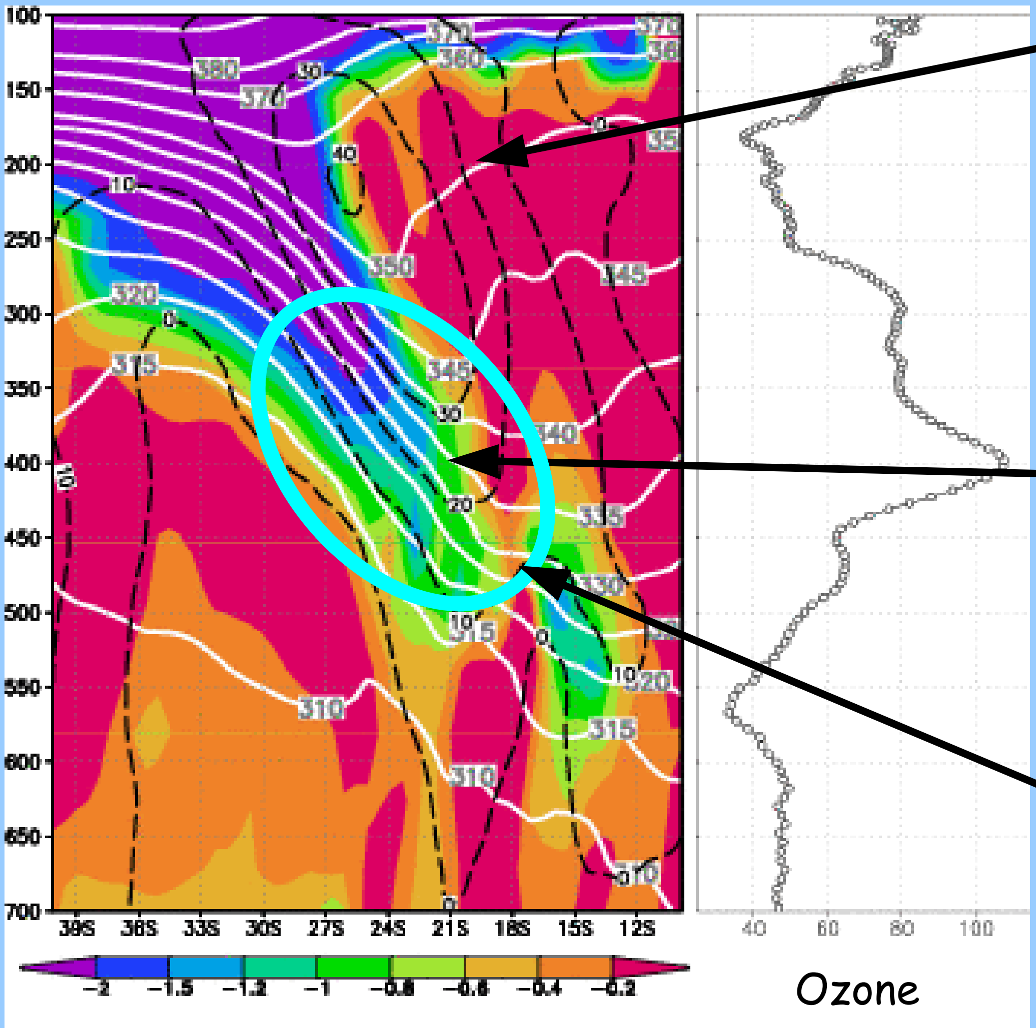

Isolines of the along front wind (across figure)

Isentropic surfaces bent into the troposphere, injecting stratospheric air

Stratospheric air mixes with tropospheric air here

CROSS-FRONT SECTION

Baray et al., GRL, 2000

Mixing barrier at the tropopause

Tracer-Tracer relations and barriers

Pre-AVE and CR-AVE campaigns

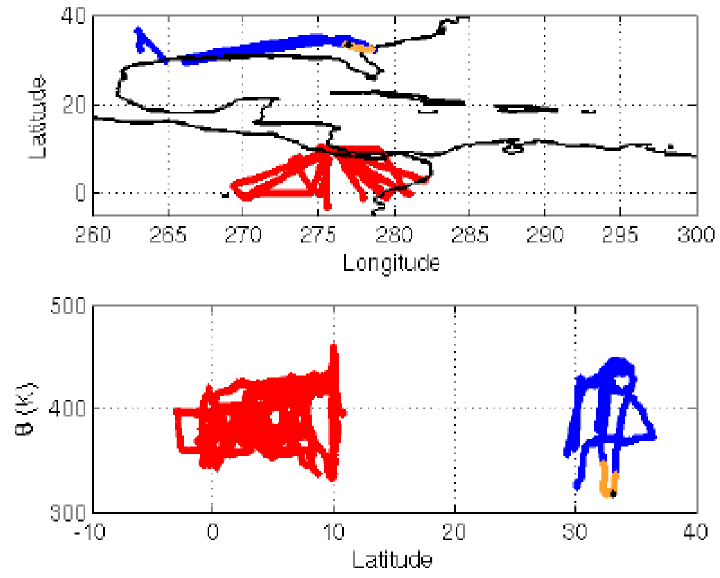

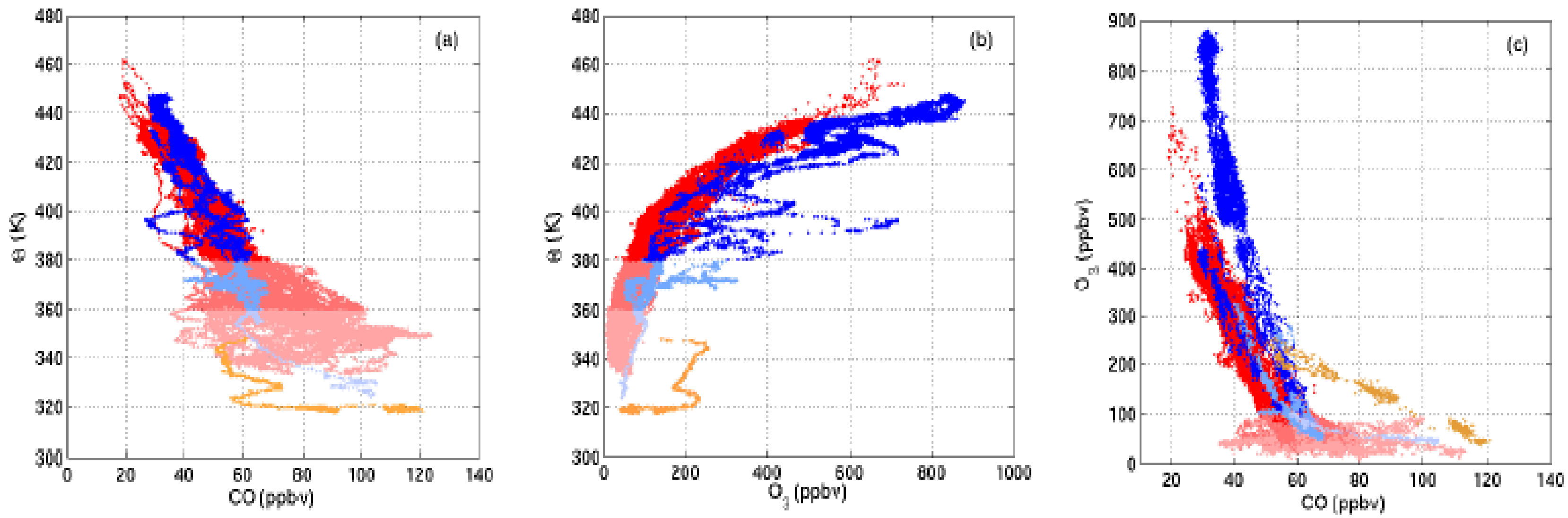

Fig. 2. (a) CO as a function of potential temperature; (b) O_3 as a function of potential temperature; (c) tracer-tracer relation with O_3 as a function of CO. Color code indicates the potential temperature (pink to red for tropical data and pale to dark blue for subtropical lower-stratosphere) with discontinuities at $\theta = 360$ K and $\theta = 380$ K, and marks the mixing line (orange). Black points in Fig. 1 are discarded from this figure.

James et Legras, ACP, 2008

Origin of parcels from Lagrangian trajectories

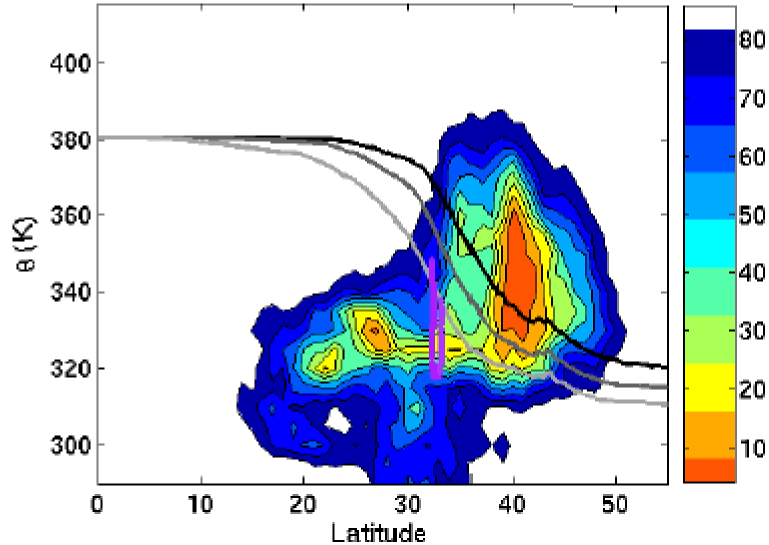

Tropopause layer

Fig. 4. Meridional distribution of the probability density function (pdf) of the particles contributing to the parcels belonging to the subtropical tropopause layer after a 9-day backward integration and as a function of latitude and potential temperature. The violet line shows the location of flight track along which the parcels have been initialized. The pdf is first calculated by binning parcels within boxes of 1 K×1deg. Contours show integrated percentage of parcels by aggregating boxes starting from the most populated. The thick line shows the average tropopause calculated as the lower level satisfying either $\theta > 380$ K or $PV > 2, 3$ or 4×10^{-6} K kg^{-1} m^2 s^{-1} (light, medium and dark gray).

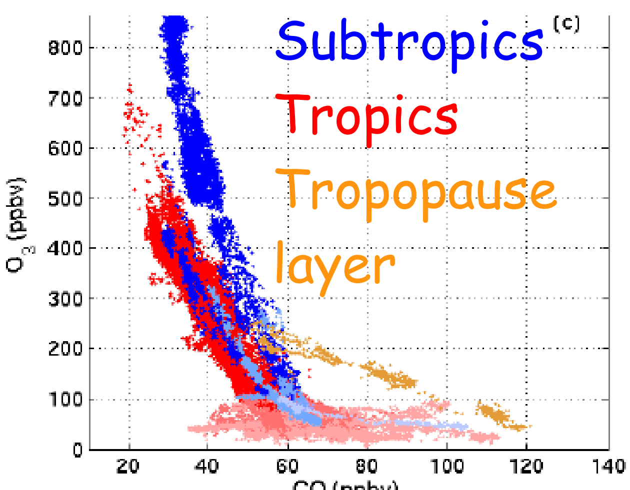

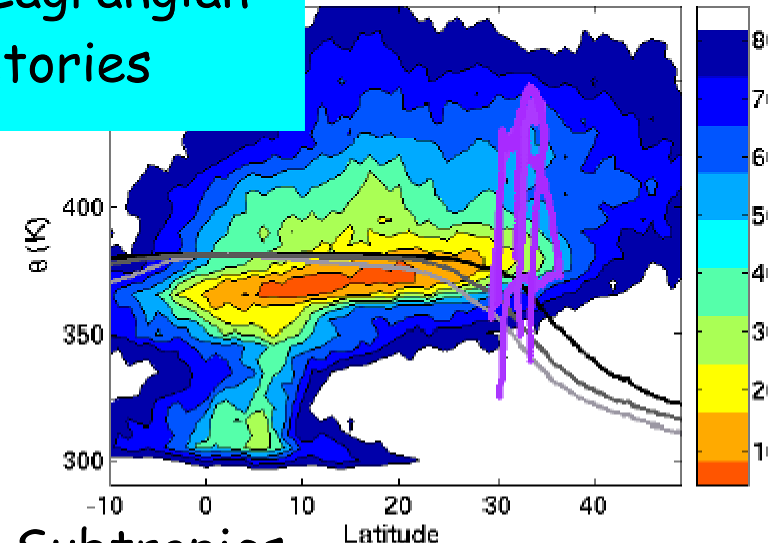

Subtropics

Fig. 7. Same as Fig. 4 for the distribution of subtropical particles initialized above 350 K after an integration of 35 days.

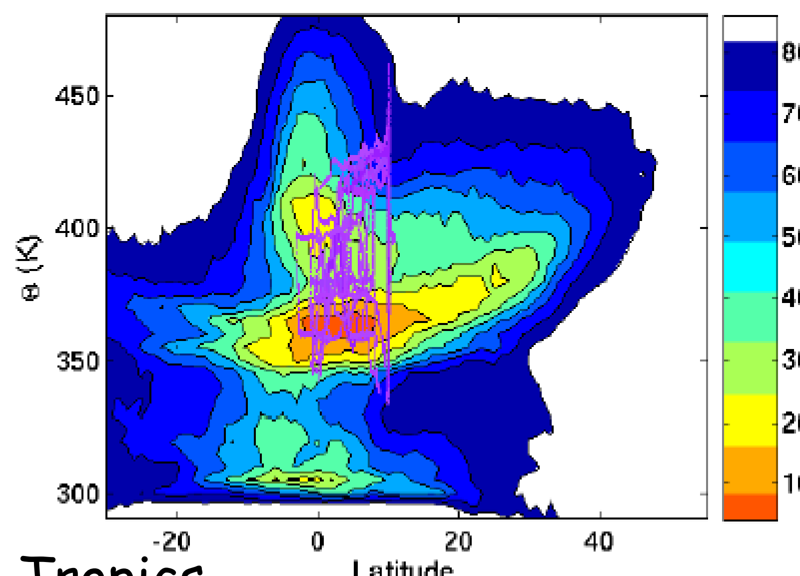

Tropics

Fig. 10. Same as Fig. 4 but for the distribution of the tropical particles after an integration of one month

James & Legras, ACP, 2008

Transport and water vapour.
(subtropical intrusions)

3858 WAUGH AND POLVANI: TRANSPORT INTO WESTERLY DUCTS

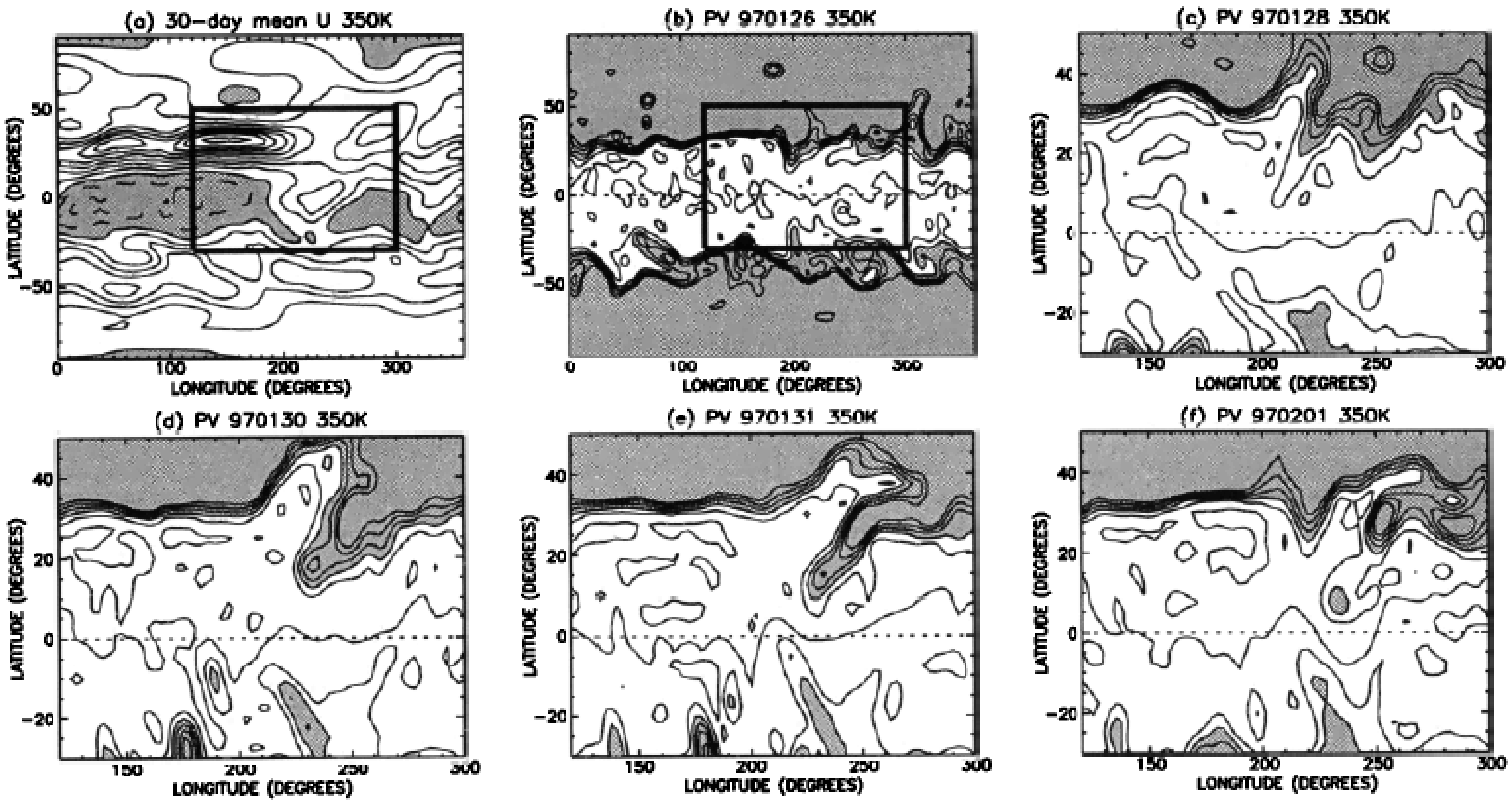

Figure 1. (a) zonal wind averaged between January 16 and February 14, 1997 (contour interval 10 m/s; negative values shaded). (b-f) PV on January 26 to February 1, 1997 (PV = (-5, -4, ..., 5) PVU contoured, with $|PV| > 2$ PVU shaded). All fields are on the 350 K isentrope.

Waugh & Polvani, GRL, 2000

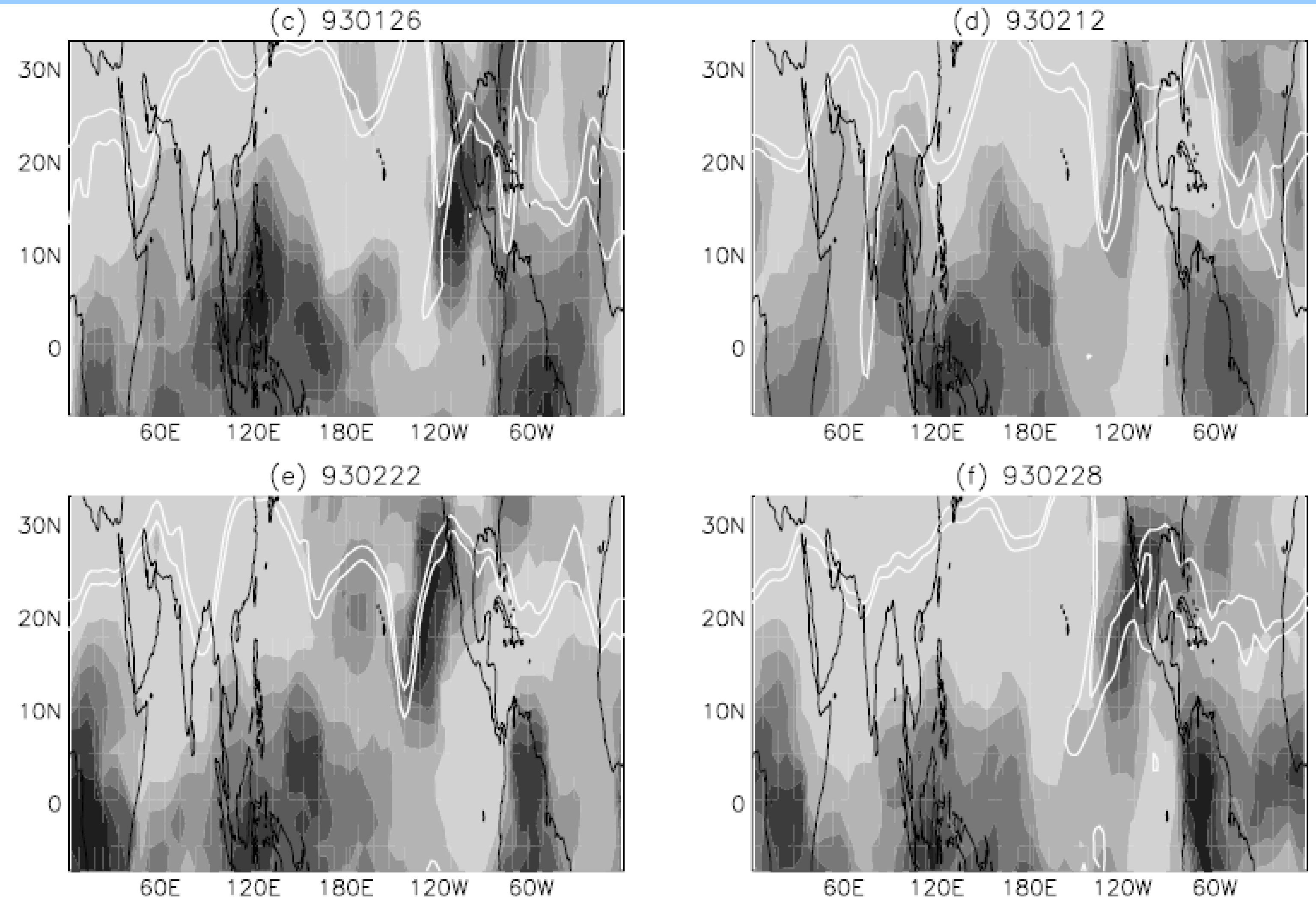

Figure 1. Maps of MLS 215 hPa RH (shading) and NCEP 350K PV (contours) for several days in January and February 1993. The shading interval for the RH is 20% with lightest shading corresponding to RH < 20% and darkest shading to RH > 120%. Contours show PV = 1 and 2 PVU.

Waugh, JGR, 2004

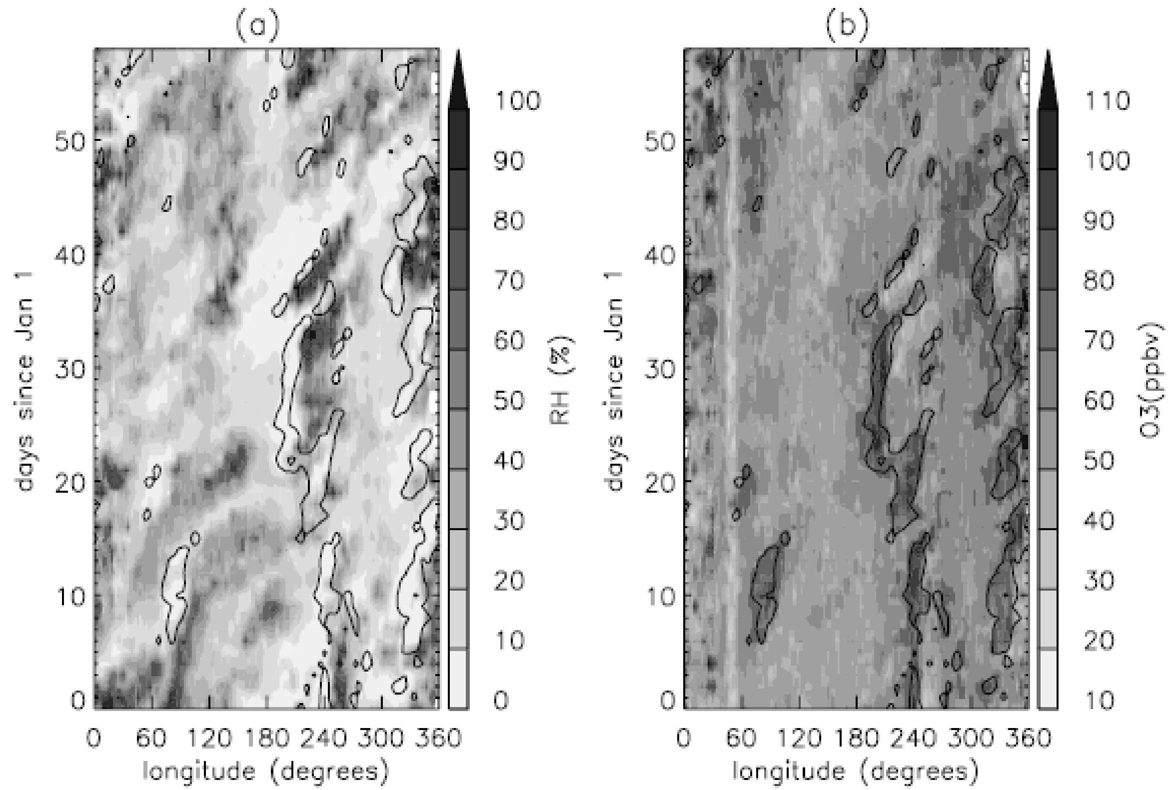

Figure 3. Longitude-time variation of AIRS 200–250 hPa (a) RH and (b) O_3 mixing ratios at 17.5°N for January–February in 2004. Contours show PV = 1.5 PVU at 17.5°N. See color version of this figure at back of this issue.

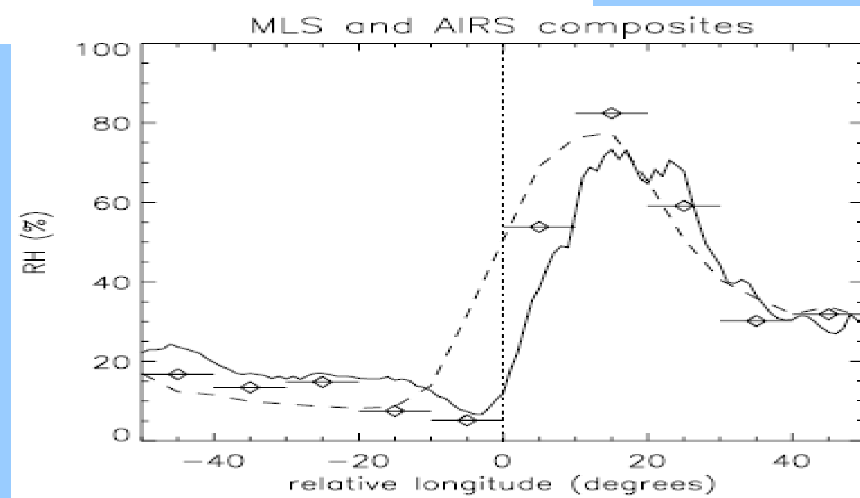

Figure 4. Longitudinal variation of the composite-mean RH for north Pacific intrusion events in January–February, for AIRS (solid curve) and MLS (dashed curve) measurements in 2003–2004 and 1992–1994, respectively. Diamonds and horizontal lines show MLS composite using individual profile data rather than gridded data. Longitude is relative to longitude of the PV intrusion (vertical dotted line).

In the subtropics at 200-300hPa , dry air from the extratropical lower stratosphere mixes with relatively moist tropical air, contributing to dry subtropical troposphere.

Waugh, JGR, 2004

Observed brightness at 6.3μm

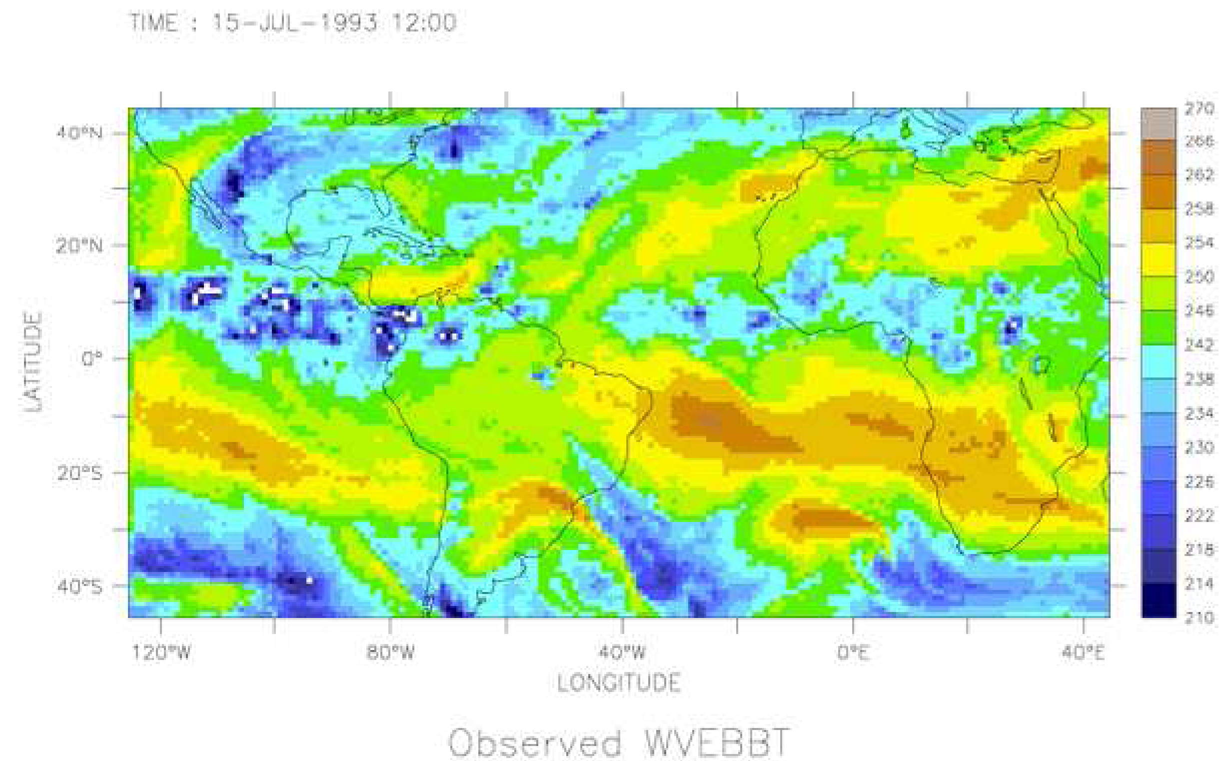

Calculated brightness

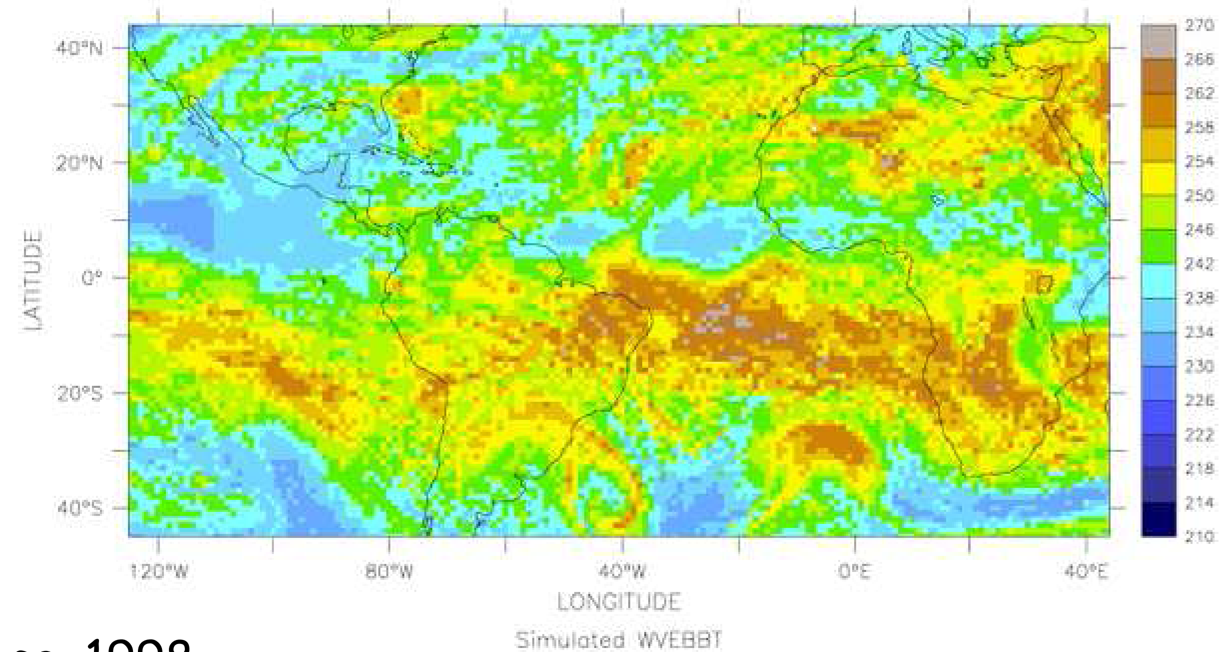

Pierremhumbert & Roca, 1998

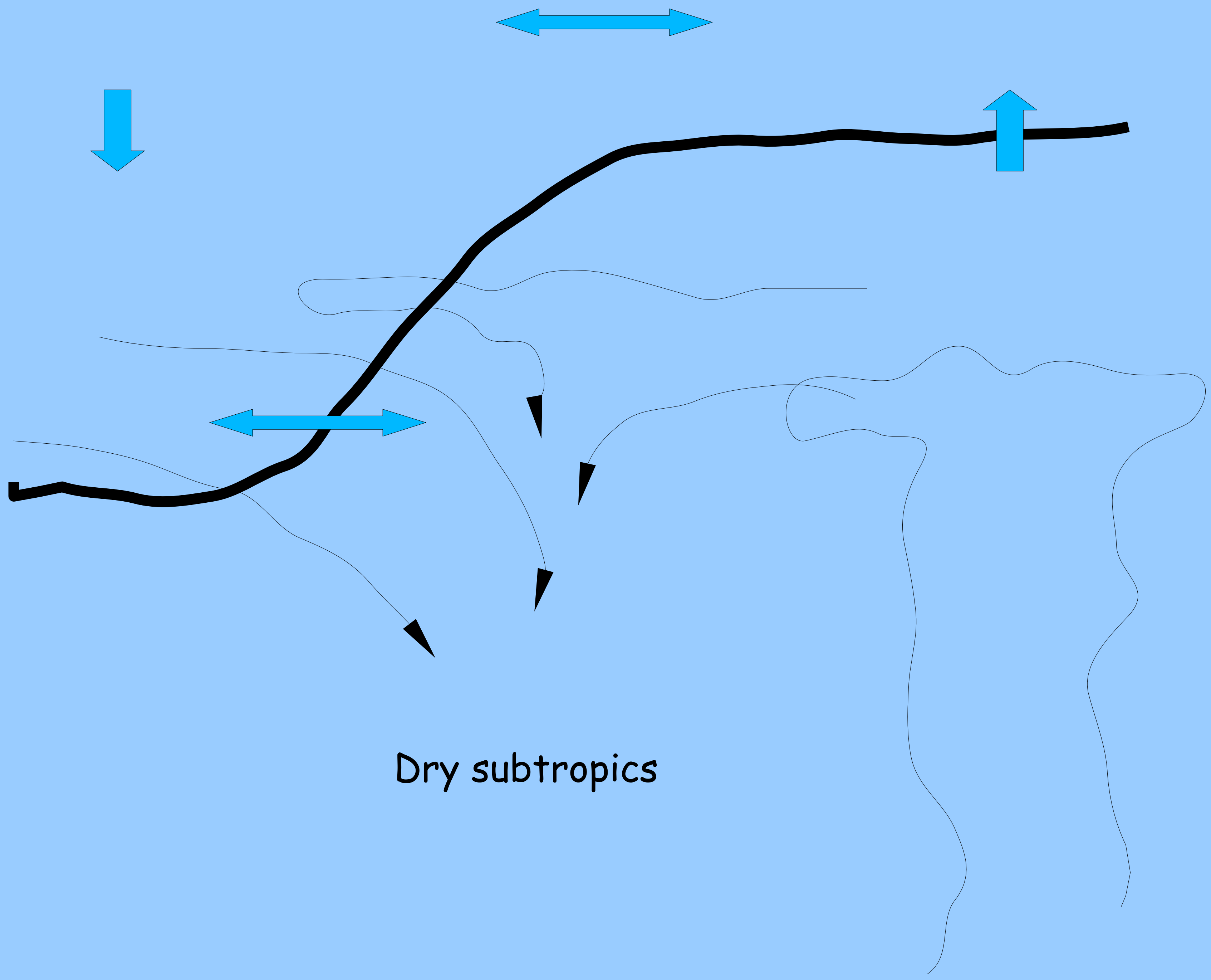
Dry subtropics

Water vapour and diffusion

Water vapour and diffusion

Consider the simple problem

$$\partial_t q = D\,\partial_{yy} q - S(q, q_s)$$

where $S(q, q_s)$ means that q is set to q_s as soon as $q > q_s$

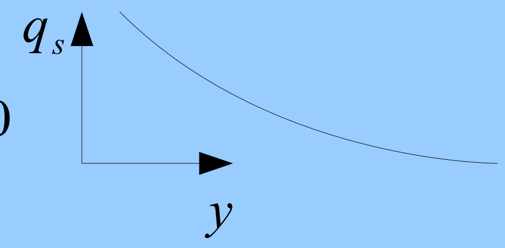

$q = q_s$ is a solution in the infinite domain as long as $\partial_{yy} q_s > 0$

In this case, diffusion flux and condensation maintain saturation everywhere.

In case of zero flux in $y=0$ and q_s decaying with y

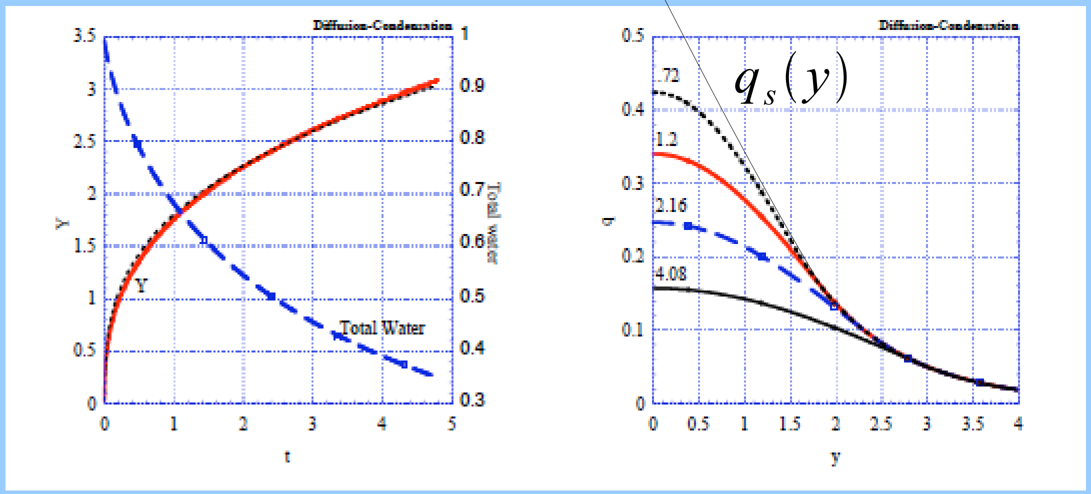

Figure 5: Numerical results for the freely decaying diffusion-condensation model with a no-flux barrier at $y = 0$. Left panel: Time evolution of the point $Y(t)$ bounding the subsaturated region, and of total moisture in the system. The short-dashed line gives the fit to the asymptotic result $Y \sim t^{1/3}$. Right panel: The profile of specific humidity at the times indicated on the curves.

Pierrehumbert et al., 2007

If now we consider instead an ensemble of particles that execute independent random walks, and are tagged with a passive tracer c_j and water vapour q_j which is bound by saturation $q_s(y)$.

If the random walk is governed by the stochastic equation

$$dy/dt = v(t) \text{ with } < v(t)v(t') \geq 2\mathrm{D}\,\delta(t-t')$$

Then the distribution of the passive tracer follows the diffusion equation

$$\partial_t c = D\,\partial_{yy} c$$

while interesting behaviour is observed for the non passive water vapour.

First dry air is generated in the infinite domain because of the excursions of parcel into the dry region .

For the same reason, the decay in the bounded domain with zero flux is faster

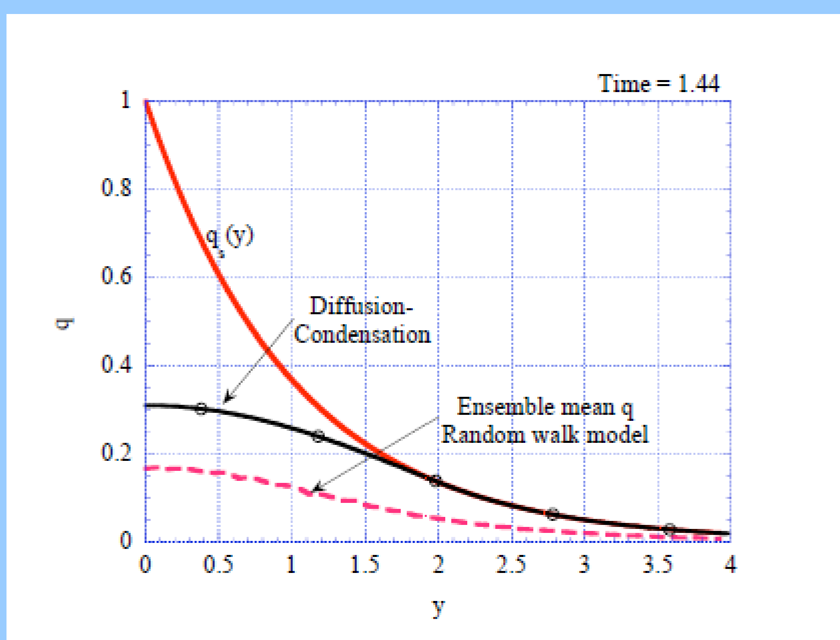

Pierrehumbert et al., 2007

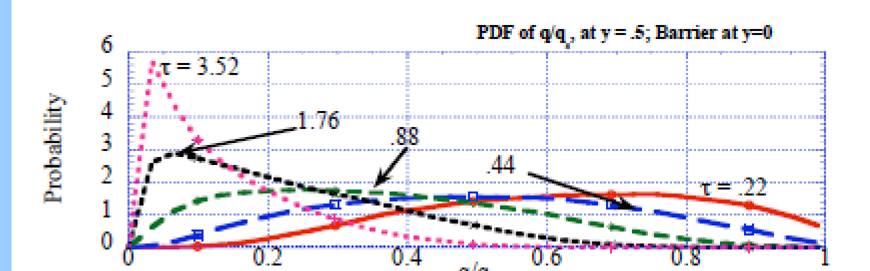

PDF of q at $y=0.5$

Non mixing particles

Hence:

Random walk and condensation do not commute (same conclusio,n holds for order 2 chemical reactions)

Turbulent diffusivity is questionable for humidity and chemical compounds.

Consequences: large-scale models (GCM, NWP) may not represent the dry part of the water vapour distribution.

This can be investigated using Lagrangian trajectories

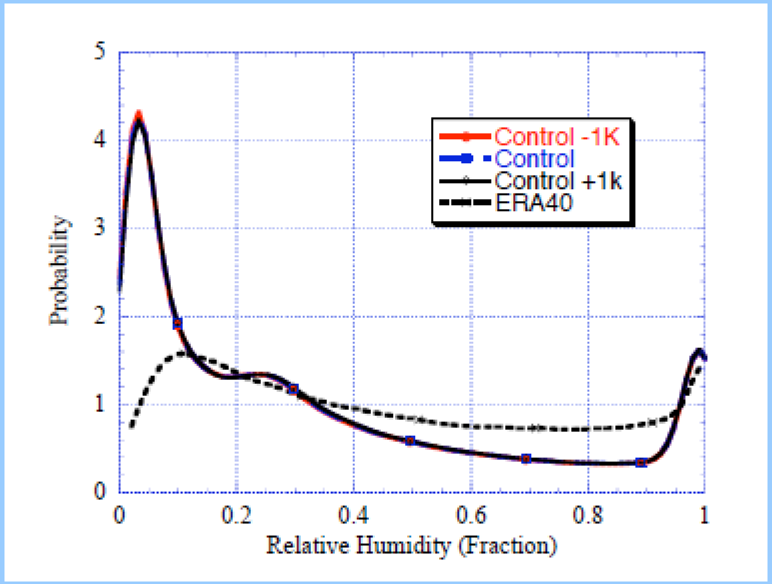

Pierrehumbert et al., 2007

Figure 15: Probability distribution of relative humidity for Dec. 1994 over the region shown in Figure 14, computed 4 times daily using NCEP winds and temperatures. Results for experiments with temperature uniformly increased or decreased by 1K are also shown, but the curves are barely visible because they lie almost exactly on the control case. For comparison, the relative humidity PDF over the same time and region for the ERA40 analysis is also shown.

Assumtion: The distribution of water vapour is essentially dependent on the transport properties of the flow + the last encounter with saturation. Then the variation of RH under climate change (where circulation is unchanged to first order) is linked to the Clausius-Clapeyron law

$$r(\Delta T) \approx (\frac{p}{p_m})\frac{e_s(T_m) + e_s(T_m)\frac{L}{R_w T_m^2}\Delta T}{e_s(T) + e_s(T)\frac{L}{R_w T^2}\Delta T} \approx r(0)(1 + \frac{L}{R_w T}(\frac{T^2}{T_m^2} - 1)\frac{\Delta T}{T})$$

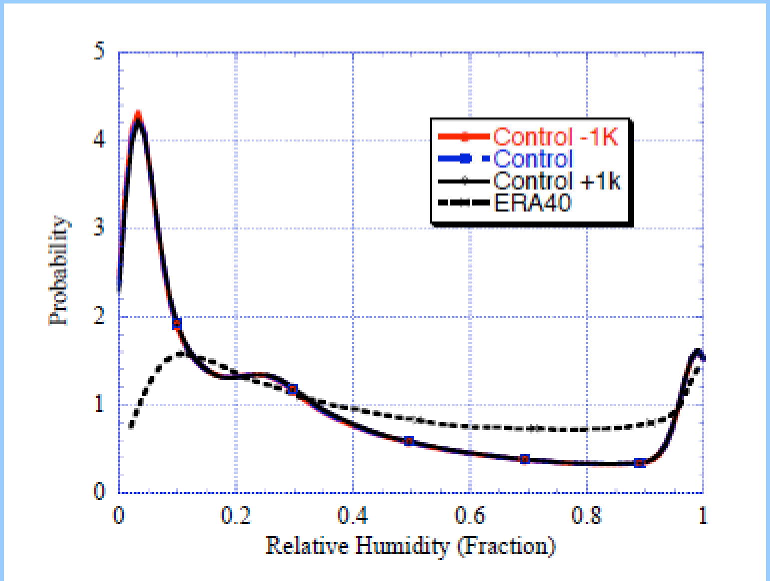

where T is the parcel temperature and T_m its minimum encountered temperature

With $T = 260\,\mathrm{K}$, $T_m = 240\,\mathrm{K}$ and $\Delta T = 1\,\mathrm{K}$ the increase is only $0.014\, r(0)$

Figure 15: Probability distribution of relative humidity for Dec. 1994 over the region shown in Figure 14, computed 4 times daily using NCEP winds and temperatures. Results for experiments with temperature uniformly increased or decreased by 1K are also shown, but the curves are barely visible because they lie almost exactly on the control case. For comparison, the relative humidity PDF over the same time and region for the ERA40 analysis is also shown.

Vertical velocities
and diabatic heating rates

- Vertical velocities dp/dt
- Standard archived product of most models.
- Offset adiabatic motion
- Instantaneous values very noisy. Remedies:
  - increase temporal resolution (3h is OK, 1h not needed)
  - Time average (but loss of mass conservation)
- Mean ascent within the grid averaging convective ascent and environment cooling.

- Heating rates $d\theta/dt$
- Archived in ECMWF reanalysis. In most cases, need radiative calculations.
- Accumulated heating rates much less noisy than vertical velocities.
- Can separate radiative/convective, clear sky/all sky effects.
- Difficulty: weak vertical gradients of θ often encountered in the troposphere
- Loss of mass conservation

Comparison of reconstructions with several advecting wind fields

No sensitivity to spatial resolution but very large sensitivity to temporal resolution

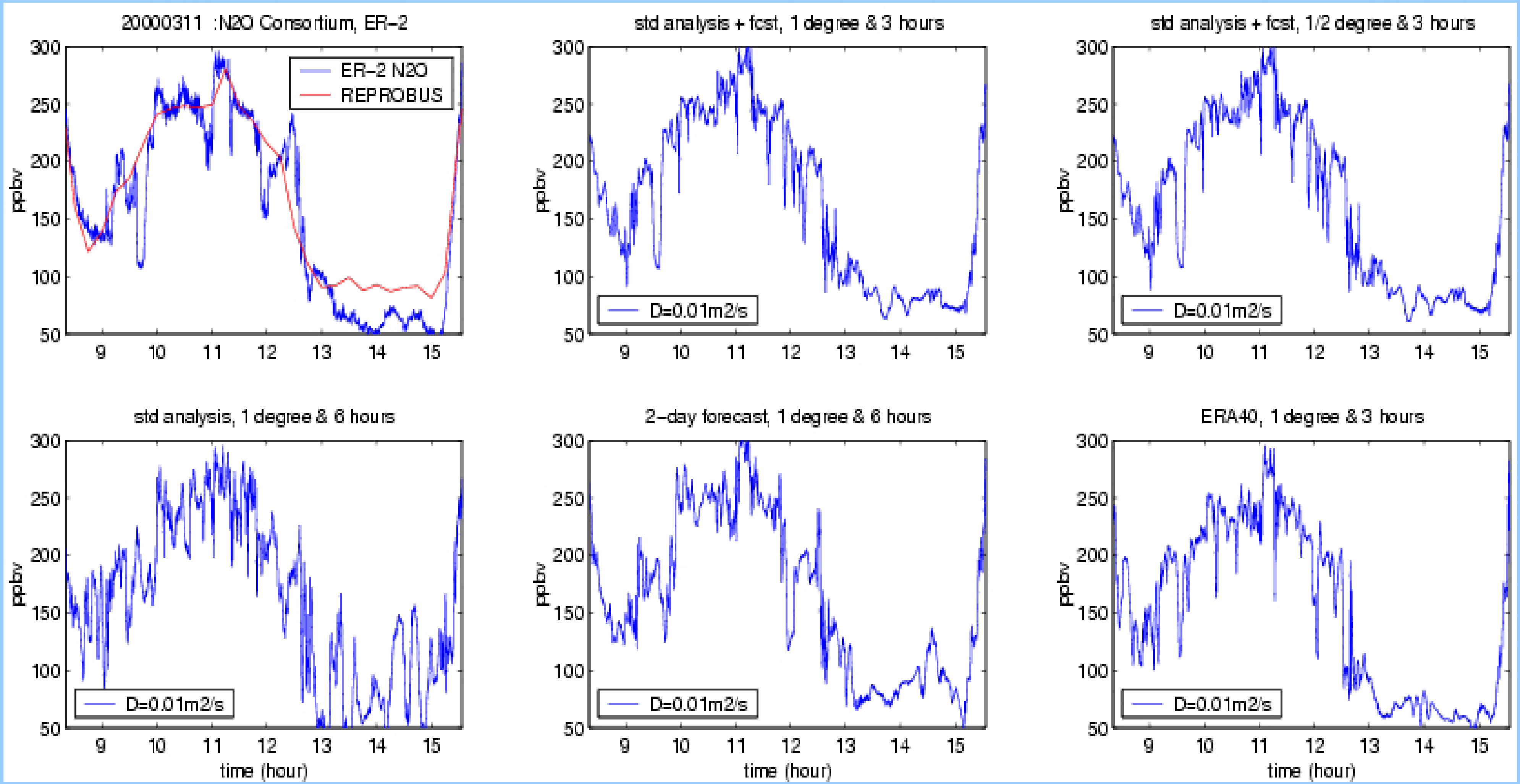

Trajectories and clouds

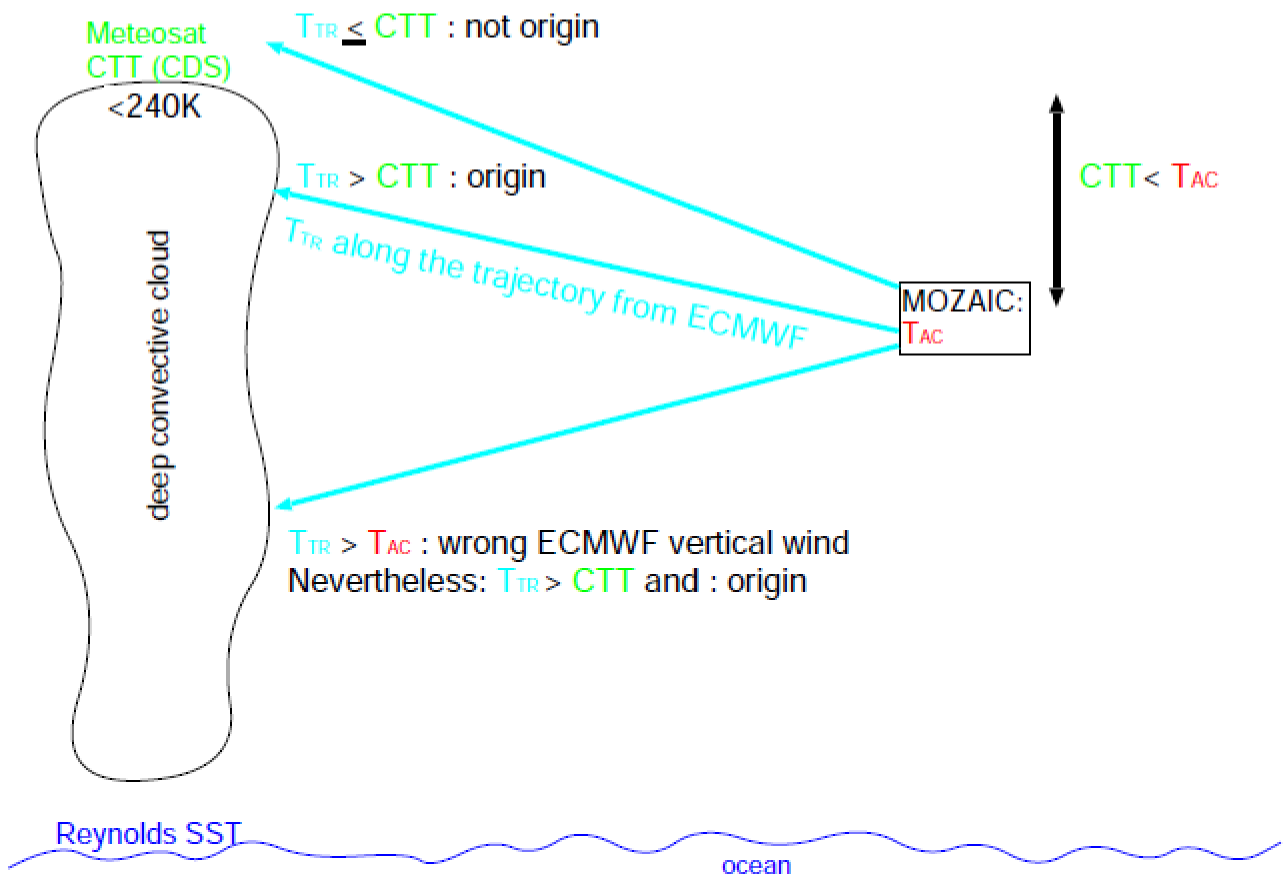

Figure 5.8: Examples of trajectory with different vertical motion to illustrate the different criteria. Only clouds where all criteria are fulfilled are interpreted as the convective origin of the measured air.

S. Nawarth, thesis, Köln, 2002

Backward Lagrangian trajectories in the TTL from 100 hPa during monsoon season.
Diabatic heating rates from ERA-Interim
Rightness temperature from CLAUS

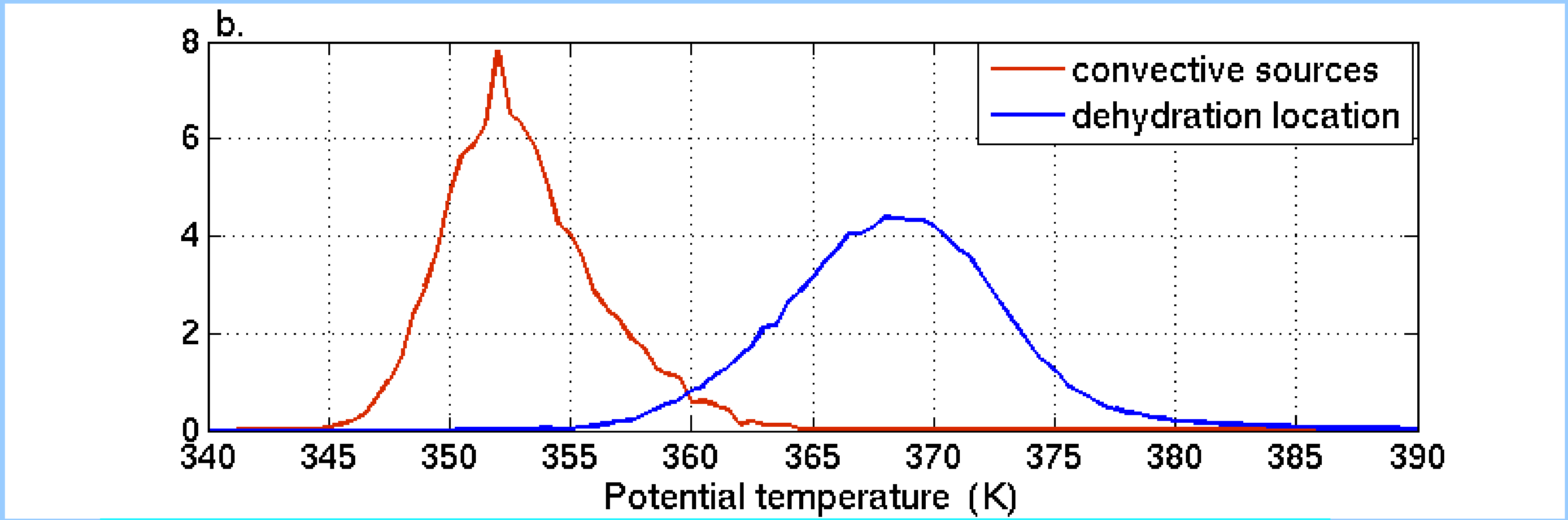

PDF of potential temperature of convective sources (CLAUS) and of locations of minimum temperature (dehydration)

James et al., GRL, 2008

Effect of clouds on transport within the TTL

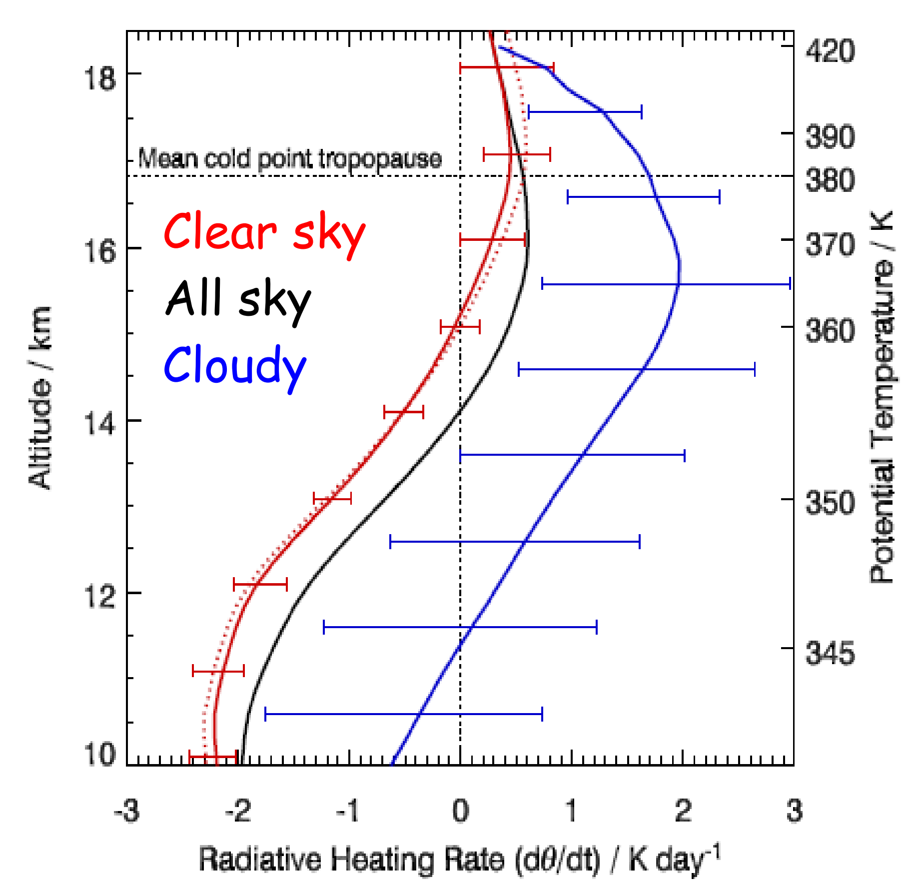

Corti et al, ACP, 2006
For soundings distributed within the tropics

ERA-Interim heating rates

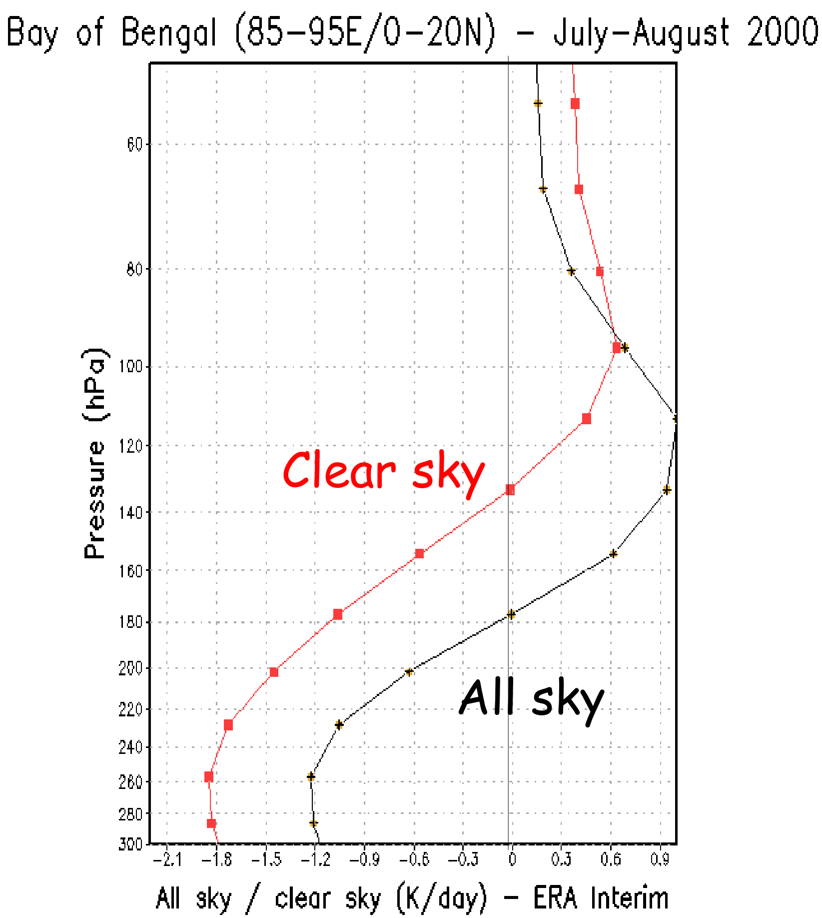

Cloud upwelling transports parcels from the outflow level to the level of zero clear sky heating rate

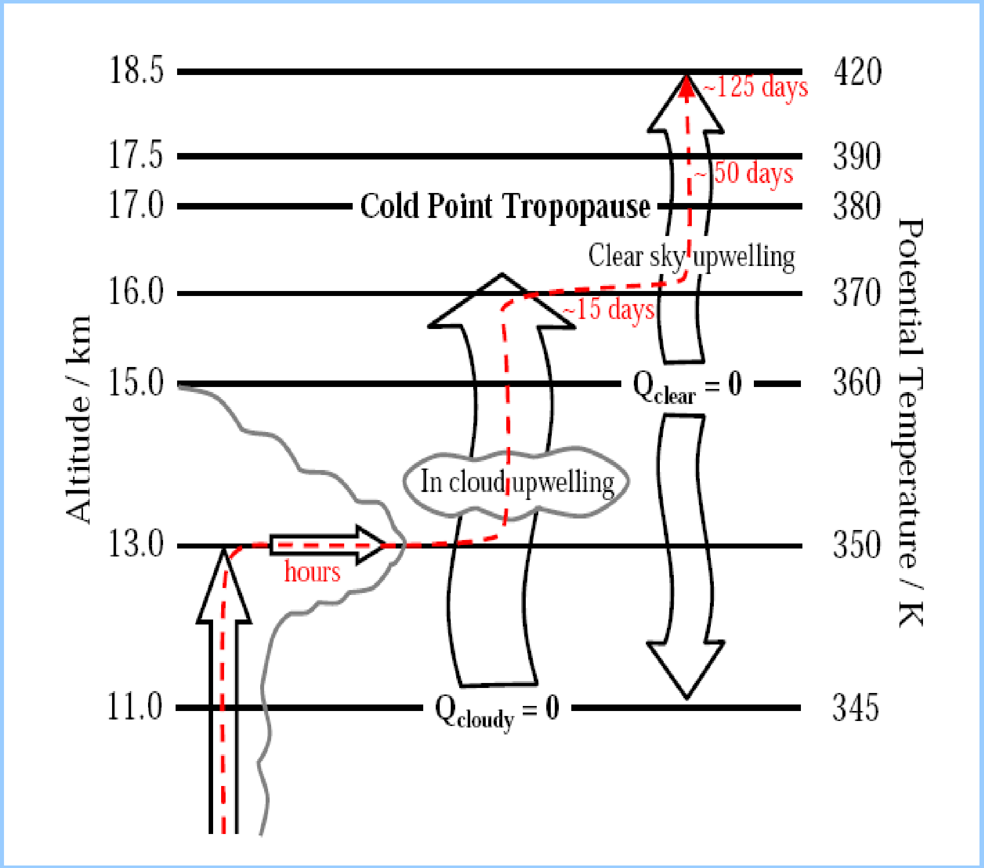

Corti et al, ACP, 2006

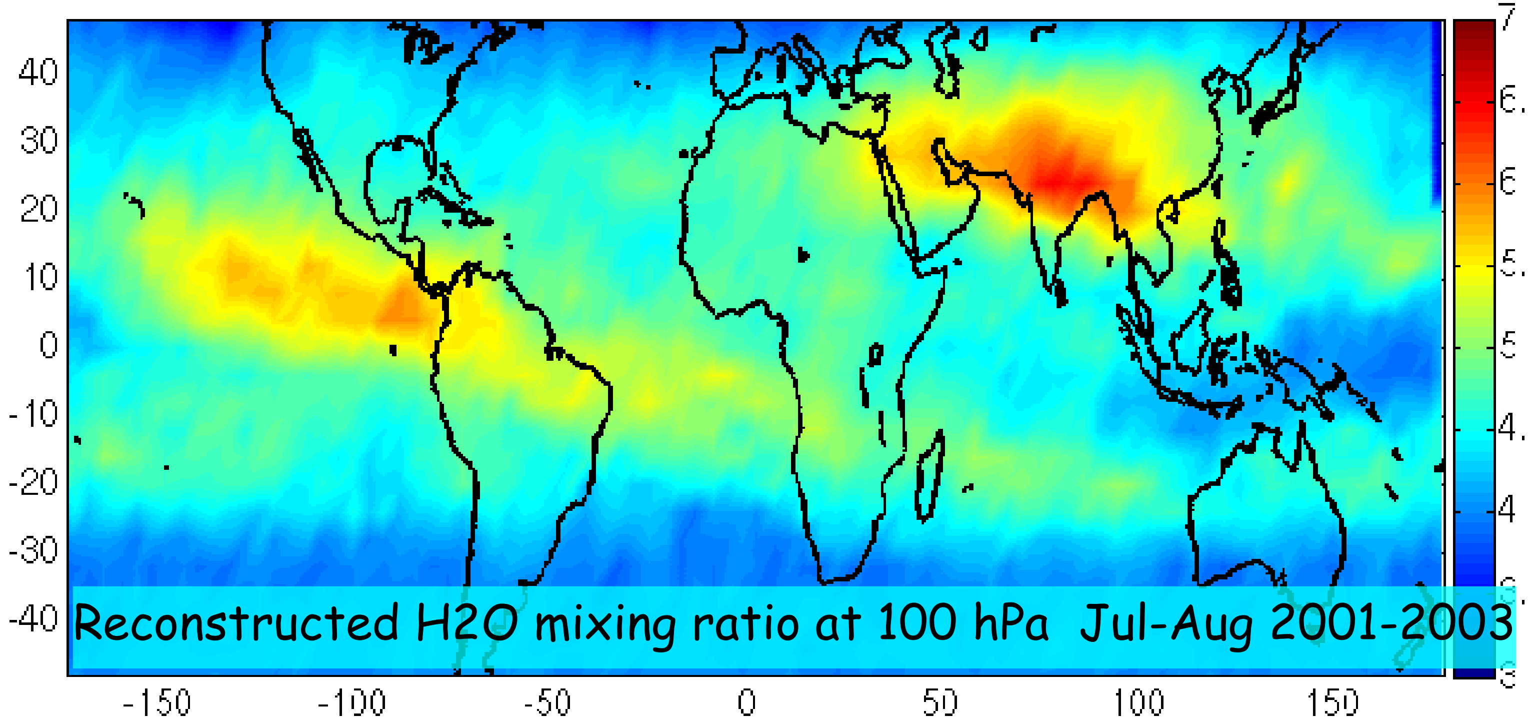
Reconstructed H2O mixing ratio at 100 hPa Jul-Aug 2001-2003

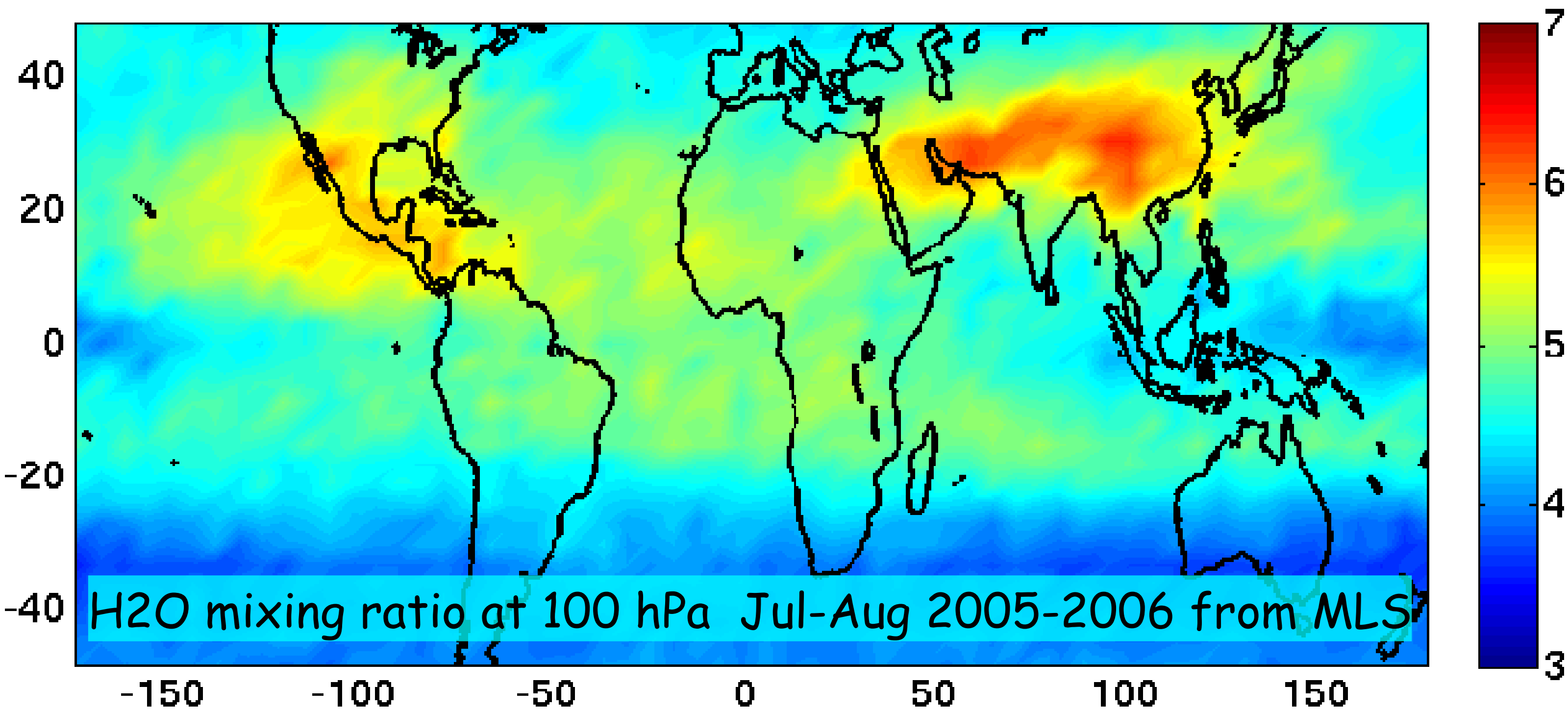
H2O mixing ratio at 100 hPa Jul-Aug 2005-2006 from MLS

S
e

Sensitivity studies

Reference - Simulation with vertical velocities (instead of heating rates)

Reference - Simulation with clear sky heating rates (instead of all sky)

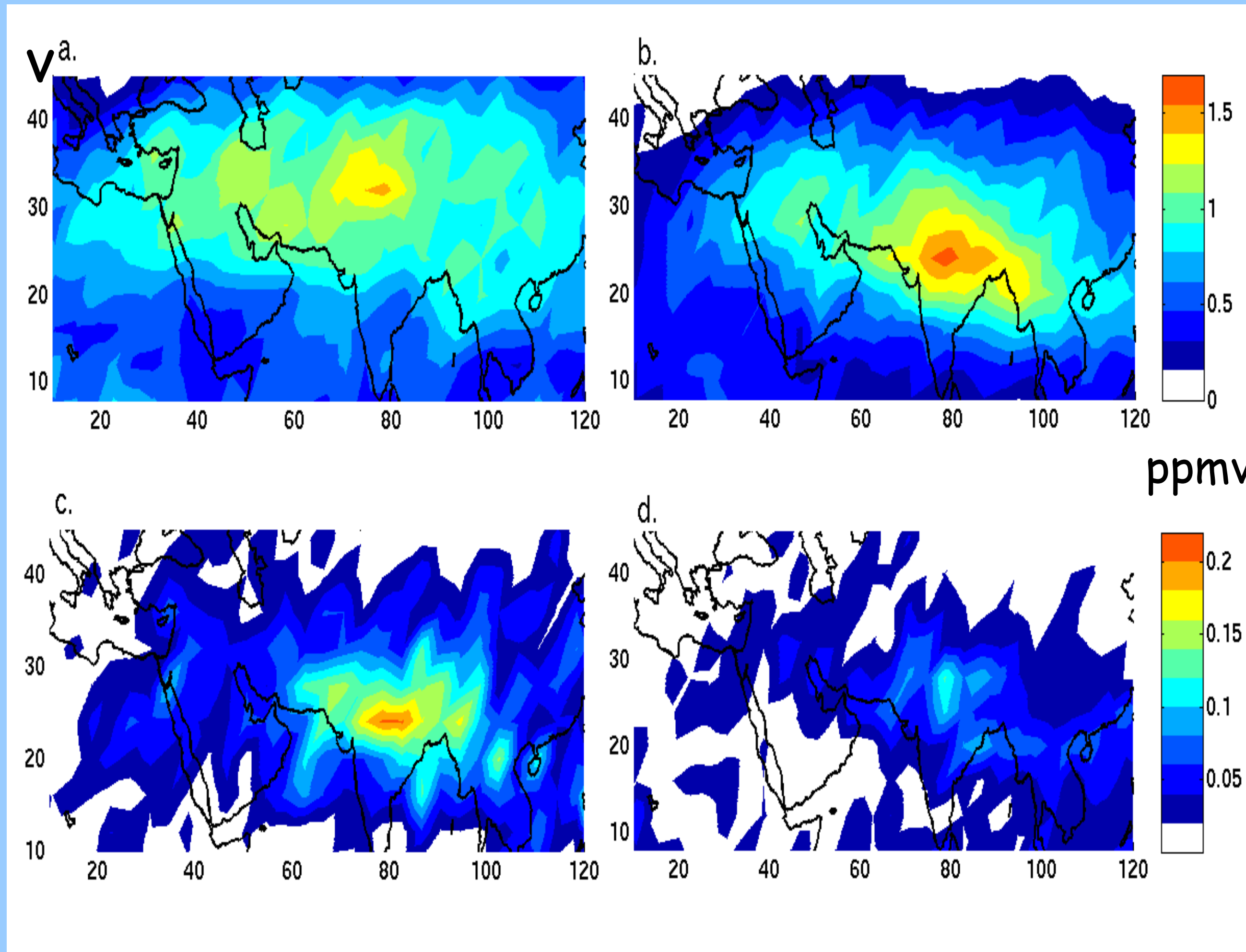

Reference - Simulation ignoring cloud tops

Simulation including overshoots - Reference

Overshoot parameterization: encounter probability with exponential decay with height adjusted to be 6% over ocean and 15% over land 1km above cloud top (10 times Liu & Zipser, 2005). Frequency needs to be multiplied by 100to get 0.3 ppmv)

agrangian transport

B. LEGRAS WAVACS 23/09